HOKKAIDO UNIVERSITY

Title	Mineral processing of complex sulfide ores combined with extraction, flotation, and cementation for sustainable development of complex sulfide deposits
Author(s)	相川, 公政
Degree Grantor	北海道大学
Degree Name	博士(工学)
Dissertation Number	甲第15380号
Issue Date	2023-03-23
DOI	https://doi.org/10.14943/doctoral.k15380
Doc URL	https://hdl.handle.net/2115/97003
Type	doctoral thesis
File Information	Kosei_Aikawa.pdf

Hokkaido University Collection of Scholarly and Academic Papers : HUSCAP

Doctoral Thesis

Mineral processing of complex sulfide ores combined with extraction, flotation, and cementation for sustainable development of complex sulfide deposits

A dissertation submitted in partial fulfillment of the requirements
for the degree of Doctorate in Engineering

by

KOSEI AIKAWA

Laboratory of Mineral Processing and Resources Recycling
Division of Sustainable Resources Engineering,
Graduate School of Engineering,
Hokkaido University, Japan
March 2023

Abstract

Complex sulfide ores, some of the most important sources of critical metals, are typically composed of several metal sulfide minerals like chalcopyrite, galena and sphalerite. Complex sulfides consisting of copper (Cu), lead (Pb), and zinc (Zn)-sulfide minerals are typically processed via flotation—a separation technique based on the differences in wettability of minerals—to produce concentrates of each mineral. Some complex sulfides (e.g., seafloor massive sulfides obtained from around Japan, one of the promising sources of critical metals in the future) contain not only galena but also anglesite, which is not typically contained in conventional ores. The presence of anglesite is problematic for the separation of Cu, Pb and Zn-sulfide minerals by flotation due to the unwanted activation of ZnS by lead ions released from anglesite. In addition, anglesite is disposed of into tailings dam and contaminates its surrounding environment. To address these problems, a sufficient method needs to be developed for depressing sphalerite floatability to separate it from Cu and Pb-minerals and preventing lead polluting the surrounding environment of tailings dam. In this study, a promising process of mineral processing for complex sulfide ores was investigated by combining extraction, flotation, and cementation for sustainable development of complex sulfide deposits in harmony with environment.

In Chapter 1, background and objectives of this study and a literature review on depression of sphalerite floatability in flotation of complex sulfide ores were described.

In Chapter 2, a process of mineral processing for complex sulfide ores combined with extraction, flotation, and cementation using ethylene diamine tetra acetic acid (EDTA) was investigated. The results of extraction tests showed that EDTA extracted 99.8% of anglesite in sphalerite-anglesite mixture and the results of cementation tests using zero-valent iron (ZVI) showed that 99.7% of extracted lead ion was recovered from the leachate after extraction with EDTA (EDTA pretreatment). The flotation results of the residue after EDTA pretreatment showed that the floatability of ZnS was depressed from 82% to 30% by applying EDTA pretreatment. The results of thermodynamics calculations for lead activation reaction and surface analysis using XPS for sphalerite with and without EDTA pretreatment indicated that lead activation of sphalerite was limited due to the decrease of lead ion concentration, resulting in depression of sphalerite floatability.

In Chapter 3, alternative extractants of anglesite to EDTA were investigated using ammonium acetate and sodium chloride. The results of extraction tests showed that ammonium acetate extracted almost of all anglesite when S/L ratio was ≤0.5 g/10 mL. The results of cementation tests using ZVI showed that almost of all extracted lead ion was recovered from the leachate after extraction with ammonium acetate. While extraction of anglesite using sodium chloride-hydrochloric acid was

limited due the solubility of lead-chloride species, almost of all anglesite was extracted and recovered when the coupled extraction and cementation (CEC) method using ZVI was applied. The flotation results of the residues after extraction using ammonium acetate or the non-magnetic fraction after CEC using sodium chloride-hydrochloric acid and ZVI showed that the floatability of sphalerite was depressed.

In Chapter 4, effects of pyrite on the separation of chalcopyrite and sphalerite were investigated to further depress the floatability of sphalerite in the cleaner stage of Cu flotation. While the floatability of sphalerite was depressed from >90% to <12% with zinc sulfate in the absence of pyrite, the floatability of sphalerite increased to >80%, indicating that pyrite inhibited the depressive effect of zinc sulfate toward sphalerite. The mechanism was proposed that pyrite inhibits the depressive effect of zinc sulfate toward sphalerite in the presence of chalcopyrite via promoting the release of copper ion due to galvanic interaction between chalcopyrite and sphalerite based on the results of contact angle measurements of sphalerite and pyrite with air bubble and flotation tests under anoxic conditions.

In Chapter 5, effects of pyrite on the floatability of lead-activated sphalerite were investigated to clarify whether the addition of activators such as copper sulfate is necessary to separate lead-activated sphalerite from pyrite in Zn flotation. The flotation results with and without pyrite showed that pyrite depressed the floatability of lead-activated sphalerite from 81.5% to 1.4%. Based on the results of contact angle measurements between PbS and air babble with and without electrical connection with pyrite and dissolution tests of PbS with and without pyrite combined with surface analysis, the mechanism that pyrite depressed the floatability of lead-activated sphalerite due to dissolution of PbS layer on sphalerite via galvanic interaction between pyrite and PbS was proposed.

And finally, Chapter 6 summarized important findings of this dissertation and proposed a possible application.

Table of Contents

List of Figures ..... **vii**

List of Tables ..... **x**

CHAPTER 1 – GENERAL INTRODUCTION **1**

1.1 Statement of the problem and objectives of this study 1

1.2 Literature review on complex sulfide ores containing anglesite and depression of sphalerite floatability 2

1.2.1 complex sulfide ores 2

1.2.2 Cu/Zn separation and Pb/Zn separation in flotation of complex sulfide ores 4

1.2.3 Depression of sphalerite 6

1.3 Outline of the dissertation 7

References 8

CHAPTER 2 – EFFECT OF ANGLESITE ON SPHALERITE FLOATABILITY, ENHANCED DEPRESSION OF SPHALERITE BY EXTRACTING ANGLESITE USING EDTA, AND RECOVERY OF EXTRACTED Pb^{2+} AS ZERO-VALENT Pb BY CEMENTATION USING ZERO-VALENT Fe **16**

2.1 Introduction 16

2.2 Materials and methods 17

2.2.1 Materials 17

2.2.2 Experimental methods 18

2.2.2.1 Extraction experiments of lead minerals using EDTA 18

2.2.2.2 Cementation experiments of the extracted Pb^{2+} 19

2.2.2.3 Flotation experiments 19

2.3 Results and discussion 20

2.3.1 Effects of $PbSO_4$ on ZnS floatability 20

2.3.2 Extraction of $PbSO_4$ using EDTA 21

2.3.3 Recovery of extracted Pb^{2+} as zero-valent Pb by cementation using zero-valent Fe 22

2.3.4 Effects of EDTA pretreatment on ZnS depression in flotation..... 25

2.3.5 Implication of this study 28

2.4 Conclusions 29

References 30

CHAPTER 3 – ALTERNATIVE EXTRACTANTS OF ANGLESITE TO EDTA USING AMMONIUM ACETATE AND SODIUM CHLORIDE-HYDROCHLORIC ACID 37

3.1 Introduction 37

3.2 Materials and methods..... 38

3.2.1 Materials..... 38

3.2.2 Experimental methods 39

3.2.2.1 Extraction of anglesite..... 39

3.2.2.2 Cementation experiments of extracted Pb^{2+} 39

3.2.2.3 Coupled extraction-cementation experiments 40

3.2.2.4 Flotation experiments..... 40

3.3 Results and discussion..... 42

3.3.1 Extraction of $PbSO_4$ *using EDTA,* CH_3COONH_4*, or NaCl-HCl* 42

3.3.2 Extraction of $PbSO_4$ *using* CH_3COONH_4 *and recovery of extracted* Pb^{2+} *as zero-valent Pb by cementation using zero-valent Fe* 45

3.3.4 Coupled Extraction-Cementation of $PbSO_4$ *using NaCl-HCl and zero-valent Fe* 46

3.3.4 Effects of pretreatments on ZnS depression in flotation..... 48

3.3.5 Implication of this study 50

3.4 Conclusions 50

References 51

CHAPTER 4 – EFFECTS OF PYRITE ON Cu/Zn SEPARATION AND AN EFFICIENT METHOD TO ENHANCE SPHALERITE DEPRESSION..... 56

4.1 Introduction 56

4.2 Materials and methods 57

4.2.1 Materials 57

4.2.2 Experimental methods 58

4.2.2.1 Flotation 58

4.2.2.2 Contact Angle Measurements 59

4.3 Results and discussion 60

4.3.1 Single Mineral Flotation of Chalcopyrite or Sphalerite 60

4.3.2 Effects of Chalcopyrite on the Floatability of Sphalerite 61

4.3.3 Effects of Pyrite on Sphalerite Floatability in the Presence of Chalcopyrite 64

4.3.4. Mechanisms of Losing the Depressive Effect of Zinc Sulfate Toward Sphalerite in the Presence of Both Pyrite and Chalcopyrite 65

4.3.4.1 Effects of Pyrite on the Hydrophilicity of Sphalerite 65

4.3.4.2 Effects of the Galvanic Interaction between Chalcopyrite and Pyrite on the Floatability of Sphalerite 66

4.3.5 A Proposed Method to Efficiently Depress Sphalerite in Flotation of Cu Ores with a High Cu/Zn Ratio 68

4.4 Conclusions 69

References 69

CHAPTER 5 – DEPRESSION OF LEAD-ACTVATED SPHALERITE BY PYRITE VIA GALVANIC INTERACTIONS 75

5.1 Introduction 75

5.2 Materials and methods 77

5.2.1 Materials 77

5.2.2 Flotation 78

5.2.2.1 Single mineral flotation tests 79

5.2.2.2 Mixed sphalerite-pyrite flotation tests 79

5.2.2.3 Single mineral flotation in the presence of Fe^{2+} or SO_4^{2-} 79

5.2.3 Contact angle measurements 79

5.2.4 Dissolution tests of galena 80

5.3 Results and discussion 81

5.3.1 Flotation experiments 81

5.3.1.1 Effects of pyrite on the floatability of lead-activated sphalerite 81

5.3.1.2 Lead-activated sphalerite flotation with dissolved Fe and S 82

5.3.1.3 Lead-activated sphalerite flotation with pyrite 83

5.3.2 Effects of pyrite on the dissolution of PbS formed on sphalerite 86

5.3.2.1 Contact angle measurements of xanthate-treated galena with and without electrical connection with pyrite 86

5.3.3 Dissolution tests of galena with and without pyrite 87

5.3.4 Proposed mechanism of depression of lead-activated sphalerite floatability by pyrite 90

5.4 Conclusions 91

References 92

CHAPTER 6 – GENERAL CONCLUSION..... 98

ACKNOLEDGEMENT 104

List of Figures

Figure 1-1. Global distribution of seafloor hydrothermal systems and related mineral deposits. Version 2.0 of the InterRidge Global Database (Beaulieu (2010) (Beaulieu, 2010)) used in this study contains information on 554 sites of seafloor hydrothermal activity (confirmed and unconfirmed) and inactive deposits. About 300 are sites of high-temperature hydrothermal venting; 165 are confirmed sites of massive sulfide accumulation. Credits: S. Beaulieu, K. Joyce, and S.A. Soule (Woods Hole Oceanographic Institution). (Edited from Hannington et al., (2011)) 3

Figure 2-1. XRD pattern of a mineral specimen of ZnS. 18

Figure 2-2. Flotation results of ZnS with SiO_2 or $PbSO_4$. 21

Figure 2-3. (a) Extraction efficiency of $PbSO_4$ after 24 h with different concentrations of EDTA (100, 200, or 500 mM) and (b) effect of time on $PbSO_4$ extraction with 500 mM EDTA. Note that the dotted line in Figure 2-3a corresponds to the ratio of EDTA/$[Pb]_{tot}$. 22

Figure 2-4. Extraction efficiency of lead minerals with 500 mM EDTA after 24 h. 22

Figure 2-5. (a) Effects of the ZVI amount on the recovery of the extracted Pb after 24 h in the leachate after $PbSO_4$ extraction using 500 mM of EDTA for 30 min and (b) effects of time on the recovery of the extracted Pb^{2+} using 1 g/10 mL of ZVI in the leachate after EDTA pretreatment using 500 mM EDTA for 30 min. 23

Figure 2-6. SEM photomicrograph of the residue of the cementation experiment using 1 g/10 mL of ZVI for 24 h with the corresponding elemental maps of Fe, Pb, and O. 24

Figure 2-7. XRD pattern of the residue of the cementation experiment using 1 g/10 mL of ZVI for 24 h. 25

Figure 2-8. Effects of EDTA pretreatment on the floatability of ZnS in the presence of $PbSO_4$. 26

Figure 2-9. XPS Pb4f7/2 spectra of (a) raw ZnS, (b) ZnS/$PbSO_4$ with EDTA pretreatment, and (c) ZnS/$PbSO_4$ without EDTA pretreatment. 27

Figure 2-10. Proposed enhanced depression of sphalerite (ZnS) by extracting anglesite ($PbSO_4$) using ethylene diamine tetra acetic acid (EDTA) and recovery of the extracted Pb^{2+} as zero-valent Pb (Pb^0) by cementation using zero-valent Fe (ZVI). 29

Figure 3-1. The extraction efficiency of Pb after 24 h with EDTA 0.5 M (circle), CH_3COONH_4 6.5 M (cross), and NaCl 5.0 M acidified with HCl 0.1 M (triangle). 43

Figure 3-2. The extraction efficiency of Pb^{2+} and SO_4^{2-} after 24 h with NaCl 5.0 M acidified with HCl 0.1 M. 43

Figure 3-3. SEM photomicrograph of the residue after extraction with NaCl 5 M acidified with HCl 0.1 M 24 h at S/L ratio = 1.0 g/10 mL 44

Figure 3-4. A diagram of log $a\mathrm{Pb}2+$ vs log $a\mathrm{Cl}-$ at pH 0.64 and 25°C created using the Geochemist's Workbench® with the MINTEQ database (Gustaffson, 2013). 44

Figure 3-5. The extraction efficiency of Pb (a) after 24 h with different concentrations of CH_3COONH_4 (0−6.5 M), (b) after .0−60 min with CH_3COONH_4 3.5 M. 45
Figure 3-6. The Pb recovery in the leachate after $PbSO_4$ extraction using CH_3COONH_4 3.5 M for 30 min (a) after 24 h with different amount of ZVI (0.1−0.5 g/10 mL), (b) after 0−2 h with ZVI 0.5 g/10 mL 46
Figure 3-7. SEM photomicrograph of the residue of the cementation experiment using 0.5 g/10 mL of ZVI for 24 h with the corresponding elemental maps of Fe, Pb, and O. 46
Figure 3-8. Effects of NaCl concentration and time on distribution of Pb in ZVI, residues, and solution: (a) NaCl 0.5−5.0 M for 24 h and (b) NaCl 5.0 M for 0−1 h. 47
Figure 3-9. SEM photomicrograph and EDS spectrum of the residue of the CEC experiment using NaCl 5.0 M for 24 h with the corresponding elemental maps of Fe, Pb, and O. 48
Figure 3-10. Effects of pretreatments using CH_3COONH_4 or NaCl on the floatability of ZnS in the presence of $PbSO_4$: (a) W/o pretreatments, (b) w/ a pretreatment using CH_3COONH_4, and (c) w/ a pretreatment using NaCl-HCl. 49
Figure 4-1. XRD patterns of mineral samples: (a) chalcopyrite ($CuFeS_2$), (b) sphalerite (ZnS), and (c) pyrite (FeS_2). Note differences in the scales of the y-axes. 58
Figure 4-2. Flotation procedure with sequential addition of the collector (PIPX). 59
Figure 4-3. Results of single mineral flotation of (a) chalcopyrite or (b) sphalerite. 61
Figure 4-4. Flotation results of sphalerite in the absence of Zn depressants (a) without chalcopyrite and (b) with chalcopyrite. Note that the data at 100 g/t of collector in Figure 4-4b were absent due to the lack of froth amounts for the XRF. 62
Figure 4-5. SEM photomicrograph of sphalerite after conditioning with chalcopyrite in the flotation cell with the corresponding elemental maps of Zn, S, Cu, Fe, and O. 62
Figure 4-6. A schematic diagram of copper activation of sphalerite in the presence of chalcopyrite. 63
Figure 4-7. Flotation results of sphalerite and chalcopyrite with zinc sulfate (a) 0 kg/t and (b) 1 kg/t. Note that the data at 100 g/t of collector in Figure 4-7a and those at 100 and 200 g/t of collector in Figure 4-7b were absent due to the lack of froth amounts for the XRF. 63
Figure 4-8. Flotation results of sphalerite and chalcopyrite (a) in the absence of pyrite and with zinc sulfate 1 kg/t, (b) in the presence of pyrite and zinc sulfate 1kg/t, and (c) in the presence of pyrite and zinc sulfate 10 kg/t. Note that the data at 100 and 200 g/t of collector in Figure 4-8a and those at 200 g/t of collector in Figure 4-8c were absent due to the lack of froth amounts for the XRF. 64
Figure 4-9. A schematic diagram of two possible mechanisms for why pyrite inhibits the depression of sphalerite with zinc sulfate in the presence of chalcopyrite: (i) the reduced amount of zinc precipitates adsorbed onto the surface of sphalerite due to the presence of pyrite whose surface

also attracts zinc precipitates, (ii) galvanic interaction between chalcopyrite and pyrite that promotes the anodic half-cell reaction of chalcopyrite, releasing more Cu^{2+} into the aqueous solution. 65
Figure 4-10. The contact angle of sphalerite in the absence and presence of pyrite. 66
Figure 4-11. Flotation results of chalcopyrite, sphalerite, and pyrite in the presence of 1 kg/t zinc sulfate (a) with air and (b) with N_2 gas 67
Figure 4-12. A schematic diagram of the proposed efficient method to depress sphalerite in flotation of Cu ores containing sphalerite and pyrite with zinc sulfate. 68
Figure 5-1. A schematic diagram of galvanic interaction between pyrite and sulfides with lower rest potentials (MS) (e.g., chalcopyrite, galena, and sphalerite). 76
Figure 5-2. XRD patterns of mineral samples of (a) sphalerite (ZnS), (b) pyrite (FeS_2), (c) galena (PbS). Note differences in the scale of the y-axes. 78
Figure 5-3. A schematic diagram of the contact angle measurements with and without electrical connection. 80
Figure 5-4. Zn recovery in single mineral flotation of sphalerite with and without lead activation. 81
Figure 5-5. Zn recovery in mixed sphalerite-pyrite flotation. 82
Figure 5-6. Schematic diagrams of three possible mechanisms for the depression of lead-activated sphalerite floatability by pyrite 82
Figure 5-7. Zn recovery in single lead-activated sphalerite flotation in the absence and presence of (a) Fe^{2+} and (b) SO_4^{2-}. 83
Figure 5-8. Conditioning methods of sphalerite flotation with various orders of pyrite addition. 84
Figure 5-9. Zn recovery in mixed sphalerite-pyrite flotation by changing when pyrite was added. 85
Figure 5-10 Change of contact angle with and without electrical connection as a function of time. 87
Figure 5-11. Dissolved Pb (blue) and S (red) concentration after the dissolution tests of galena with and without pyrite 88
Figure 5-12. XPS spectra of Pb $4f_{(7/2)}$ of residues after dissolution tests: (a) galena only, and (b) galena with pyrite. 89
Figure 5-13. A diagram of log $\boldsymbol{a}\mathbf{Pb2+}$ vs log $\boldsymbol{a}\mathbf{SO42-}$ at pH 7 and 25°C created using the Geochemist's Workbench® with the MINTEQ database (Gustaffson, 2013). 90
Figure 5-14. A schematic diagram of the proposed depression mechanism of lead-activated sphalerite floatability by pyrite 91
Figure 6-1. The proposed flowsheet of selective flotation of complex sulfide ores based on pretreatments to extract $PbSO_4$ in complex sulfide ores. 102
Figure 6-2. The detailed flowsheet of pretreatments to extract $PbSO_4$ using EDTA and CH_3COONH_4 combined with cementation using ZVI, and to extract and recover $PbSO_4$ using a CEC method using NaCl-HCl and ZVI. 103

List of Tables

Table 2-1. Chemical composition of a mineral specimen of ZnS based on XRF. 18
Table 2-2. Calculation results of the change in free energy with and without EDTA pretreatment. .26
Table 2-3. XPS peak parameters for Pb4$f_{7/2}$ spectra and relative abundances of Pb species. 28
Table 3-1. Calculation results of the change in free energy without pretreatments or with CH_3COONH_4 or NaCl-HCl pretreatment.....50
Table 4-1. The chemical composition of mineral samples based on XRF.....57
Table 5-1. Chemical composition of mineral samples based on XRF.....78
Table 5-2. XPS peak parameters for Pb $4f_{(7/2)}$ spectra and the relative abundances of Pb species....89

CHAPTER 1 – GENERAL INTRODUCTION

1.1 Statement of the problem and objectives of this study

In 2015, 193 governments adopted 17 sustainable development goals (SDGs) aiming to eradicate poverty, protect the planet, and ensure peaceful and prosperous lives for everyone by 2030 (Hák et al., 2016; Park et al., 2021b; Tabelin et al., 2021). Number 13 of the SDGs—"Climate Action"—envisions drastic carbon dioxide (CO_2) emission reductions to combat climate change and achieve a carbon-neutral society by 2050 (Goal 13 | Department of Economic and Social Affairs). Copper (Cu), lead (Pb), and zinc (Zn) are classified as critical metals defined by the World Bank as essential in renewable energy and clean storage technologies (e.g., wind turbines, solar photovoltaic (PV) panels, batteries, etc.), and thus their demands are projected to significantly increase in the future to achieve a carbon-neutral society (Nansai et al., 2014; WBG, 2020). To keep up with the high demand for critical metals like Cu, Pb, and Zn, the development of new metal resources is an important issue for the future.

Complex sulfide ores, some of the most important sources of critical metals, are typically composed of several metal sulfide minerals like chalcopyrite, galena and sphalerite. Complex sulfides consisting of copper (Cu), lead (Pb), and zinc (Zn)-sulfide minerals are typically processed via flotation—a separation technique based on the differences in wettability of minerals—to produce concentrates of each mineral. In the general flotation circuit of Cu-Pb-Zn sulfide ores, Cu and Pb sulfides are first recovered as froth, and then Zn sulfides are separated from gangue minerals with the assistance of activators (e.g., $CuSO_4$) (Wills and Finch, 2016; Woodcock et al., 2007).

Terrestrial deposits being developed are large-scale, and their mineralogical compositions are typically uniform. Because of this, concentrates that meet the requirements of smelters can be produced stably, so the modification of the operating conditions is not often required once optimized. Meanwhile, large-scale deposits are getting depleted, and the remaining deposits are small-scale, complex, and heterogeneous, which make the conventional mineral processing inapplicable. Therefore, the development of future-oriented mineral processing is necessary; in particular, (i) monitoring (to check ore characteristics), (ii) simulation (to optimize flotation process/conditions based on ore characteristics), and (iii) automatic control (to operate with optimized flotation process).

In the case of the ores where there are no interactions between mineral-mineral and mineral-dissolved ion, it is easy to develop simulation models for optimization of flotation process/conditions based on ore characteristics. In flotation of salt-type minerals, dissolved ions are known to strongly affect the floatability of co-existing minerals due to their higher solubilities compared to other minerals such as oxide and sulfide minerals (Tsunekawa et al., 1990). While the solubilities of

sulfide minerals are much lower than salt-type minerals, metal ions can be dissolved by electrochemical interactions between minerals because some sulfide minerals are semi-conductive. In addition, dissolved ions from soluble minerals can affect the floatability of sulfide minerals. Therefore, interactions between mineral-mineral and mineral-dissolved ion should be considered to develop simulation models for optimization of flotation process/conditions based on ore characteristics.

In this study, seafloor massive sulfide (SMS) deposit was chosen as a representative of the future deposits. Some complex sulfides (e.g., seafloor massive sulfides obtained from around Japan, one of the promising sources of critical metals in the future) contain not only galena but also anglesite, which is not typically contained in conventional ores. The presence of anglesite is problematic for the separation of Cu, Pb and Zn-sulfide minerals by flotation due to the unwanted activation of Zn sulfides by lead ions released from anglesite. Anglesite is regarded as a gangue mineral because it is less valuable than galena for Pb smelting, thus, the flotation circuit is typically composed of three stages—(i) Cu-Pb bulk flotation, (ii) Cu flotation from Cu-Pb bulk concentrate, and (iii) Zn flotation from Cu-Pb bulk tailing. However, the presence of anglesite causes problems in (i) Cu-Pb bulk flotation due to interactions between mineral-dissolved ion, (ii) Cu flotation due to interactions between mineral-mineral/dissolved ion, and (iii) Zn flotation due to interactions between mineral-mineral.

In addition, when anglesite is disposed of into tailings dam after recovering Cu, Pb, and Zn-sulfide minerals, Pb would be leached out and contaminates the surrounding environment of tailings dam. To address these problems, a sufficient method needs to be developed for depressing sphalerite floatability to separate it from Cu and Pb-minerals and preventing lead pollution to the surrounding environment of tailings dam. In this study, a promising process of mineral processing for complex sulfide ores was investigated by combining extraction, flotation, and cementation for sustainable development of complex sulfide deposits in harmony with environment.

1.2 Literature review on complex sulfide ores containing anglesite and depression of sphalerite floatability

1.2.1 complex sulfide ores

One of the most widespread and promising deposits that contain many critical metals like copper (Cu), Pb (lead), and zinc (Zn), is loosely classified as ‘complex sulfides’ (Herzig and Hannington, 1995a; Ikumapayi and Rao, 2015; Marston et al., 1981; Martin et al., 1989). Complex sulfide ores are typically composed of several metal sulfide minerals such as chalcopyrite ($CuFeS_2$), galena

(PbS), and sphalerite (ZnS). Some complex sulfide ores (e.g., seafloor massive sulfide ores) contain not only PbS but also anglesite ($PbSO_4$). Seafloor massive sulfide (SMS) deposits have gained increasing attention as one of new metal resources because they consist of polymetallic sulfide including Cu, Pb, Zn, Au, Ag, etc. A number of scholars have studied SMS deposits, examples of which include formation mechanisms (Halbach et al., 1993; Janecky and Seyfried, 1984; Leybourne et al., 2012), exploration (German et al., 2016; Hannington et al., 2011; Monecke et al., 2014), mining methods (Asakawa et al., 2014; Fallon et al., 2018; Fuchida et al., 2018; Zha et al., 2020), and environmental impacts (Collins et al., 2013; Narita et al., 2015; Van Dover, 2014); however, only few studies on mineral processing of SMS ores have been carried out (Ministry of Economic and Japan Oil, 2018; Oki et al., 2015). SMS deposits have been found in a variety of volcanic and tectonic settings on the modern ocean floor at water depths ranging from about 3700 to 1500 m (Herzig and Hannington, 1995b), and almost all have been found at the plate boundaries including oceanic spreading centers, submarine volcanic arcs, and backarc basins, where there is a strong spatial and temporal correlation between magmatism, seismicity, and high-temperature hydrothermal venting (Figure 1-1) (Hannington et al., 2011).

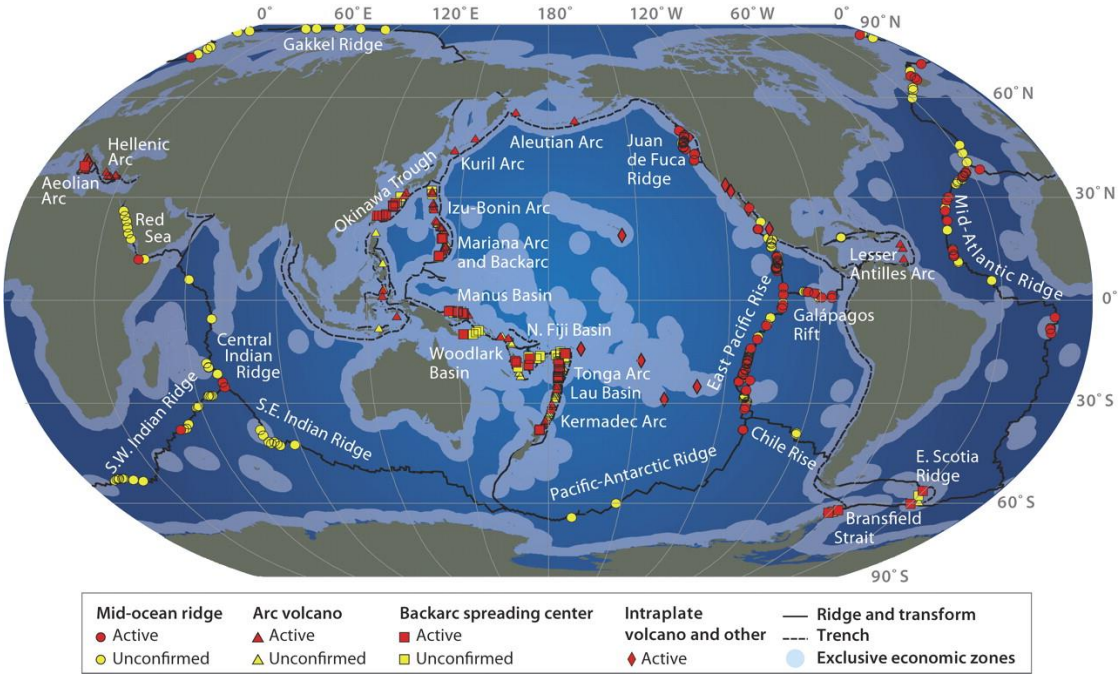

Figure 1-1. Global distribution of seafloor hydrothermal systems and related mineral deposits. Version 2.0 of the InterRidge Global Database (Beaulieu (2010) (Beaulieu, 2010)) used in this study contains information on 554 sites of seafloor hydrothermal activity (confirmed and unconfirmed) and inactive deposits. About 300 are sites of high-temperature hydrothermal venting; 165 are confirmed sites of massive sulfide accumulation. Credits: S. Beaulieu, K. Joyce, and S.A. Soule (Woods Hole Oceanographic Institution). (Edited from Hannington et al., (2011))

SMS deposits form through hydrothermal activity; cold seawater percolates down through the seafloor, is heated through geothermal energy, becomes buoyant and rises, dissolving metals and sulfides from the surrounding rocks. These hydrothermal systems can be low intensity (typically <200°C), which are generally thought unimportant in the formation of SMS deposits, or high-intensity (typically 200–400°C), which although located at fewer more discreet sites, tend to concentrate mineral deposits (Rona, 1985). Typically, SMS ores are enriched with base metals (iron, zinc, copper and lead), sulfides and numerous other elements, including gold, silver, arsenic, cobalt, molybdenum and platinum (Krasnov et al., 1995). The exact mineral composition of deposits varies according to hydrothermal activity, tectonic setting and the section of the deposit sampled. For example, Okinawa Trough is comparably rich in iron, zinc, and copper (Halbach et al., 1989).

In Japan, the program for the development of SMS deposits around Japan has been conducted by the Ministry of Economic, Trade and Industry (METI) and Japan Oil, Gas and Metals National Corporation (JOGMEC). Not only seafloor mining, but also mineral processing and extractive metallurgy of SMS ores have been studied. Masuda, (2011) reported that SMS resembles the Kuroko on land in terms of deposit origin, which implies that similar processing and refining technologies applied to Kuroko can also be utilized for SMS ores. However, the previous studies on mineral processing of SMS ores conducted by JOGMEC indicated that mineral processing behaviors of the SMS ores are quite different compared to those of Kuroko (Oki et al., 2015). METI and JOGMEC (2018) reported distinct features of SMS ores obtained from around Japan: (1) lead minerals in the SMS ores are mostly present as anglesite ($PbSO_4$) with a minor amount of galena (PbS), and (2) metal ions are highly dissolved from the SMS ores (e.g., [Zn^{2+}], 1700–3000 ppm). Moreover, some researchers reported various metal ions like Cu^{2+}, Pb^{2+}, and Zn^{2+} are released from the SMS ores obtained from the Trans-Atlantic Geotraverse active mound on the Mid-Atlantic Ridge (Fallon et al., 2018) and the Izena Hole in the middle Okinawa Trough, Japan (Fuchida et al., 2018). These distinct features of SMS ores around Japan—the presence of anglesite and the release of metal ions—would make mineral processing of SMS ores composed of Cu-Pb-Zn sulfide minerals complicated. Therefore, in flotation of SMS ores, the effects of dissolved ions should be investigated for the development of SMS deposits.

1.2.2 Cu/Zn separation and Pb/Zn separation in flotation of complex sulfide ores

Typical complex sulfide ores contain sphalerite (ZnS), chalcopyrite ($CuFeS_2$), galena (PbS), pyrite (FeS_2), and barite ($BaSO_4$). In selective flotation of complex sulfide ores, $CuFeS_2$ and PbS are floated first. After that ZnS is recovered by surface modification using an ‘activator’ such as copper

sulfate ($CuSO_4$) to form CuS-like surface compounds as illustrated in Equation (1-1) (Wills and Finch, 2016).

$$ZnS(s) + Cu^{2+} = CuS(s) + Zn^{2+} \quad (1\text{-}1)$$

These CuS-like surface compounds have higher affinities for short-chained thiol collectors like xanthate than ZnS (the solubility product (K_{sp}) of Cu^{2+} and Zn^{2+} are $10^{-24.2}$ and $10^{-8.2}$, respectively (Du Reitz, 1975)), so the surface modification of sphalerite using $CuSO_4$ enhances collector adsorption on and floatability of the mineral (Chandra and Gerson, 2009; Leppinen, 1990; Wills and Finch, 2016). The surface modifications of sulfide minerals using metal ions have been studied in great detail for many years and are typically composed of two steps (Finkelstein, 1997; Fornasiero and Ralston, 2006; Gerson et al., 1999): (1) activation to form surface compounds with strong affinities to xanthate (e.g., CuS-like and PbS-like compounds), and (2) xanthate adsorption on the surface of activated sphalerite.

Some complex sulfide ores contain not only PbS but also anglesite ($PbSO_4$), the presence of which is problematic for the separation of Cu, Pb, and Zn by flotation due to the unwanted activation of ZnS by Pb^{2+} released from $PbSO_4$ (Ministry of Economic and Japan Oil, 2018; Zeng et al., 2021). When $PbSO_4$ is contained in complex sulfide ores, however, Pb^{2+} is readily released from $PbSO_4$ during conditioning and/or flotation due to its higher solubility compared to PbS—K_{sp} of $PbSO_4$ and PbS is $10^{-7.79}$ and $10^{-26.77}$, respectively (Ball and Nordstrom, 1991)—and activates the surface of ZnS via the formation of PbS-like compounds, as illustrated in Equation (1-2) (Laskowski et al., 1997; Rashchi et al., 2002a);

$$ZnS(s) + Pb^{2+} = PbS(s) + Zn^{2+} \quad (1\text{-}2)$$

The activation of ZnS by Pb^{2+} increases the ZnS floatability because of a higher affinity of PbS-like compounds for xanthate compared to ZnS (Houot and Raveneau, 1992; Trahar et al., 1997). As a result, when the unwanted activation of ZnS occurs, ZnS is recovered as froth together with $CuFeS_2$ and PbS, making their separation difficult . Therefore, a proper way of depressing ZnS floatability during flotation of complex sulfide ores containing $PbSO_4$ should be established.

Not only in the processing of complex sulfide ores but also in the selective flotation to separate Cu/Zn and Pb/Zn (i.e., $CuFeS_2$/ZnS and PbS/ZnS), unwanted activation of ZnS by metal ions such as Cu^{2+} and Pb^{2+} can occur, resulting in the difficulty in their separation. For example, oxidation and/or weathering of $CuFeS_2$ and PbS during storage and grinding causes the release of Cu^{2+} and Pb^{2+} from metal oxides, (Azizi et al., 2013; Huang and Grano, 2005; Lascelles and Finch, 2002; Palm et al., 2010; Rabieh et al., 2018; Seng et al., 2019b; Wei et al., 2021). Thus, a suitable way to depress ZnS sphalerite floatability affected by unwanted activation during flotation of complex sulfide ores should be established even in the absence of $PbSO_4$.

Cu/Zn separation is an important issue in flotation of Cu ores from porphyry copper deposits (PCDs) as well as complex sulfide ores composed of Cu, Pb, and Zn -sulfide minerals. To meet the

high forecasted demand for copper, mining industries are finding it necessary to mine ores at increasingly deeper positions since copper reserves are finite and easy-to-mine ore deposits are dwindling (Hornn et al., 2021; Park, 2022; Tabelin et al., 2021). In the case of PCDs, as mining areas become deeper laterally, it could be extended to the peripheral zone, where the amount of sphalerite (ZnS) increases compared to the ore zone (John et al., 2010). When processing copper ores containing sphalerite via flotation, the depression of sphalerite floatability is an important issue for producing saleable copper concentrates because the impurities in copper concentrates have a negative impact on copper smelting and penalties are imposed for their treatment in the smelting process (Haga et al., 2012, 2018; Tongamp et al., 2009). In general, Cu-Zn sulfide ores consisting of a Cu/Zn ratio of 0.4–1:1 (*w*/*w*) (Bıçak et al., 2012; Kant et al., 1994; Natarajan et al., 1997; Sinche-Gonzalez and Fornasiero, 2021; Soltani et al., 2014) are processed by a two-step flotation: (i) the selective flotation of Cu minerals while depressing sphalerite using zinc sulfate ($ZnSO_4$)—a sphalerite depressant—and other gangue minerals such as pyrite (FeS_2) and silicate minerals under alkaline conditions, and (ii) the recovery of sphalerite after its activation using copper sulfate ($CuSO_4$) (Woodcock et al., 2007). However, it is unclear whether the conventional approach for Cu-Zn and Cu-Zn-Pb ores (i.e., depression of sphalerite using zinc sulfate) is effective in Cu/Zn separation in the processing of the copper ores excavated from PCDs with a much lower level of Zn (e.g., a Cu/Zn ratio of 7:1 (*w*/*w*)) compared to Cu-Zn or Cu-Zn-Pb sulfide ores (Ito et al., 2020).

The difficulty in Cu/Zn separation may occur in Cu flotation of SMS ores as well as Cu ores when sphalerite could not be depressed in Cu/Zn flotation of SMS ores. Conventionally, Cu/Zn ratios in cleaner stage of Cu flotation of complex sulfide ores are very low, and thus saleable Cu concentrates are produced because the floatability of sphalerite is properly depressed in Cu-Pb/Zn flotation. As mentioned above, unwanted activation of sphalerite by Pb^{2+} released from anglesite would occur in Cu-Pb/Zn flotation of SMS ores, causing higher Cu/Zn ratios in cleaner stage of Cu flotation compared to that of complex sulfide ores.

1.2.3 Depression of sphalerite

In flotation of Cu-Pb-Zn sulfides, Cu- and Pb-sulfide minerals are first recovered, followed by floating Zn-sulfide minerals like sphalerite (Woodcock et al., 2007). However, in the presence of anglesite, it is readily dissolved and releases Pb^{2+} that activates sphalerite via the formation of PbS-like compounds on sphalerite surface. Activation of sphalerite by Pb^{2+} increases the sphalerite floatability because PbS-like compound has a higher affinity with xanthate than sphalerite (Houot and Raveneau, 1992; Laskowski et al., 1997; Rashchi et al., 2002b; Trahar et al., 1997). Thus, lead-sphalerite is recovered together with chalcopyrite and galena, and lead activation of sphalerite makes their separation difficult. To separate chalcopyrite and galena from lead-activated sphalerite, the

suppression of lead-activated sphalerite is necessary. Some researchers examined the depression of lead-activated sphalerite using the conventional depressant for "non-activated" sphalerite (e.g., zinc sulfate, sulfoxy reagents, etc.) or other reagents like sodium hydrogen phosphate.

El-Shall et al. (2000) evaluated the possibility of depression of lead-activated sphalerite in the presence of 1×10^{-4} mol/L of Pb^{2+} and 1×10^{-4} mol/L of Zn^{2+} at about pH 7.0 by calculating the change in free energy based on the equilibrium constant (Equations (1-2) and (1-3), where K = 1000). It was concluded that depression of lead-activated sphalerite by zinc sulfate is most probably due to the reverse reaction of Equation (1-2).

$$ZnS + Pb^{2+} = PbS + Zn^{2+} \quad (1\text{-}2)$$

$$\Delta G = -RT \ln K + \ln(Zn^{2+}/Pb^{2+}) \quad (1\text{-}3)$$

Basilio et al. (1996) also evaluated the possibility of lead activation of sphalerite in the presence of 1 ppm of Pb^{2+} and 400 ppm of Zn^{2+} at natural pH based on the change in free energy (Equation (1-2)) using equilibrium constants of Equation (1-2) calculated based on Equation (1-4) using K_{sp} values of ZnS and PbS in the literature. Because the possibility of lead activation of sphalerite is strongly affected by the calculated equilibrium constants of Equation (1-2) which were in the range of 32.3 and 3.3×10^{6}, it was suggested that it is difficult to conclude whether the thermodynamic calculation provides a definitive answer to the question concerning lead activation of sphalerite. However it was suggested that most of the calculated values of equilibrium constants support lead activation of sphalerite I the presence of 1 ppm of Pb^{2+} and 400 ppm of Zn^{2+}.

$$K = \frac{K_{sp}^{ZnS}}{K_{sp}^{PbS}} \quad (1\text{-}4)$$

Wang (2019) reported the depression effects of the combination of hydrogen phosphate and zinc sulfate on the floatability of lead-activated sphalerite at neutral pH 6.5. It was concluded that the addition of hydrogen phosphate results in oxidation of PbS formed on sphalerite by lead activation and zinc sulfate makes lead activation of sphalerite difficult in the consideration of thermodynamics.

1.3 Outline of the dissertation

The dissertation is comprised of five chapters and summaries of each chapter are outlined as follows:

In Chapter 1, background and objectives of this study and a literature review on depression of sphalerite floatability in flotation of complex sulfide ores were described.

In Chapter 2, a process of mineral processing for complex sulfide ores combined with extraction, flotation, and cementation using ethylene diamine tetra acetic acid (EDTA) was investigated. This chapter is edited from "Aikawa et al., 2022. Development of a sustainable process

for complex sulfide ores containing anglesite: Effect of anglesite on sphalerite floatability, enhanced depression of sphalerite by extracting anglesite, and recovery of extracted Pb^{2+} as zero-valent Pb by cementation using zero-valent Fe. Minerals 723, 12(6)."

In Chapter 3, alternative extractants of anglesite to EDTA were investigated using ammonium acetate and sodium chloride-hydrochloric acid.

In Chapter 4, effects of pyrite on the separation of chalcopyrite and sphalerite were investigated to further depress the floatability of sphalerite in the cleaner stage of Cu flotation. This chapter is edited from "Aikawa et al., 2022b. Flotation of copper ores with high Cu/Zn Ratio: Effects of Pyrite on Cu/Zn Separation and an Efficient Method to Enhance Sphalerite Depression. Minerals 1103, 12(9)."

In Chapter 5, effects of pyrite on the floatability of lead-activated sphalerite were investigated to clarify whether the addition of activators such as copper sulfate is necessary to separate lead-activated sphalerite from pyrite in Zn flotation. This chapter is edited from "Aikawa et al., 2020. Depression of lead-activated sphalerite by pyrite via galvanic interactions: Implications to the selective flotation of complex sulfide ores. Miner. Eng. 152, 106367."

And finally, Chapter 6 summarized important findings of this dissertation and proposed a possible application.

References

Asakawa, E., Murakami, F., Tsukahara, H., Mizohata, S., 2014. Development of vertical cable seismic (VCS) system for seafloor massive sulfide (SMS), in: 2014 Oceans - St. John's. IEEE, St. John's, NL, Canada, pp. 1–7. https://doi.org/10.1109/OCEANS.2014.7003171

Azizi, A., Shafaei, S.Z., Noaparast, M., Karamoozian, M., 2013. Galvanic interaction between chalcopyrite and pyrite with low alloy and high carbon chromium steel ball. J Chem 2013. https://doi.org/10.1155/2013/817218

Ball, J.W., Nordstrom, D.K., 1991. User's manual for WATEQ4F, with revised thermodynamic data base and text cases for calculating speciation of major, trace, and redox elements in natural waters, U.S. Geological Survey Water-Resources Investigations Report. Reston, VA, USA. https://doi.org/10.3133/ofr91183

Basilio, C.I., Kartio, I.J., Yoon, R.-H., 1996. Lead activation of sphalerite during galena flotation. Miner Eng 9, 869–879. https://doi.org/10.1016/0892-6875(96)00078-7

Beaulieu, S., 2010. InterRidge Global Database of Active Submarine Hydrothermal Vent Fields: prepared for InterRidge, Version 2.0. [WWW Document]. World Wide Web electronic publication. URL http://www.interridge.org/irvents/ (accessed 2.1.21).

Bıçak, Ö., Ekmekçi, Z., Can, M., Öztürk, Y., 2012. The effect of water chemistry on froth stability and surface chemistry of the flotation of a Cu–Zn sulfide ore. Int J Miner Process 102–103, 32–37. https://doi.org/10.1016/j.minpro.2011.09.005

Chandra, A.P., Gerson, A.R., 2009. A review of the fundamental studies of the copper activation mechanisms for selective flotation of the sulfide minerals, sphalerite and pyrite. Adv Colloid Interface Sci. https://doi.org/10.1016/j.cis.2008.09.001

Collins, P.C., Croot, P., Carlsson, J., Colaço, A., Grehan, A., Hyeong, K., Kennedy, R., Mohn, C., Smith, S., Yamamoto, H., Rowden, A., 2013. A primer for the Environmental Impact Assessment of mining at seafloor massive sulfide deposits. Mar Policy 42, 198–209. https://doi.org/10.1016/j.marpol.2013.01.020

El-Shall, H.E., Elgillani, D.A., Abdel-Khalek, N.A., 2000. Role of zinc sulfate in depression of lead-activated sphalerite. Int J Miner Process 58, 67–75. https://doi.org/10.1016/S0301-7516(99)00055-1

Fallon, E.K., Niehorster, E., Brooker, R.A., Scott, T.B., 2018. Experimental leaching of massive sulphide from TAG active hydrothermal mound and implications for seafloor mining. Mar Pollut Bull 126, 501–515. https://doi.org/10.1016/j.marpolbul.2017.10.079

Finkelstein, N.P., 1997. The activation of sulphide minerals for flotation: a review. Int J Miner Process 52, 81–120. https://doi.org/10.1016/S0301-7516(97)00067-7

Fornasiero, D., Ralston, J., 2006. Effect of surface oxide/hydroxide products on the collectorless flotation of copper-activated sphalerite. Int J Miner Process 78, 231–237. https://doi.org/10.1016/j.minpro.2005.10.006

Fuchida, S., Ishibashi, J., Shimada, K., Nozaki, T., Kumagai, H., Kawachi, M., Matsushita, Y., Koshikawa, H., 2018. Onboard experiment investigating metal leaching of fresh hydrothermal sulfide cores into seawater. Geochem Trans 19, 15. https://doi.org/10.1186/s12932-018-0060-9

German, C.R., Petersen, S., Hannington, M.D., 2016. Hydrothermal exploration of mid-ocean ridges: Where might the largest sulfide deposits be forming? Chem Geol 420, 114–126. https://doi.org/10.1016/j.chemgeo.2015.11.006

Gerson, A.R., Lange, A.G., Prince, K.E., Smart, R.St.C., 1999. The mechanism of copper activation of sphalerite. Appl Surf Sci 137, 207–223. https://doi.org/10.1016/S0169-4332(98)00499-1

Goal 13 | Department of Economic and Social Affairs [WWW Document], n.d. URL https://sdgs.un.org/goals/goal13 (accessed 4.26.22).

Haga, K., Altansukh, B., Shibayama, A., 2018. Volatilization of Arsenic and Antimony from Tennantite/Tetrahedrite Ore by a Roasting Process. Mater Trans 59, 1396–1403. https://doi.org/10.2320/matertrans.M2017400

Haga, K., Tongamp, W., Shibayama, A., 2012. Investigation of Flotation Parameters for Copper Recovery from Enargite and Chalcopyrite Mixed Ore. Mater Trans 53, 707–715. https://doi.org/10.2320/matertrans.M2011354

Hák, T., Janoušková, S., Moldan, B., 2016. Sustainable Development Goals: A need for relevant indicators. Ecol Indic 60, 565–573. https://doi.org/10.1016/j.ecolind.2015.08.003

Halbach, P., Nakamura, K., Wahsner, M., Lange, J., Sakai, H., Käselitz, L., Hansen, R.-D., Yamano, M., Post, J., Prause, B., Seifert, R., Michaelis, W., Teichmann, F., Kinoshita, M., Märten, A., Ishibashi, J., Czerwinski, S., Blum, N., 1989. Probable modern analogue of Kuroko-type massive sulphide deposits in the Okinawa Trough back-arc basin. Nature 338, 496–499. https://doi.org/10.1038/338496a0

Halbach, P., Pracejus, B., Maerten, A., 1993. Geology and mineralogy of massive sulfide ores from the central Okinawa Trough, Japan. Economic Geology 88, 2210–2225. https://doi.org/10.2113/gsecongeo.88.8.2210

Hannington, M., Jamieson, J., Monecke, T., Petersen, S., Beaulieu, S., 2011. The abundance of seafloor massive sulfide deposits. Geology 39, 1155–1158. https://doi.org/10.1130/G32468.1

Herzig, P.M., Hannington, M.D., 1995a. Polymetallic massive sulfides at the modern seafloor a review. Ore Geol Rev 10, 95–115. https://doi.org/10.1016/0169-1368(95)00009-7

Herzig, P.M., Hannington, M.D., 1995b. Polymetallic massive sulfides at the modern seafloor a review. Ore Geol Rev 10, 95–115. https://doi.org/10.1016/0169-1368(95)00009-7

Hornn, V., Park, I., Ito, M., Shimada, H., Suto, T., Tabelin, C.B., Jeon, S., Hiroyoshi, N., 2021. Agglomeration-flotation of finely ground chalcopyrite using surfactant-stabilized oil emulsions: Effects of co-existing minerals and ions. Miner Eng 171, 107076. https://doi.org/10.1016/J.MINENG.2021.107076

Houot, R., Raveneau, P., 1992. Activation of sphalerite flotation in the presence of lead ions. Int J Miner Process 35, 253–271. https://doi.org/10.1016/0301-7516(92)90037-W

Huang, G., Grano, S., 2005. Galvanic interaction of grinding media with pyrite and its effect on floatation. Miner Eng 18, 1152–1163. https://doi.org/10.1016/j.mineng.2005.06.005

Ikumapayi, F., Rao, K.H., 2015. Recycling process water in complex sulfide ore flotation: Effect of calcium and sulfate on sulfide minerals recovery. Mineral Processing and Extractive Metallurgy Review 36, 45–64. https://doi.org/10.1080/08827508.2013.868346

Ito, M., Orii, N., Aikawa, K., Jeon, S., Park, I., Hiroyoshi, N., Magwaneng, R., Kudo, K., Sunada, K., Takahashi, T., 2020. Effects of several depressants on the floatability of sphalerite in the flotation of copper-zinc sulfides, in: The Mining and Materials Processing Institute of Japan (MMIJ) Fall Meeting 2020. The Mining and Materials Processing Institute of Japan.

Janecky, D.R., Seyfried, W.E., 1984. Formation of massive sulfide deposits on oceanic ridge crests: Incremental reaction models for mixing between hydrothermal solutions and seawater. Geochim Cosmochim Acta 48, 2723–2738. https://doi.org/10.1016/0016-7037(84)90319-3

John, D.A., Ayuso, R.A., Barton, M.D., Blakely, R.J., Bodnar, R.J., Dilles, J.H., Gray, F., Graybeal, F.T., Mars, J.C., McPhee, D.K., Seal, R.R., Taylor, R.D., Vikre, P.G., 2010. Porphyry Copper Deposit Model, Chapter B of Mineral Deposit Models for Resource Assessment. Menlo Park, CA, USA.

Kant, C., Rao, S.R., Finch, J.A., 1994. Distribution of surface metal ions among the products of chalcopyrite flotation. Miner Eng 7, 905–916. https://doi.org/10.1016/0892-6875(94)90132-5

Krasnov, S.G., Cherkashev, G.A., Stepanova, T. V., Batuyev, B.N., Krotov, A.G., Malin, B. V., Maslov, M.N., Markov, V.F., Poroshina, I.M., Samovarov, M.S., Ashadze, A.M., Lazareva, L.I., Ermolayev, I.K., 1995. Detailed geological studies of hydrothermal fields in the North Atlantic. Geological Society, London, Special Publications 87, 43–64. https://doi.org/10.1144/GSL.SP.1995.087.01.05

Lascelles, D., Finch, J.A., 2002. Quantifying accidental activation. Part I. Cu ion production. Miner Eng 15, 567–571. https://doi.org/10.1016/S0892-6875(02)00081-X

Laskowski, J.S., Liu, Q., Zhan, Y., 1997. Sphalerite activation: Flotation and electrokinetic studies. Miner Eng 10, 787–802. https://doi.org/10.1016/S0892-6875(97)00057-5

Leppinen, J.O., 1990. FTIR and flotation investigation of the adsorption of ethyl xanthate on activated and non-activated sulfide minerals. Int J Miner Process 30, 245–263. https://doi.org/10.1016/0301-7516(90)90018-T

Leybourne, M.I., de Ronde, C.E.J., Wysoczanski, R.J., Walker, S.L., Timm, C., Gibson, H.L., Layton-Matthews, D., Baker, E.T., Clark, M.R., Tontini, F.C., Faure, K., Lupton, J.E., Fornari, D.J., Soule, S.A., Massoth, G.J., 2012. Geology, Hydrothermal Activity, and Sea-Floor Massive Sulfide Mineralization at the Rumble II West Mafic Caldera. Economic Geology 107, 1649–1668. https://doi.org/10.2113/econgeo.107.8.1649

Marston, R.J., Groves, D.I., Hudson, D.R., Ross, J.R., 1981. Nickel sulfide deposits in Western Australia: a review. Economic Geology 76, 1330–1363. https://doi.org/10.2113/gsecongeo.76.6.1330

Martin, C.J., Rao, S.R., Finch, J.A., Leroux, M., 1989. Complex sulphide ore processing with pyrite flotation by nitrogen. Int J Miner Process 26, 95–110. https://doi.org/10.1016/0301-7516(89)90045-8

Masuda, N., 2011. Challenges toward the sea-floor massive sulfide mining with more advanced technologies, in: 2011 IEEE Symposium on Underwater Technology and Workshop on Scientific Use of Submarine Cables and Related Technologies. IEEE, pp. 1–4. https://doi.org/10.1109/UT.2011.5774153

Ministry of Economic, T. and I. (METI), Japan Oil, G. and M.N.C. (JOGMEC), 2018. Summary report on comprehensive evaluations of development plan of seafloor massive sulfide deposits [WWW Document]. URL http://www.jogmec.go.jp/content/300359550.pdf (accessed 2.26.21).

Monecke, T., Petersen, S., Hannington, M.D., 2014. Constraints on Water Depth of Massive Sulfide Formation: Evidence from Modern Seafloor Hydrothermal Systems in Arc-Related Settings. Economic Geology 109, 2079–2101. https://doi.org/10.2113/econgeo.109.8.2079

Nansai, K., Nakajima, K., Kagawa, S., Kondo, Y., Suh, S., Shigetomi, Y., Oshita, Y., 2014. Global Flows of Critical Metals Necessary for Low-Carbon Technologies: The Case of Neodymium, Cobalt, and Platinum. Environ Sci Technol 48, 1391–1400. https://doi.org/10.1021/es4033452

Narita, T., Oshika, J., Toyohara, T., Okamoto, N., Shirayama, Y., 2015. The Environmental Impact Assessment for Mining Seafloor Massive Sulphides in Japan. Journal of MMIJ 131, 634–638. https://doi.org/10.2473/journalofmmij.131.634

Natarajan, R., Nirdosh, I., Muthuswami, S. v., 1997. Flotation of a Copper-Zinc Ore Using p-Nonylcupferron as Collector. Developments in Chemical Engineering and Mineral Processing 5, 183–193. https://doi.org/10.1002/apj.5500050302

Oki, T., Nishisu, Y., Hoshino, M., 2015. Characteristics of The Existing Mineral Phases of Japanese Submarine Hydrothermal Polymetallic Sulfides and Their Influence on Respective Mineral Processing Properties. Journal of MMIJ 131, 619–626. https://doi.org/10.2473/journalofmmij.131.619

Palm, N.A., Shackleton, N.J., Malysiak, V., O'Connor, C.T., 2010. The effect of using different comminution procedures on the flotation of sphalerite. Miner Eng 23, 1053–1057. https://doi.org/10.1016/j.mineng.2010.08.001

Park, I., 2022. Advances in Selective Flotation and Leaching Process in Metallurgy. Metals (Basel) 12, 144. https://doi.org/10.3390/met12010144

Park, I., Kanazawa, Y., Sato, N., Galtchandmani, P., Jha, M.K., Tabelin, C.B., Jeon, S., Ito, M., Hiroyoshi, N., 2021. Beneficiation of Low-Grade Rare Earth Ore from Khalzan Buregtei Deposit (Mongolia) by Magnetic Separation. Minerals 11, 1432. https://doi.org/10.3390/min11121432

Rabieh, A., Eksteen, J.J., Albijanic, B., 2018. Galvanic interaction of grinding media with arsenopyrite and pyrite and its effect on gold cyanide leaching. Miner Eng 116, 46–55. https://doi.org/10.1016/j.mineng.2017.10.018

Rashchi, F., Sui, C., Finch, J.A., 2002a. Sphalerite activation and surface Pb ion concentration. Int J Miner Process 67, 43–58. https://doi.org/10.1016/S0301-7516(02)00005-4

Rashchi, F., Sui, C., Finch, J.A., 2002b. Sphalerite activation and surface Pb ion concentration. Int J Miner Process 67, 43–58. https://doi.org/10.1016/S0301-7516(02)00005-4

Rona, P.A., 1985. Hydrothermal mineralization at slow-spreading center: Red Sea, Atlantic Ocean, and Indian Ocean. Deep Sea Research Part B. Oceanographic Literature Review 32, 1023. https://doi.org/10.1016/0198-0254(85)93839-7

Seng, S., Tabelin, C.B., Makino, Y., Chea, M., Phengsaart, T., Park, I., Hiroyoshi, N., Ito, M., 2019. Improvement of flotation and suppression of pyrite oxidation using phosphate-enhanced galvanic microencapsulation (GME) in a ball mill with steel ball media. Miner Eng 143, 105931. https://doi.org/10.1016/j.mineng.2019.105931

Sinche-Gonzalez, M., Fornasiero, D., 2021. Understanding the effect of sulphate in mining-process water on sulphide flotation. Miner Eng 165, 106865. https://doi.org/10.1016/j.mineng.2021.106865

Soltani, F., Koleini, S.M.J., Abdollahy, M., 2014. Optimization of Cu–Zn Massive Sulphide Flotation by Selective Reagents. Journal of The Institution of Engineers (India): Series D 95, 125–134. https://doi.org/10.1007/s40033-014-0043-7

Tabelin, C.B., Park, I., Phengsaart, T., Jeon, S., Villacorte-Tabelin, M., Alonzo, D., Yoo, K., Ito, M., Hiroyoshi, N., 2021. Copper and critical metals production from porphyry ores and E-wastes: A review of resource availability, processing/recycling challenges, socio-environmental aspects, and sustainability issues. Resour Conserv Recycl 170, 105610. https://doi.org/10.1016/J.RESCONREC.2021.105610

Tongamp, W., Takasaki, Y., Shibayama, A., 2009. Arsenic removal from copper ores and concentrates through alkaline leaching in NaHS media. Hydrometallurgy 98, 213–218. https://doi.org/10.1016/j.hydromet.2009.04.020

Trahar, W.J., Senior, G.D., Heyes, G.W., Creed, M.D., 1997. The activation of sphalerite by lead — a flotation perspective. Int J Miner Process 49, 121–148. https://doi.org/10.1016/S0301-7516(96)00041-5

Tsunekawa, M., Ogata, E., Habata, N., Takamori, T., Hirajima, T., 1990. Solution chemistry and interfacial phenomena in an aqueous system containing plural salt-type minerals. Coexistence of fluorite and calcite. Journal of the Society of Powder Technology, Japan 27, 603–608. https://doi.org/10.4164/sptj.27.603

Van Dover, C.L., 2014. Impacts of anthropogenic disturbances at deep-sea hydrothermal vent ecosystems: A review. Mar Environ Res 102, 59–72. https://doi.org/10.1016/j.marenvres.2014.03.008

Wang, A., 2019. Depression of Lead-activated Sphalerite by Sodium Hydrogen Phosphate for Red Dog Mine Operation. https://doi.org/10.7939/R3-75XG-1868

WBG, 2020. Minerals for Climate Action: The Mineral Intensity of the Clean Energy Transition [WWW Document]. URL https://pubdocs.worldbank.org/en/961711588875536384/Minerals-for-Climate-Action-The-Mineral-Intensity-of-the-Clean-Energy-Transition.pdf (accessed 4.25.22).

Wei, Q., Jiao, F., Dong, L., Liu, X., Qin, W., 2021. Selective depression of copper-activated sphalerite by polyaspartic acid during chalcopyrite flotation. Transactions of Nonferrous Metals Society of China 31, 1784–1795. https://doi.org/10.1016/S1003-6326(21)65616-9

Wills, B.A., Finch, J.A., 2016. Mineral processing technology: an introduction to the practical aspects of ore treatment and mineral recovery, 8th ed.

Woodcock, J.T., Sparrow, G.J., Bruckard, W.J., Johnson, N.W., Dunne, R., 2007. Plant Practice: Sulfide Minerals and Precious Metals, in: Froth Flotation A Century of Innovation. pp. 781–844.

Zeng, Z., Chen, Z., Qi, H., 2021. Two Processes of Anglesite Formation and a Model of Secondary Supergene Enrichment of Bi and Ag in Seafloor Hydrothermal Sulfide Deposits. J Mar Sci Eng 10, 35. https://doi.org/10.3390/jmse10010035

Zha, L., Li, H., Wang, N., 2020. Electrochemical Study of Galena Weathering in NaCl Solution: Kinetics and Environmental Implications. Minerals 10, 416. https://doi.org/10.3390/min10050416

CHAPTER 2 – EFFECT OF ANGLESITE ON SPHALERITE FLOATABILITY, ENHANCED DEPRESSION OF SPHALERITE BY EXTRACTING ANGLESITE USING EDTA, AND RECOVERY OF EXTRACTED Pb^{2+} AS ZERO-VALENT Pb BY CEMENTATION USING ZERO-VALENT Fe

2.1 Introduction

In 2015, 193 governments adopted 17 sustainable development goals (SDGs) aiming to eradicate poverty, protect the planet, and ensure peaceful and prosperous lives for everyone by 2030 (Hák et al., 2016; Park et al., 2021b; Tabelin et al., 2021). Number 13 of the SDGs—"Climate Action"—envisions drastic carbon dioxide (CO_2) emission reductions to combat climate change and achieve a carbon-neutral society by 2050 (Goal 13 | Department of Economic and Social Affairs). Copper (Cu), lead (Pb), and zinc (Zn) are classified as critical metals defined by the World Bank as essential in renewable energy and clean storage technologies (e.g., wind turbines, solar photovoltaic (PV) panels, batteries, etc.), and thus their demands are projected to significantly increase in the future to achieve a carbon-neutral society (Nansai et al., 2014; WBG, 2020).

Complex sulfide ores, some of the most important sources of critical metals, are typically composed of several types of metal sulfide minerals such as chalcopyrite ($CuFeS_2$), galena (PbS), and sphalerite (ZnS). In the mineral processing of complex sulfide ores consisting of $CuFeS_2$-PbS-ZnS (Cu-Pb-Zn sulfide minerals), flotation has been commonly adopted to produce concentrates of each mineral (Bilal et al., 2022a, 2021; Hornn et al., 2021, 2020a, 2020b, 2020c; Park et al., 2021a, 2020a, 2020b; Seng et al., 2019b). Some complex sulfide ores contain not only PbS but also anglesite ($PbSO_4$), the presence of which is problematic for the separation of Cu, Pb, and Zn by flotation due to the unwanted activation of ZnS by Pb^{2+} released from $PbSO_4$ (Aikawa et al., 2021; Ministry of Economic and Japan Oil, 2018; Zeng et al., 2021). In the general flotation circuit of Cu-Pb-Zn sulfide ores, Cu and Pb sulfides are first recovered as froth, and then ZnS is recovered with the assistance of activators (e.g., $CuSO_4$) (Wills and Finch, 2016; Woodcock et al., 2007). When $PbSO_4$ is contained in complex sulfide ores, however, Pb^{2+} is readily released from $PbSO_4$ during conditioning and/or flotation due to its higher solubility compared to PbS—the solubility products (K_{sp}) of $PbSO_4$ and PbS are $10^{-7.79}$ and $10^{-26.77}$, respectively (Ball and Nordstrom, 1991)—and activates the surface of ZnS via the formation of PbS-like compounds, as illustrated in Equation (2-1) (Laskowski et al., 1997; Rashchi et al., 2002a);

$$ZnS(s) + Pb^{2+} = PbS(s) + Zn^{2+} \quad (2\text{-}1)$$

The activation of ZnS by Pb^{2+} is known to increase the ZnS floatability because of a higher affinity of PbS-like compounds for xanthate compared to ZnS (e.g., K_{sp} of Zn^{2+} and Pb^{2+} with ethyl xanthate are $10^{-8.2}$ and $10^{-16.7}$, respectively) (Aikawa et al., 2020; du Reitz, 1975; Houot and

Raveneau, 1992; Trahar et al., 1997). As a result, ZnS is recovered as froth together with $CuFeS_2$ and PbS, making their separation difficult (Aikawa et al., 2021). Therefore, a proper way of depressing ZnS floatability during flotation of complex sulfide ores containing $PbSO_4$ should be established.

In addition, $PbSO_4$ is typically distributed into flotation tailings because it has poor affinity for the collector (e.g., xanthate) (Fuerstenau et al., 1987; Rashchi et al., 2005). The disposal of $PbSO_4$ into tailings storage facilities (TSFs) would cause lead pollution in the surrounding environment (Schindler et al., 2021; Silwamba et al., 2022). That is, the presence of $PbSO_4$ in complex sulfide ores would cause not only difficulties in the separation of ZnS from Cu and Pb sulfide minerals but also lead pollution in the surrounding environment of TSFs.

To address the above-mentioned problems, this chapter investigated the improvement of ZnS depression by extracting $PbSO_4$ and the recovery of extracted Pb^{2+} as zero-valent Pb (Pb^0) by cementation using zero-valent iron (ZVI). Specifically, this chapter was devoted not only to optimizing the conditions for the extraction of $PbSO_4$ by ethylene diamine tetra acetic acid (EDTA) as well as the recovery of extracted Pb^{2+} as Pb^0 via cementation using ZVI but also to understanding how the absence/presence of $PbSO_4$ affected the floatability of ZnS through flotation experiments and surface characterizations of ZnS/$PbSO_4$ mixtures with and without EDTA pretreatment. Finally, a sustainable flowsheet for the processing of complex sulfide ores containing $PbSO_4$ with the combination of EDTA pretreatment, flotation, and cementation is proposed.

2.2 Materials and methods

2.2.1 Materials

Five types of minerals were used in this study: sphalerite (ZnS, Kamioka Mine, Hida, Japan), lead sulfate ($PbSO_4$, 98% purity), lead carbonate ($PbCO_3$, 99% purity), lead chloride ($PbCl_2$, 99% purity), and quartz (SiO_2, 99% purity). The lead compounds and quartz were obtained from FUJIFILM Wako Pure Chemical Corporation (Osaka, Japan). A mineral specimen of ZnS was characterized using X-ray fluorescence spectroscopy (XRF, EDXL300, Rigaku Corporation, Tokyo, Japan) and X-ray powder diffraction (XRD, MultiFlex, Rigaku Corporation, Tokyo, Japan), and its chemical and mineralogical compositions ware shown in Table 2-1 and Figure 2-1, respectively. The XRD pattern of ZnS implied that ZnS was relatively pure due to the absence of the peaks of common minerals such as SiO_2. In preparation for the flotation experiments, ZnS was ground by a vibratory disc mill (RS 200, Retsch Inc., Haan, Germany) and screened to obtain a size fraction of −75 + 38 μm.

Table 2-1. Chemical composition of a mineral specimen of ZnS based on XRF.

Elements	Zn	Fe	Pb	S	Si
Mass fraction (%)	55.7	6.2	0.2	21.3	8.4

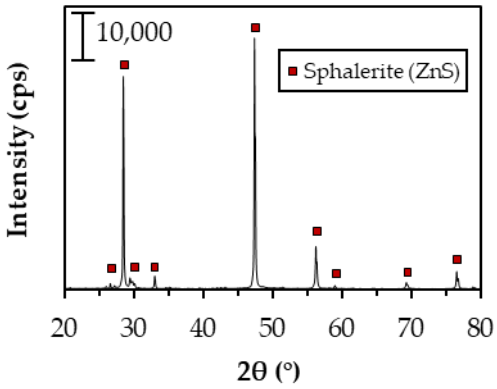

Figure 2-1. XRD pattern of a mineral specimen of ZnS.

For the flotation experiments, potassium amyl xanthate (KAX, Tokyo Chemical Industry Co., Ltd., Tokyo, Japan) and methyl isobutyl carbinol (MIBC, FUJIFILM Wako Pure Chemical Corporation, Osaka, Japan) were used as collector and frother, respectively. Zinc sulfate ($ZnSO_4$) and sodium sulfite (Na_2SO_3), purchased from FUJIFILM Wako Pure Chemical Corporation (Osaka, Japan), were used as depressants for ZnS. Sulfuric acid (H_2SO_4, FUJIFILM Wako Pure Chemical Corporation, Osaka, Japan) and sodium hydroxide (NaOH, FUJIFILM Wako Pure Chemical Corporation, Osaka, Japan) were used as pH adjusters. For the extraction experiments, ethylene diamine tetra acetic acid (EDTA, FUJIFILM Wako Pure Chemical Corporation, Osaka, Japan) was used as an extractant. For the cementation experiments, zero-valent Fe (ZVI) powder (Fe^0, −45 μm, FUJIFILM Wako Pure Chemical Corporation, Osaka, Japan) was used as a reductant.

2.2.2 Experimental methods

2.2.2.1 Extraction experiments of lead minerals using EDTA

The extraction experiments of lead minerals were conducted in 50 mL Erlenmeyer flasks containing 1 g of the lead mineral and an EDTA solution (solid/liquid ratio: 1 g/10 mL). The solutions containing 100, 200, or 500 mM EDTA were used without pH adjustment (natural pH: 11.3). The flasks were shaken in a thermostat water bath shaker at a shaking speed of 120 rpm and an amplitude of 40 mm at 25 °C. After this, the leachates were collected by filtration using 0.2 μm syringe-driven membrane filters and immediately analyzed using an inductively coupled plasma atomic emission spectrometer (ICP-AES, ICPE 9820, Shimadzu Corporation, Kyoto, Japan) (margin of error = ±2%)

to measure the concentration of Pb^{2+}. The experiments were performed in triplicate to ascertain that the differences observed were statistically significant, and the extraction efficiency of the lead mineral (E_{Pb}) was calculated using the following equation:

$$E_{Pb} = \frac{[Pb]_i}{[Pb]_{tot}} \times 100 \quad (2\text{-}2)$$

where $[Pb]_{tot}$ and $[Pb]_i$ are total Pb (mM) and extracted Pb (mM), respectively.

2.2.2.2 Cementation experiments of the extracted Pb^{2+}

The cementation experiments of Pb^{2+} extracted from $PbSO_4$ were conducted in 50 mL Erlenmeyer flasks. A volume of 10 mL of the leachate collected by filtration using 0.2 μm syringe-driven membrane filters after the extraction experiments ([EDTA], 500 mM; S/L ratio, 1 g/10 mL; time, 30 min) was added to the flask, and ultrapure nitrogen gas (N_2; 99.99%) was introduced for 15 min to remove the dissolved oxygen (DO) present in the leachate. Then, a known amount of ZVI powder was added to the flask, and N_2 was further introduced for 5 min. The flask was tightly capped with a silicon rubber plug and parafilm and shaken in a thermostat water bath shaker at a shaking speed of 120 rpm and an amplitude of 40 mm at 25 °C. After this, the leachate was filtered using a 0.2 μm syringe-driven membrane filter, and the filtrate was immediately analyzed using ICP-AES to measure the concentration of Pb^{2+}. Meanwhile, the residue was washed thoroughly with distilled water, dried in a vacuum-drying oven at 40 °C, and analyzed by scanning electron microscopy with energy-dispersive X-ray spectroscopy (SEM-EDS, JSM-IT200TM, JEOL Co., Ltd., Tokyo, Japan). The experiments were performed in triplicate to ascertain that the differences observed were statistically significant. Pb recovery (R_{Pb}) was calculated using the following equation:

$$R_{Pb} = \frac{[Pb]_I - [Pb]_F}{[Pb]_I} \times 100 \quad (2\text{-}3)$$

where $[Pb]_I$ and $[Pb]_F$ are the initial and the final concentrations of Pb (mM) in the leachate, respectively.

2.2.2.3 Flotation experiments

The flotation experiments were carried out using an agitator-type flotation machine (ASH-F30H, Kankyo-kanri Engineering, Akita, Japan) equipped with a 400 mL flotation cell under the following conditions: pH, 6.5; temperature, 25 °C; pulp density, 5%; impeller speed, 1000 rpm; air flow rate, 1 L/min. In a 500 mL beaker, a model sample containing 15 g of ZnS and 5 g of $PbSO_4$ or SiO_2 was suspended in 300 mL of distilled water, and the supernatant was decanted to remove fine particles (<38 μm) (Aikawa et al., 2021). After desliming, a model sample was repulped to 400 mL with distilled water in the flotation cell and conditioned for 3 min after adding the following reagents in sequence: ~5 kg/t of $ZnSO_4$ (100 ppm Zn^{2+}), 1 kg/t of Na_2SO_3, 20 g/t of KAX, and 20 μL/L of MIBC.

Afterwards, air was introduced at a flowrate of 1 L/min, and froth was recovered for 3 min. The recovered froth/tailing products were dried at 105 °C for 24 h and analyzed by XRF to determine the Zn recovery. The experiments were performed in duplicate to ascertain that the differences observed were statistically significant. An aliquot of the pulp of about 5 mL was collected 3 min after adding the depressant, filtered through a 0.2 μm syringe-driven membrane filter, and immediately analyzed using ICP-AES to check the extent of lead activation of ZnS. Meanwhile, the collected residues were washed thoroughly with distilled water, dried in a vacuum-drying oven at 40 °C, and analyzed by X-ray photoelectron spectroscopy (XPS, JPS-9200, JEOL Co., Ltd., Tokyo, Japan). The XPS analysis was conducted using an Al Kα X-ray source (1486.7 eV) operated at 100 W (voltage = 10 kV; current = 10 mA) under ultrahigh vacuum conditions (~10^{-7} Pa). The binding energies of photoelectrons were calibrated using C1s (285 eV) or $Zn2p_{3/2}$ (1022.0 eV) for charge correction. The XPS data were analyzed by Casa XPS, and deconvolutions of the spectra were carried out using an 80% Gaussian–20% Lorentzian peak model and a Shirley background (Park et al., 2020c; Shirley, 1972; Tabelin et al., 2019; Zoleta et al., 2020a).

In addition, flotation experiments of ZnS/$PbSO_4$ mixture after EDTA pretreatment were conducted to check how effective the removal of $PbSO_4$ was on the depression of ZnS floatability. A mixture of 15 g ZnS and 5 g $PbSO_4$ was mixed with 200 mL of a 500 mM EDTA solution (i.e., solid/liquid ratio: 20 g/200 mL) and shaken in a thermostat water bath shaker at a shaking speed of 120 rpm and an amplitude of 40 mm at 25 °C for 30 min. After this, the leachate was filtered using a 0.2 μm syringe-driven membrane filter, the filtrate was immediately analyzed using ICP-AES to measure the concentration of Pb^{2+}, and the cementation experiments to recover the extracted Pb^{2+} in the filtrate were carried out using 1 g/10 mL of ZVI for 24 h under the same conditions and with the same procedures mentioned in Section 2.2.2. Meanwhile, the residue obtained after EDTA pretreatment was washed thoroughly with distilled water and deslimed to remove fine particles (Aikawa et al., 2021). After desliming, the residue was repulped to 400 mL with distilled water, and then flotation was conducted under the same conditions mentioned above. An aliquot of the pulp of about 5 mL was also collected 3 min after adding the depressant ($ZnSO_4$) and filtered through a 0.2 μm syringe-driven membrane filter, and the filtrate and residue were analyzed by ICP-AES and XPS, respectively.

2.3 Results and discussion

2.3.1 Effects of $PbSO_4$ on ZnS floatability

Figure 2-2 shows the flotation results of ZnS mixed with SiO_2 or $PbSO_4$. As can be seen, Zn recovery in the presence of SiO_2 was ~12% but significantly increased to >80% when $PbSO_4$ was

present. It was reported that the affinity between ZnS and xanthate is poor, so the surface of ZnS needs to be modified using activators (Wills and Finch, 2016). Since the solubility of $PbSO_4$ is higher than that of PbS, a substantial amount of Pb^{2+} might be released into the pulp during the conditioning process when the ore contains $PbSO_4$ (Aikawa et al., 2021). As a result, lead activation of ZnS could occur (Equation (2-1)), thus increasing its floatability due to the formation of PbS-like compounds, having a higher affinity for xanthate than ZnS, on the mineral surface. In short, the presence of $PbSO_4$ in the complex sulfide ores containing $CuFeS_2$, PbS, and ZnS would negatively affect the separation of Cu-Pb from Zn. In addition, some portion of $PbSO_4$ will remain undissolved and be rejected as tailings due to the poor affinity of $PbSO_4$ for the collector (e.g., xanthate), which can cause lead contamination of the surrounding environment (Fuerstenau et al., 1987; Rashchi et al., 2005; Silwamba et al., 2020b).

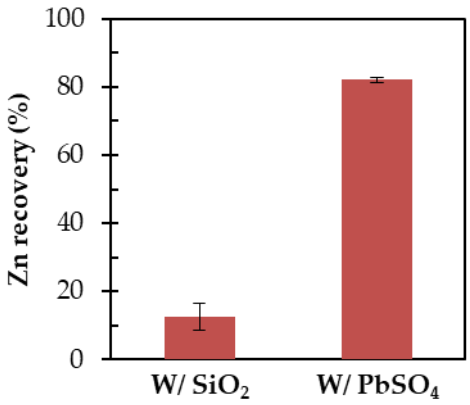

Figure 2-2. Flotation results of ZnS with SiO_2 or $PbSO_4$.

2.3.2 Extraction of $PbSO_4$ using EDTA

To address the above-mentioned problems caused by the presence of $PbSO_4$ (i.e., unwanted activation of ZnS and lead contamination), its extraction prior to flotation was investigated. Among the extractants, EDTA was chosen in this study because of its ability to extract metal ions from sulfates like $PbSO_4$, without dissolving metal sulfides (e.g., PbS and ZnS) (Bicak, 2019; Grano et al., 1988; Kant et al., 1994; Rumball and Richmond, 1996).

Figure 2-3a shows the extraction efficiency of $PbSO_4$ after 24 h with different concentrations of EDTA (100, 200, or 500 mM). When the stoichiometric ratio of EDTA/$[Pb]_{tot}$ was lower than 1, the amount of Pb^{2+} extracted was identical to the concentration of EDTA, which indicated that Pb^{2+} and EDTA formed a 1:1 complex (i.e., $[Pb(EDTA)]^{2-}$). When the stoichiometric ratio of EDTA/$[Pb]_{tot}$ was >1, almost all $PbSO_4$ (~98%) was extracted. The rate of $PbSO_4$ extraction was further studied with 500 mM EDTA, and the result showed that ~97% of $PbSO_4$ was extracted within 15 min (Figure 2-3b). EDTA could extract not only $PbSO_4$ but also other Pb minerals like $PbCO_3$ and $PbCl_2$

(Figure 2-4). These minerals are also unfloatable and will be rejected into the TSFs, indicating that their presence in the ores may result in the contamination of the TSFs with Pb minerals. It was confirmed that EDTA pretreatment can extract almost all Pb minerals except for PbS, thus suppressing lead pollution to the surrounding environment of TSFs. It is noted that the concentration of EDTA should be chosen in the consideration of the amount of soluble minerals contained in ores, because EDTA would be consumed not only by Pb^{2+} but also by other metal ions from soluble minerals such as sulfates, oxides, hydroxides, and carbonates.

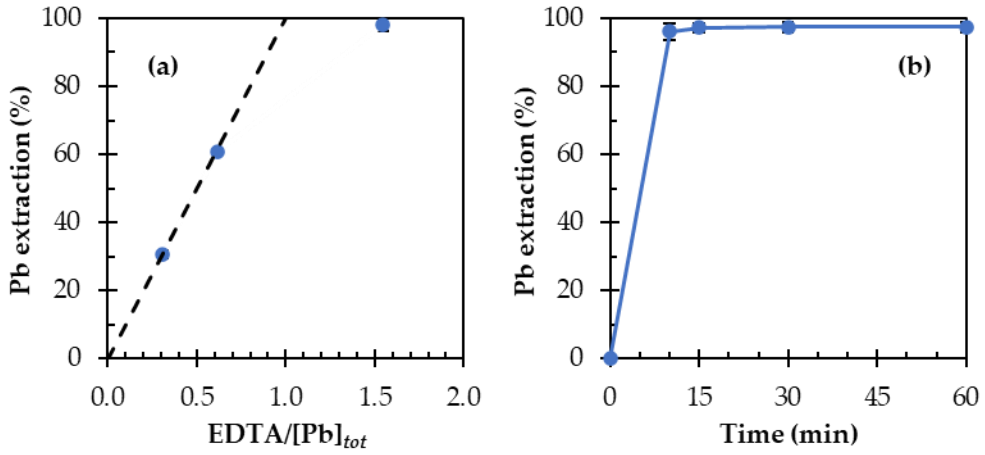

Figure 2-3. (a) Extraction efficiency of $PbSO_4$ after 24 h with different concentrations of EDTA (100, 200, or 500 mM) and (b) effect of time on $PbSO_4$ extraction with 500 mM EDTA. Note that the dotted line in Figure 2-3a corresponds to the ratio of EDTA/$[Pb]_{tot}$.

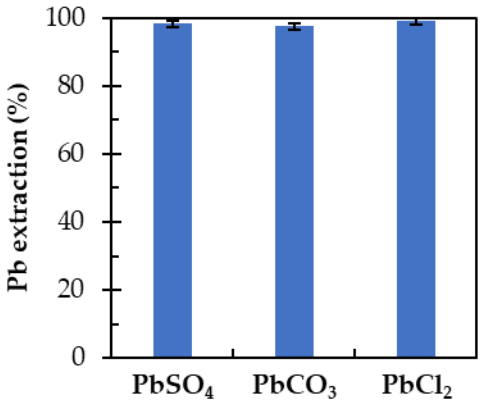

Figure 2-4. Extraction efficiency of lead minerals with 500 mM EDTA after 24 h.

2.3.3 Recovery of extracted Pb^{2+} as zero-valent Pb by cementation using zero-valent Fe

After EDTA pretreatment, the recovery of Pb^{2+} from the leachate will not only add economic value but also protect the environment. Cementation is one of the effective methods to recover metal ions

as zero-valent metals (Choi et al., 2021a, 2021c; Jeon et al., 2021, 2020a, 2020b). A general cementation reaction is illustrated in Equation (2-4): a metal (A^0) gives electrons to metal ion (B^{b+}), driven by the difference in standard redox potentials of the interacting metals and their ions, and as a result, B^{b+} is deposited on the surface of A^0 as B^0 (Choi et al., 2021b, 2020a; Jeon et al., 2022a, 2022b):

$$b\,A^0 + a\,B^{b+} \rightarrow b\,A^{a+} + a\,B^0 \quad (2\text{-}4)$$

To recover the extracted Pb^{2+} as zero-valent Pb (Pb^0) from the EDTA leachate, cementation experiments were carried out using ZVI powder as a reductant after removing DO from the solution by purging with ultrapure nitrogen gas. Figure 2-5a shows the effects of the ZVI amount on the recovery of the extracted Pb^{2+} from the leachate after EDTA pretreatment using 500 mM EDTA for 30 min. When the amount of ZVI was 0.5 g/10 mL, ~40% of Pb^{2+} was recovered, although ~0.18 g/10 mL ZVI was stoichiometrically sufficient to recover all Pb^{2+} in the solution. As the cementation reaction progressed, the surface of ZVI was covered with cementation products (i.e., Pb^0), which hindered a further cementation reaction. This was probably the reason why 1 g/10 mL of ZVI was required to recover all Pb^{2+} from the EDTA leachate.

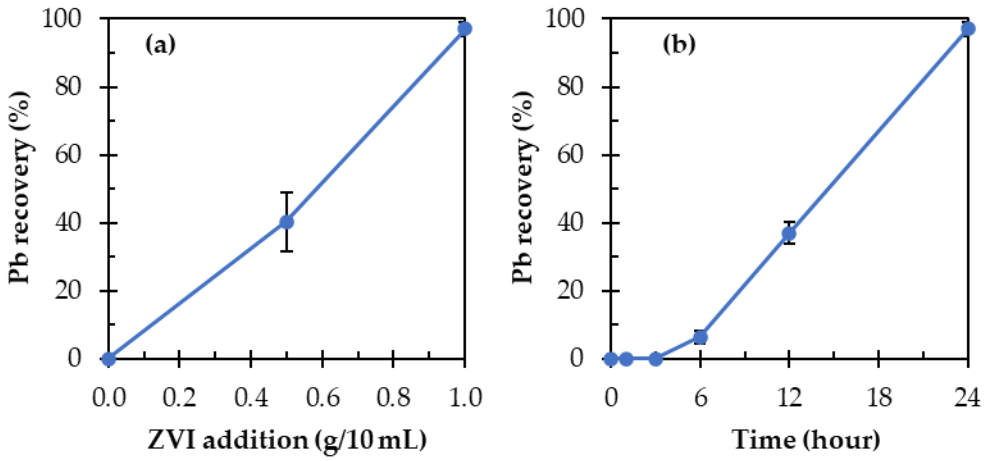

Figure 2-5. (a) Effects of the ZVI amount on the recovery of the extracted Pb after 24 h in the leachate after $PbSO_4$ extraction using 500 mM of EDTA for 30 min and (b) effects of time on the recovery of the extracted Pb^{2+} using 1 g/10 mL of ZVI in the leachate after EDTA pretreatment using 500 mM EDTA for 30 min.

Figure 2-5b shows the cementation results of Pb^{2+} by ZVI in time. As can be seen, almost no cementation occurred for 3 h, and then Pb^{2+} started being cemented gradually. The initial slow rate of Pb cementation can have two reasons: (i) the presence of Fe oxide films formed on the ZVI surface that limited the cementation of Pb^{2+} and (ii) an excess amount of free EDTA that redissolved the cemented Pb^0. After 3 h, the concentration of free EDTA ligands was most likely decreased due to its consumption in dissolving Fe oxide films and/or in forming complexes with Fe species

released by the cementation reaction. It is important to note that after 24 h, ~97% cementation was achieved. To confirm the recovery of Pb^{2+} on ZVI, the residue obtained from the cementation experiment using 1 g/10 mL of ZVI for 24 h was analyzed using SEM-EDS. As shown in Figure 2-6, the deposition of Pb compounds on ZVI powder was observed, suggesting that the extracted Pb^{2+} was reductively deposited via the cementation reaction:

$$Pb(EDTA)^{2-} + Fe^0 = Pb^0 + EDTA + Fe^{2+} \quad (2\text{-}5)$$

Equation (2-5) consists of two half-cell reactions (Silwamba et al., 2021):

$$Pb(EDTA)^{2-} + 2e^- = Pb^0 + EDTA^{4-} \quad (2\text{-}6)$$

$$Fe^0 = Fe^{2+} + 2e^- \quad (2\text{-}7)$$

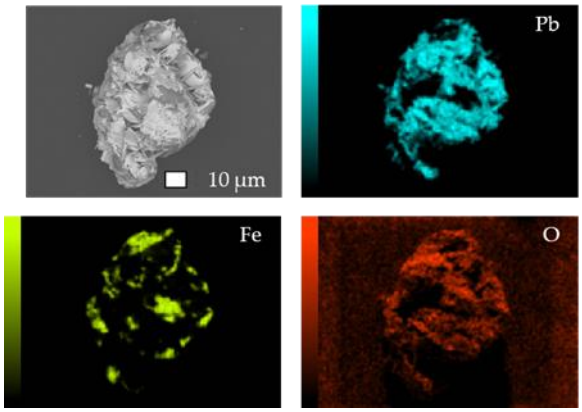

Figure 2-6. SEM photomicrograph of the residue of the cementation experiment using 1 g/10 mL of ZVI for 24 h with the corresponding elemental maps of Fe, Pb, and O.

The above-mentioned residue was also analyzed by XRD to further characterize Pb compounds formed on ZVI (Figure 2-7). As shown in the XRD pattern, the peaks of Fe^0, Fe_2O_3, Pb^0, and PbO were detected, indicating that Pb^{2+} was reductively deposited as Pb^0 on the surface of ZVI, as illustrated in Equation (2-5). The presence of PbO and Fe_2O_3 was due most likely to the oxidation of Pb^0 and ZVI surface during drying and storing of the sample (Silwamba et al., 2020a; Taylor and Perry, 1998; Xi et al., 2010).

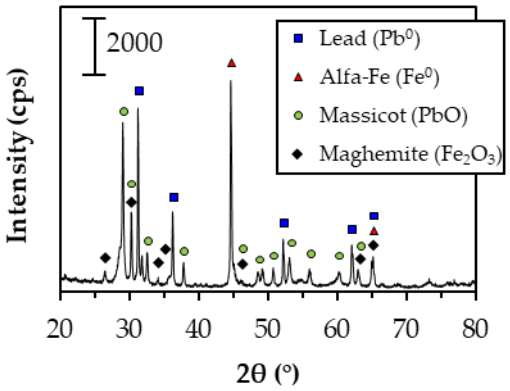

Figure 2-7. XRD pattern of the residue of the cementation experiment using 1 g/10 mL of ZVI for 24 h.

2.3.4 Effects of EDTA pretreatment on ZnS depression in flotation

As described in Section 2.3.2, almost all $PbSO_4$ was extracted with EDTA, so the effects of EDTA pretreatment on ZnS depression in flotation were investigated. Flotation experiments using model samples (ZnS/$PbSO_4$ mixture) with and without EDTA pretreatment were conducted (Figure 2-8). Prior to the flotation experiments, the mixture of 15 g ZnS and 5 g $PbSO_4$ was treated with 500 mM of EDTA for 30 min (solid/liquid ratio: 20 g/200 mL), and ~99.8% of $PbSO_4$ was extracted. The cementation experiments using 1 g/10 mL of ZVI for 24 h were also carried out to recover the extracted Pb^{2+} in the filtrate obtained after EDTA pretreatment , and ~99.7% of the extracted Pb^{2+} was recovered. Meanwhile, the residue obtained after EDTA pretreatment was deslimed and repulped to 400 mL with distilled water in the flotation cell, and then the flotation experiments were conducted with ~5 kg/t of $ZnSO_4$ (100 ppm Zn^{2+}) and 1 kg/t of Na_2SO_3 as depressants at pH 6.5. As shown in Figure 2-8, the floatability of Zn was clearly depressed from ~82% to ~30% when EDTA pretreatment was applied.

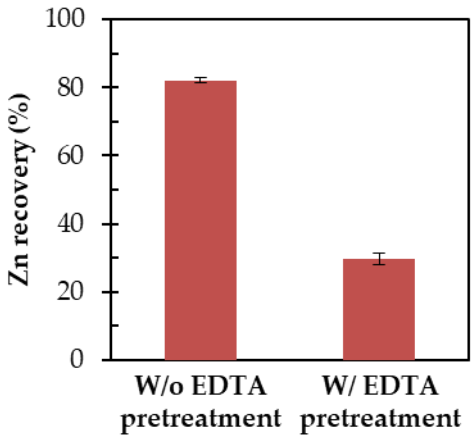

Figure 2-8. Effects of EDTA pretreatment on the floatability of ZnS in the presence of $PbSO_4$.

To confirm the depression of ZnS floatability after EDTA pretreatment, a pretreated sample reacted with $ZnSO_4$ for 3 min, a ~5 mL aliquot of the pulp was collected, and the filtrate and the residue were analyzed by ICP-AES and XPS, respectively. The concentration of Pb^{2+} in the filtrate without EDTA pretreatment was 5.3 ppm; it decreased to 0.2 ppm with EDTA pretreatment. On the other hand, the concentrations of Zn^{2+} in the filtrates with and without EDTA pretreatment were 101 and 99.4 ppm, respectively. Based on thermodynamics calculations using Equation (2-8), the possibility of lead activation of ZnS (Equation (2-1)) could be evaluated using the measured values of Pb^{2+} and Zn^{2+} (Aikawa et al., 2021; Basilio et al., 1996; El-Shall et al., 2000). In this study, the changes in free energy were calculated using measured values of Pb^{2+} and Zn^{2+} concentrations.

Table 2-2 shows the calculated results of the changes in free energy based on the equilibrium constants of lead activation of ZnS (Equation (2-1)). The change in free energy without EDTA pretreatment was negative, while that with EDTA pretreatment was positive. When the change in free energy is positive, the reverse reaction of lead activation (Equation (2-1)) would occur spontaneously, indicating that lead activation would be limited by EDTA pretreatment. These results support the flotation results that the depression of ZnS floatability was achieved by the pretreatment, which decreased Pb^{2+} concentration during flotation by extracting $PbSO_4$ in advance.

$$\Delta G = -RT \ln K + \ln(Zn^{2+}/Pb^{2+}) \quad (2\text{-}8)$$

$$K = \frac{K_{sp}^{ZnS}}{K_{sp}^{PbS}} \quad (2\text{-}9)$$

Table 2-2. Calculation results of the change in free energy with and without EDTA pretreatment.

K	ΔG (kJ/mol) Without EDTA Pretreatment	ΔG (kJ/mol) With EDTA Pretreatment
1000 [a]	−6.9	1.8
704 [b]	−6.1	2.7

1059 [c]	−7.1	1.7
1127 [d]	−7.2	1.5

[a] The equilibrium constant was obtained from a previous study (El-Shall et al., 2000). [b, c, d] The equilibrium constants were calculated using Equation (2-9) by the reported K_{sp} values of *ZnS* and *PbS*, respectively (Helgeson, 1969; Latimer, 1952; Leckie and James, 1974).

To confirm whether the lead activation of sphalerite was limited by the extraction of $PbSO_4$ using EDTA, untreated ZnS as well as $ZnSO_4$-pretreated $ZnS/PbSO_4$ mixtures with and without EDTA pretreatment were analyzed by XPS. The $Pb4f_{7/2}$ core-level spectra of the samples are shown in Figure 2-9, and the corresponding curve-fitting parameters are summarized in Table 2-3. Since the Zn3s peak overlapped with the $Pb4f_{7/2}$ signals, the spectrum was resolved by curve fitting to subtract the area due to the Zn3s peak (Basilio et al., 1996; Liu et al., 2020). As illustrated in Figure 2-9b and c, the deconvoluted XPS spectra of the residues with and without $PbSO_4$ extraction showed two types of Pb species: (1) Pb^{2+}—S of PbS (143.6 and 138.6 eV) and (2) Pb^{2+}—SO_4 of $PbSO_4$ (144.7 and 139.8 eV), while the deconvoluted XPS spectrum of untreated ZnS showed no Pb species (Figure 2-9a) (Aikawa et al., 2020; Hernan et al., 1995). The decrease in the intensity of Pb^{2+}—SO_4 was in a good agreement with the extraction efficiency of $PbSO_4$ using EDTA for the $ZnS/PbSO_4$ mixture (~99.8%). When EDTA pretreatment was applied prior to the flotation experiments, the peak intensity ratio of PbS/ZnS decreased from 2.3 to 0.2, indicating that EDTA pretreatment was effective in limiting lead activation of ZnS. This is in line with the calculated results of the change in free energy based on thermodynamics (Table 2-2).

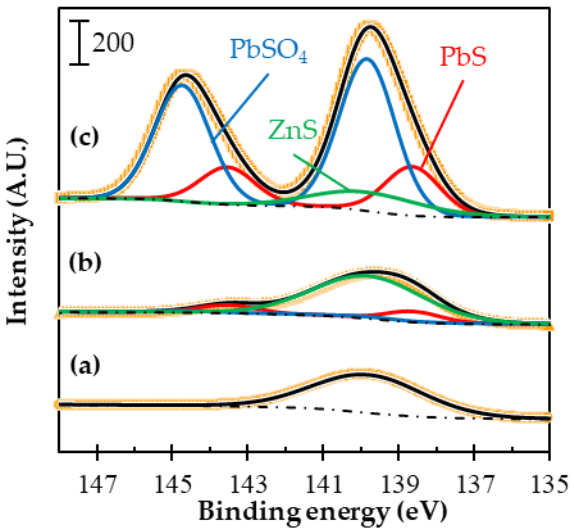

Figure 2-9. XPS Pb4f7/2 spectra of (a) raw ZnS, (b) $ZnS/PbSO_4$ with EDTA pretreatment, and (c) $ZnS/PbSO_4$ without EDTA pretreatment.

Table 2-3. XPS peak parameters for $Pb4f_{7/2}$ spectra and relative abundances of Pb species.

Binding Energy (eV)	FWHM	Assignments	Contents (at.%)		
			Untreated [a]	W/ EDTA [b] Pretreatment	W/o EDTA [a] Pretreatment
138.6 ± 0.05 143.5 ± 0.05	1.7	PbS	0	17.1	21.5
139.8 ± 0.05 144.7 ± 0.05	1.7	$PbSO_4$	0	8.8	48.4
139.8 ± 0.05	3.4	ZnS	100	80.5	9.5

[a] The binding energies of photoelectrons were calibrated using C1s (285 eV) for charge correction.

[b] The binding energies of photoelectrons were calibrated using $Zn2p_{3/2}$ (1022.0 eV) for charge correction.

2.3.5 Implication of this study

The results of this study have significant implications not only for understanding how the presence of $PbSO_4$ in complex sulfide ores affects the floatability of ZnS but also for proposing a sustainable process flowsheet covering both the improved flotation separation of complex sulfide ores and the detoxification of solid/solution wastes contaminated with Pb species. Firstly, the presence of $PbSO_4$ might have a detrimental impact on the flotation separation of complex sulfide ores due to unwanted lead activation of ZnS that improves its floatability, which could not be depressed with $ZnSO_4$—the conventional depressant for ZnS. Secondly, EDTA washing could extract almost all $PbSO_4$ from the ZnS/$PbSO_4$ mixture, and consequently, the floatability of ZnS decreased due to the limited amount of PbS-like compounds formed on the ZnS surface by lead activation. Finally, cementation using ZVI could recover Pb^{2+} extracted from $PbSO_4$ during EDTA pretreatment as Pb^0, which will not only add economic value but also protect the environment.

Based on the findings of this study, a sustainable process flowsheet for complex sulfide ores is proposed (Figure 2-10). In this proposed flowsheet, $PbSO_4$ is first extracted by EDTA pretreatment before flotation. The residue obtained after EDTA pretreatment is fed to a flotation stage where ZnS floatability is effectively depressed by the conventional depressant for ZnS due to the decrease in the ratio of Pb^{2+}/Zn^{2+} of the flotation pulp, and then gangue minerals like SiO_2 and FeS_2 would be disposed of into a tailings dam after the recovery of ZnS with the assistance of activators (e.g., $CuSO_4$). Meanwhile, the leachate obtained from EDTA pretreatment is rich in Pb^{2+} that can be recovered via cementation using ZVI as Pb^0. To keep up with the high demand for critical metals following the SDGs, mine developments should be in harmony with the environment. This proposed flowsheet can achieve enhanced selective flotation of complex sulfide ores (depression of ZnS floatability) while preventing lead pollution to the surrounding environment of tailings dams

(removal of toxic $PbSO_4$ before flotation) and maximizing the recovery of critical elements by cementation (recovery of Pb^0 using ZVI).

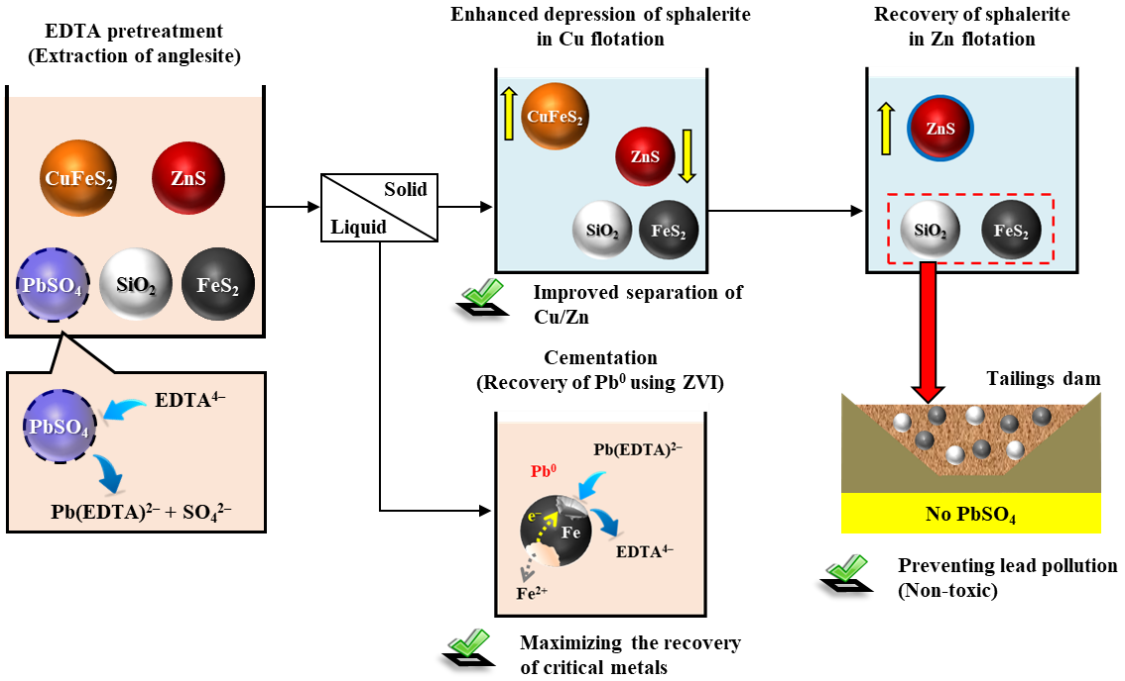

Figure 2-10. Proposed enhanced depression of sphalerite (ZnS) by extracting anglesite ($PbSO_4$) using ethylene diamine tetra acetic acid (EDTA) and recovery of the extracted Pb^{2+} as zero-valent Pb (Pb^0) by cementation using zero-valent Fe (ZVI).

2.4 Conclusions

In this chapter, a pretreatment of flotation to extract $PbSO_4$ for the prevention of lead pollution to the surrounding environment of tailings dams and the depression of ZnS floatability combined with the recovery of extracted Pb^{2+} by cementation was investigated, and the findings of this chapter are summarized as follows:

1. ZnS floatability increased in the presence of $PbSO_4$.
2. The conventional depressants for ZnS, $ZnSO_4$ and Na_2SO_3, were not effective in depressing the floatability of ZnS when $PbSO_4$ was present.
3. Almost of all $PbSO_4$ (>97%) was extracted using EDTA, and >97% of the extracted Pb^{2+} could be recovered as Pb^0 by cementation using ZVI.
4. A pretreatment of flotation extracting $PbSO_4$ using EDTA was effective in depressing ZnS floatability.

5. The proposed method for complex sulfide ores containing $PbSO^4$, a combination of extraction of $PbSO_4$ using EDTA and recovery of extracted Pb^{2+} as zero-valent Pb by cementation using ZVI, could achieve enhanced selective flotation of complex sulfide ores (depression of ZnS floatability) while preventing lead pollution to the surrounding environment of tailings dams (removal of toxic $PbSO_4$ before flotation) and maximizing the recovery of critical elements by cementation (recovery of Pb^0 using ZVI).

This chapter is edited from "Aikawa et al., 2022. Development of a sustainable process for complex sulfide ores containing anglesite: Effect of anglesite on sphalerite floatability, enhanced depression of sphalerite by extracting anglesite, and recovery of extracted Pb^{2+} as zero-valent Pb by cementation using zero-valent Fe. Minerals 723, 12(6)."

References

Aikawa, K., Ito, M., Kusano, A., Park, I., Oki, T., Takahashi, T., Furuya, H., Hiroyoshi, N., 2021. Flotation of Seafloor Massive Sulfide Ores: Combination of Surface Cleaning and Deactivation of Lead-Activated Sphalerite to Improve the Separation Efficiency of Chalcopyrite and Sphalerite. Metals (Basel) 11, 253. https://doi.org/10.3390/met11020253

Aikawa, K., Ito, M., Segawa, T., Jeon, S., Park, I., Tabelin, C.B., Hiroyoshi, N., 2020. Depression of lead-activated sphalerite by pyrite via galvanic interactions: Implications to the selective flotation of complex sulfide ores. Miner Eng 152, 106367. https://doi.org/10.1016/j.mineng.2020.106367

Ball, J.W., Nordstrom, D.K., 1991. User's manual for WATEQ4F, with revised thermodynamic data base and text cases for calculating speciation of major, trace, and redox elements in natural waters, U.S. Geological Survey Water-Resources Investigations Report. Reston, VA, USA. https://doi.org/10.3133/ofr91183

Basilio, C.I., Kartio, I.J., Yoon, R.-H., 1996. Lead activation of sphalerite during galena flotation. Miner Eng 9, 869–879. https://doi.org/10.1016/0892-6875(96)00078-7

Bicak, O., 2019. A technique to determine ore variability in a sulphide ore. Miner Eng 142, 105927. https://doi.org/10.1016/j.mineng.2019.105927

Bilal, M., Ito, M., Akishino, R., Bu, X., Ul Hassan, F., Park, I., Jeon, S., Aikawa, K., Hiroyoshi, N., 2022. Heterogenous carrier flotation technique for recovering finely ground chalcopyrite

particles using coarse pyrite particles as a carrier. Miner Eng 180, 107518. https://doi.org/10.1016/j.mineng.2022.107518

Bilal, M., Ito, M., Koike, K., Hornn, V., Ul Hassan, F., Jeon, S., Park, I., Hiroyoshi, N., 2021. Effects of coarse chalcopyrite on flotation behavior of fine chalcopyrite. Miner Eng 163, 106776. https://doi.org/10.1016/J.MINENG.2021.106776

Choi, S., Jeon, S., Park, I., Ito, M., Hiroyoshi, N., 2021a. Addition of Fe3O4 as electron mediator for enhanced cementation of Cd2+ and Zn2+ on aluminum powder from sulfate solutions and magnetic separation to concentrate cemented metals from cementation products. J Environ Chem Eng 9, 106699. https://doi.org/10.1016/J.JECE.2021.106699

Choi, S., Jeon, S., Park, I., Ito, M., Hiroyoshi, N., 2021b. Enhanced Cementation of Co2+ and Ni2+ from Sulfate and Chloride Solutions Using Aluminum as an Electron Donor and Conductive Particles as an Electron Pathway. Metals 2021, Vol. 11, Page 248 11, 248. https://doi.org/10.3390/MET11020248

Choi, S., Jeon, S., Park, I., Tabelin, C.B., Ito, M., Hiroyoshi, N., 2021c. Enhanced cementation of Cd2+, Co2+, Ni2+, and Zn2+ on Al from sulfate solutions by activated carbon addition. Hydrometallurgy 201, 105580. https://doi.org/10.1016/J.HYDROMET.2021.105580

Choi, S., Yoo, K., Alorro, R.D., Tabelin, C.B., 2020. Cementation of Co ion in leach solution using Zn powder followed by magnetic separation of cementation-precipitate for recovery of unreacted Zn powder. Miner Eng 145, 106061. https://doi.org/10.1016/J.MINENG.2019.106061

Du Reitz, C., 1975. Chemisorption of collectors in flotation, in: The 11th International Mineral Processing Congress. Instituto di Arte Mineraria e Preperazione dei Minerali, Rome, pp. 395–403.

El-Shall, H.E., Elgillani, D.A., Abdel-Khalek, N.A., 2000. Role of zinc sulfate in depression of lead-activated sphalerite. Int J Miner Process 58, 67–75. https://doi.org/10.1016/S0301-7516(99)00055-1

Fuerstenau, M.C., Olivas, S.A., Herrera-Urbina, R., Han, K.N., 1987. The surface characteristics and flotation behavior of anglesite and cerussite. Int J Miner Process 20, 73–85. https://doi.org/10.1016/0301-7516(87)90018-4

Goal 13 | Department of Economic and Social Affairs [WWW Document], n.d. URL https://sdgs.un.org/goals/goal13 (accessed 4.26.22).

Grano, S.R., Ralston, J., Johnson, N.W., 1988. Characterization and treatment of heavy medium slimes in the Mt. Isa mines lead-zinc concentrator. Miner Eng 1, 137–150. https://doi.org/10.1016/0892-6875(88)90004-0

Hák, T., Janoušková, S., Moldan, B., 2016. Sustainable Development Goals: A need for relevant indicators. Ecol Indic 60, 565–573. https://doi.org/10.1016/j.ecolind.2015.08.003

Helgeson, H.C., 1969. Thermodynamics of hydrothermal systems at elevated temperatures and pressures. Am J Sci 267, 729–804. https://doi.org/10.2475/ajs.267.7.729

Hernan, L., Morales, J., Sanchez, L., Tirado, J.L., Espinos, J.P., Gonzalez Elipe, A.R., 1995. Diffraction and XPS Studies of Misfit Layer Chalcogenides Intercalated with Cobaltocene. Chem. Mater 7, 1576–1582.

Hornn, V., Ito, M., Shimada, H., Tabelin, C.B., Jeon, S., Park, I., Hiroyoshi, N., 2020a. Agglomeration-Flotation of Finely Ground Chalcopyrite and Quartz: Effects of Agitation Strength during Agglomeration Using Emulsified Oil on Chalcopyrite. Minerals 10, 380. https://doi.org/10.3390/min10040380

Hornn, V., Ito, M., Shimada, H., Tabelin, C.B., Jeon, S., Park, I., Hiroyoshi, N., 2020b. Agglomeration–Flotation of Finely Ground Chalcopyrite Using Emulsified Oil Stabilized by Emulsifiers: Implications for Porphyry Copper Ore Flotation. Metals 2020, Vol. 10, Page 912 10, 912. https://doi.org/10.3390/MET10070912

Hornn, V., Ito, M., Yamazawa, R., Shimada, H., Tabelin, C.B., Jeon, S., Park, I., Hiroyoshi, N., 2020c. Kinetic Analysis for Agglomeration-Flotation of Finely Ground Chalcopyrite: Comparison of First Order Kinetic Model and Experimental Results. Mater Trans 61, 1940–1948. https://doi.org/10.2320/MATERTRANS.M-M2020843

Hornn, V., Park, I., Ito, M., Shimada, H., Suto, T., Tabelin, C.B., Jeon, S., Hiroyoshi, N., 2021. Agglomeration-flotation of finely ground chalcopyrite using surfactant-stabilized oil emulsions: Effects of co-existing minerals and ions. Miner Eng 171, 107076. https://doi.org/10.1016/J.MINENG.2021.107076

Houot, R., Raveneau, P., 1992. Activation of sphalerite flotation in the presence of lead ions. Int J Miner Process 35, 253–271. https://doi.org/10.1016/0301-7516(92)90037-W

Jeon, S., Bright, S., Park, I., Kuze, A., Ito, M., Hiroyoshi, N., 2022a. A Kinetic Study on Enhanced Cementation of Gold Ions by Galvanic Interactions between Aluminum (Al) as an Electron Donor and Activated Carbon (AC) as an Electron Mediator in Ammonium Thiosulfate System. Minerals 2022, Vol. 12, Page 91 12, 91. https://doi.org/10.3390/MIN12010091

Jeon, S., Bright, S., Park, I., Tabelin, C.B., Ito, M., Hiroyoshi, N., 2022b. A simple and efficient recovery technique for gold ions from ammonium thiosulfate medium by galvanic interactions of zero-valent aluminum and activated carbon: A parametric and mechanistic study of cementation. Hydrometallurgy 208, 105815. https://doi.org/10.1016/J.HYDROMET.2021.105815

Jeon, S., Bright, S., Park, I., Tabelin, C.B., Ito, M., Hiroyoshi, N., 2021. The Effects of Coexisting Copper, Iron, Cobalt, Nickel, and Zinc Ions on Gold Recovery by Enhanced Cementation via Galvanic Interactions between Zero-Valent Aluminum and Activated Carbon in Ammonium Thiosulfate Systems. Metals 2021, Vol. 11, Page 1352 11, 1352. https://doi.org/10.3390/MET11091352

Jeon, S., Tabelin, C.B., Park, I., Nagata, Y., Ito, M., Hiroyoshi, N., 2020a. Ammonium thiosulfate extraction of gold from printed circuit boards (PCBs) of end-of-life mobile phones and its recovery from pregnant leach solution by cementation. Hydrometallurgy 191, 105214. https://doi.org/10.1016/j.hydromet.2019.105214

Jeon, S., Tabelin, C.B., Takahashi, H., Park, I., Ito, M., Hiroyoshi, N., 2020b. Enhanced cementation of gold via galvanic interactions using activated carbon and zero-valent aluminum: A novel approach to recover gold ions from ammonium thiosulfate medium. Hydrometallurgy 191, 105165. https://doi.org/10.1016/j.hydromet.2019.105165

Kant, C., Rao, S.R., Finch, J.A., 1994. Distribution of surface metal ions among the products of chalcopyrite flotation. Miner Eng 7, 905–916. https://doi.org/10.1016/0892-6875(94)90132-5

Laskowski, J.S., Liu, Q., Zhan, Y., 1997. Sphalerite activation: Flotation and electrokinetic studies. Miner Eng 10, 787–802. https://doi.org/10.1016/S0892-6875(97)00057-5

Latimer, W.M., 1952. The oxidation states of the elements and their potentials in aqueous solutions, 2nd ed.

Leckie, J.O., James, R.O., 1974. Aqueous Environmental Chemistry of Metals. Ann Arbor Science Publishers.

Liu, J., Ejtemaei, M., Nguyen, A. v, Wen, S., Zeng, Y., 2020. Surface chemistry of Pb-activated sphalerite. Miner Eng 145, 106058. https://doi.org/10.1016/j.mineng.2019.106058

Ministry of Economic, T. and I. (METI), Japan Oil, G. and M.N.C. (JOGMEC), 2018. Summary report on comprehensive evaluations of development plan of seafloor massive sulfide deposits [WWW Document]. URL http://www.jogmec.go.jp/content/300359550.pdf (accessed 2.26.21).

Nansai, K., Nakajima, K., Kagawa, S., Kondo, Y., Suh, S., Shigetomi, Y., Oshita, Y., 2014. Global Flows of Critical Metals Necessary for Low-Carbon Technologies: The Case of Neodymium, Cobalt, and Platinum. Environ Sci Technol 48, 1391–1400. https://doi.org/10.1021/es4033452

Park, I., Hong, S., Jeon, S., Ito, M., Hiroyoshi, N., 2021a. Flotation Separation of Chalcopyrite and Molybdenite Assisted by Microencapsulation Using Ferrous and Phosphate Ions: Part II. Flotation. Metals 2021, Vol. 11, Page 439 11, 439. https://doi.org/10.3390/MET11030439

Park, I., Hong, S., Jeon, S., Ito, M., Hiroyoshi, N., 2020a. Flotation Separation of Chalcopyrite and Molybdenite Assisted by Microencapsulation Using Ferrous and Phosphate Ions: Part I. Selective Coating Formation. Metals (Basel) 10, 1667. https://doi.org/10.3390/met10121667

Park, I., Hong, S., Jeon, S., Ito, M., Hiroyoshi, N., 2020b. A Review of Recent Advances in Depression Techniques for Flotation Separation of Cu–Mo Sulfides in Porphyry Copper Deposits. Metals (Basel) 10, 1269. https://doi.org/10.3390/met10091269

Park, I., Kanazawa, Y., Sato, N., Galtchandmani, P., Jha, M.K., Tabelin, C.B., Jeon, S., Ito, M., Hiroyoshi, N., 2021b. Beneficiation of Low-Grade Rare Earth Ore from Khalzan Buregtei Deposit (Mongolia) by Magnetic Separation. Minerals 11, 1432. https://doi.org/10.3390/min11121432

Park, I., Tabelin, C.B., Seno, K., Jeon, S., Inano, H., Ito, M., Hiroyoshi, N., 2020c. Carrier-microencapsulation of arsenopyrite using Al-catecholate complex: nature of oxidation products, effects on anodic and cathodic reactions, and coating stability under simulated weathering conditions. Heliyon 6, e03189. https://doi.org/10.1016/j.heliyon.2020.e03189

Rashchi, F., Dashti, A., Arabpour-Yazdi, M., Abdizadeh, H., 2005. Anglesite flotation: a study for lead recovery from zinc leach residue. Miner Eng 18, 205–212. https://doi.org/10.1016/J.MINENG.2004.10.014

Rashchi, F., Sui, C., Finch, J.A., 2002. Sphalerite activation and surface Pb ion concentration. Int J Miner Process 67, 43–58. https://doi.org/10.1016/S0301-7516(02)00005-4

Rumball, J.A., Richmond, G.D., 1996. Measurement of oxidation in a base metal flotation circuit by selective leaching with EDTA. Int J Miner Process 48, 1–20. https://doi.org/10.1016/s0301-7516(96)00010-5

Schindler, M., Santosh, M., Dotto, G., Silva, L.F.O., Hochella, M.F., 2021. A review on Pb-bearing nanoparticles, particulate matter and colloids released from mining and smelting activities. Gondwana Research. https://doi.org/10.1016/j.gr.2021.07.011

Seng, S., Tabelin, C.B., Makino, Y., Chea, M., Phengsaart, T., Park, I., Hiroyoshi, N., Ito, M., 2019. Improvement of flotation and suppression of pyrite oxidation using phosphate-enhanced galvanic microencapsulation (GME) in a ball mill with steel ball media. Miner Eng 143, 105931. https://doi.org/10.1016/j.mineng.2019.105931

Shirley, D.A., 1972. High-Resolution X-Ray Photoemission Spectrum of the Valence Bands of Gold. Phys Rev B 5, 4709–4714. https://doi.org/10.1103/PhysRevB.5.4709

Silwamba, M., Ito, M., Hiroyoshi, N., Tabelin, C.B., Fukushima, T., Park, I., Jeon, S., Igarashi, T., Sato, T., Nyambe, I., Chirwa, M., Banda, K., Nakata, H., Nakayama, S., Ishizuka, M., 2020a. Detoxification of lead-bearing zinc plant leach residues from Kabwe, Zambia by coupled extraction-cementation method. J Environ Chem Eng 8, 104197. https://doi.org/10.1016/J.JECE.2020.104197

Silwamba, M., Ito, M., Hiroyoshi, N., Tabelin, C.B., Hashizume, R., Fukushima, T., Park, I., Jeon, S., Igarashi, T., Sato, T., Chirwa, M., Banda, K., Nyambe, I., Nakata, H., Nakayama, S., Ishizuka, M., 2020b. Recovery of Lead and Zinc from Zinc Plant Leach Residues by Concurrent Dissolution-Cementation Using Zero-Valent Aluminum in Chloride Medium. Metals 2020, Vol. 10, Page 531 10, 531. https://doi.org/10.3390/MET10040531

Silwamba, M., Ito, M., Hiroyoshi, N., Tabelin, C.B., Hashizume, R., Fukushima, T., Park, I., Jeon, S., Igarashi, T., Sato, T., Nyambe, I., Nakata, H., Nakayama, S., Ishizuka, M., 2022. Alkaline Leaching and Concurrent Cementation of Dissolved Pb and Zn from Zinc Plant Leach Residues. Minerals 2022, Vol. 12, Page 393 12, 393. https://doi.org/10.3390/MIN12040393

Silwamba, M., Ito, M., Tabelin, C.B., Park, I., Jeon, S., Takada, M., Kubo, Y., Hokari, N., Tsunekawa, M., Hiroyoshi, N., 2021. Simultaneous extraction and recovery of lead using citrate and micro-scale zero-valent iron for decontamination of polluted shooting range soils. Environmental Advances 5, 100115. https://doi.org/10.1016/J.ENVADV.2021.100115

Tabelin, C.B., Corpuz, R.D., Igarashi, T., Villacorte-Tabelin, M., Ito, M., Hiroyoshi, N., 2019. Hematite-catalysed scorodite formation as a novel arsenic immobilisation strategy under ambient conditions. Chemosphere 233, 946–953. https://doi.org/10.1016/j.chemosphere.2019.06.020

Tabelin, C.B., Park, I., Phengsaart, T., Jeon, S., Villacorte-Tabelin, M., Alonzo, D., Yoo, K., Ito, M., Hiroyoshi, N., 2021. Copper and critical metals production from porphyry ores and E-wastes: A review of resource availability, processing/recycling challenges, socio-environmental aspects, and sustainability issues. Resour Conserv Recycl 170, 105610. https://doi.org/10.1016/J.RESCONREC.2021.105610

Taylor, J.A., Perry, D.L., 1998. An x-ray photoelectron and electron energy loss study of the oxidation of lead. Journal of Vacuum Science & Technology A: Vacuum, Surfaces, and Films 2, 771. https://doi.org/10.1116/1.572569

Trahar, W.J., Senior, G.D., Heyes, G.W., Creed, M.D., 1997. The activation of sphalerite by lead — a flotation perspective. Int J Miner Process 49, 121–148. https://doi.org/10.1016/S0301-7516(96)00041-5

WBG, 2020. Minerals for Climate Action: The Mineral Intensity of the Clean Energy Transition [WWW Document]. URL https://pubdocs.worldbank.org/en/961711588875536384/Minerals-for-Climate-Action-The-Mineral-Intensity-of-the-Clean-Energy-Transition.pdf (accessed 4.25.22).

Wills, B.A., Finch, J.A., 2016. Mineral processing technology: an introduction to the practical aspects of ore treatment and mineral recovery, 8th ed.

Woodcock, J.T., Sparrow, G.J., Bruckard, W.J., Johnson, N.W., Dunne, R., 2007. Plant Practice: Sulfide Minerals and Precious Metals, in: Froth Flotation A Century of Innovation. pp. 781–844.

Xi, Y., Mallavarapu, M., Naidu, R., 2010. Reduction and adsorption of Pb2+ in aqueous solution by nano-zero-valent iron—A SEM, TEM and XPS study. Mater Res Bull 45, 1361–1367. https://doi.org/10.1016/J.MATERRESBULL.2010.06.046

Zeng, Z., Chen, Z., Qi, H., 2021. Two Processes of Anglesite Formation and a Model of Secondary Supergene Enrichment of Bi and Ag in Seafloor Hydrothermal Sulfide Deposits. J Mar Sci Eng 10, 35. https://doi.org/10.3390/jmse10010035

Zoleta, J.B., Itao, G.B., Resabal, V.J.T., Lubguban, A.A., Corpuz, R.D., Ito, M., Hiroyoshi, N., Tabelin, C.B., 2020. Improved pyrolysis behavior of ammonium polyphosphate-melamine-expandable (APP-MEL-EG) intumescent fire retardant coating system using ceria and dolomite as additives for I-beam steel application. Heliyon 6, e03119. https://doi.org/10.1016/J.HELIYON.2019.E03119

CHAPTER 3 – ALTERNATIVE EXTRACTANTS OF ANGLESITE TO EDTA USING AMMONIUM ACETATE AND SODIUM CHLORIDE-HYDROCHLORIC ACID

3.1 Introduction

Complex sulfide ores, some of the most important sources of critical metals, are typically composed of several metal sulfide minerals such as chalcopyrite ($CuFeS_2$), galena (PbS), and sphalerite (ZnS). In the mineral processing of complex sulfide ores consisting of Cu-Pb-Zn sulfide minerals, flotation has been commonly adopted to produce concentrates of each mineral (Bilal et al., 2022a, 2021; Hornn et al., 2021, 2020a, 2020b, 2020c; Park et al., 2021a, 2020a, 2020b; Seng et al., 2019b). Some complex sulfide ores contain not only PbS but also anglesite ($PbSO_4$), the presence of which is problematic for the separation of Cu, Pb, and Zn by flotation due to the unwanted activation of ZnS by Pb^{2+} released from $PbSO_4$ (Aikawa et al., 2021; Ministry of Economic and Japan Oil, 2018; Zeng et al., 2021). In the general flotation circuit of Cu-Pb-Zn sulfide ores, Cu and Pb sulfides are first recovered as froth, and then ZnS is recovered with the assistance of activators (e.g., $CuSO_4$) (Wills and Finch, 2016; Woodcock et al., 2007). When $PbSO_4$ is contained in complex sulfide ores, however, Pb^{2+} is readily released from $PbSO_4$ during conditioning and/or flotation due to its higher solubility compared to PbS—the solubility product (K_{sp}) of $PbSO_4$ and PbS is $10^{-7.79}$ and $10^{-26.77}$, respectively (Ball and Nordstrom, 1991)—and activates the surface of ZnS via the formation of PbS-like compounds, as illustrated in Equation (3-1) (Laskowski et al., 1997; Rashchi et al., 2002a);

$$ZnS(s) + Pb^{2+} = PbS(s) + Zn^{2+} \quad (3\text{-}1)$$

The activation of ZnS by Pb^{2+} is known to increase the ZnS floatability because of a higher affinity of PbS-like compounds for xanthate compared to ZnS (Aikawa et al., 2020; Houot and Raveneau, 1992; Trahar et al., 1997). As a result, ZnS is recovered as froth together with $CuFeS_2$ and PbS, making their separation difficult (Aikawa et al., 2021). Therefore, a proper way of depressing ZnS floatability during flotation of complex sulfide ores containing $PbSO_4$ should be established.

In addition, $PbSO_4$ is typically distributed into flotation tailings because it has poor affinity for the collector (e.g., xanthate) (Fuerstenau et al., 1987; Rashchi et al., 2005). The disposal of $PbSO_4$ into tailings storage facilities (TSFs) would cause lead pollution in the surrounding environment (Schindler et al., 2021; Silwamba et al., 2022). That is, the presence of $PbSO_4$ in complex sulfide ores would cause not only difficulties in the separation of ZnS from Cu and Pb sulfide minerals but also lead pollution in the surrounding environment of TSFs.

To address these problems, Aikawa et al. (2022a) developed a sustainable process for complex sulfide ores containing anglesite by combining extraction, flotation, and cementation. Firstly,

removal of $PbSO_4$ from the ores is conducted by extracting $PbSO_4$ with ethylene diamine tetra acetic acid (EDTA) as a pretreatment of flotation. After solid-liquid separation, residues containing valuable minerals are fed to flotation and filtrate containing extracted Pb^{2+} is treated using cementation to recover extracted Pb^{2+} as zero-valent Pb (Pb^0). Secondly, in flotation, zinc sulfate and sodium sulfite are used as depressants for sphalerite and extraction of $PbSO_4$ prior to flotation is effective to enhance Cu/Zn separation by depressing sphalerite floatability. Cementation is one of the effective methods to recover metal ions as zero-valent metals using the difference in standard redox potentials of the interacting metals and their ions. Finally, extracted Pb^{2+} by EDTA is recovered as Pb^0 using zero-valent iron as a reductant (Equation (3-2)), which will not only add economic value but also protect the environment (Aikawa et al., 2022).

$$Pb(EDTA)^{2-} + Fe^0 = Pb^0 + EDTA + Fe^{2+} \quad (3\text{-}2)$$

Though (Aikawa et al., 2022) achieved the improved Cu/Zn separation by extracting $PbSO_4$ using EDTA, EDTA has some disadvantages such as its excessive cost, low selectivity, corrosiveness, difficulty in reuse due to its ability to form complexes with metal ions (e.g., ferrous dissolved from ZVI). For the application of the process combined with extraction, flotation, and cementation, alternative extractants of anglesite to EDTA is necessary to overcome these disadvantages of EDTA. In this study, the applicability of ammonium acetate and sodium chloride-hydrochloric acid was investigated as alternative extractants of anglesite to EDTA.

3.2 Materials and methods

3.2.1 Materials

Sphalerite (ZnS) and $PbSO_4$ samples used in this study are the same as Aikawa et al., 2022. In preparation for the flotation experiments, ZnS was ground by a vibratory disc mill (RS 200, Retsch Inc., Germany) and screened to obtain a size fraction of –75+38 μm.

For the flotation experiments, potassium amyl xanthate (KAX, Tokyo Chemical Industry Co., Ltd., Japan) and methyl isobutyl carbinol (MIBC, FUJIFILM Wako Pure Chemical Corporation, Tokyo, Japan) were used as collector and frother, respectively. Zinc sulfate ($ZnSO_4$) and sodium sulfite (Na_2SO_3) purchased from FUJIFILM Wako Pure Chemical Corporation (Japan) were used as depressants for ZnS. Sulfuric acid (H_2SO_4, FUJIFILM Wako Pure Chemical Corporation, Japan) and sodium hydroxide (NaOH, FUJIFILM Wako Pure Chemical Corporation, Japan) were used as pH adjusters. For the extraction experiments and coupled extraction-cementation, ethylene diamine tetra acetic acid (EDTA, FUJIFILM Wako Pure Chemical Corporation, Osaka, Japan), ammonium acetate (CH_3COONH_4, FUJIFILM Wako Pure Chemical Corporation, Japan) or sodium chloride (NaCl,

FUJIFILM Wako Pure Chemical Corporation, Japan) acidified with hydrochloric acid (HCl, FUJIFILM Wako Pure Chemical Corporation, Japan) were used.

For the cementation experiments and coupled extraction-cementation, zero-valent Fe (ZVI) powder (Fe^0, –45 μm, FUJIFILM Wako Pure Chemical Corporation, Japan) was used as a reductant.

3.2.2 Experimental methods

3.2.2.1 Extraction of anglesite

Extraction experiments of anglesite were conducted in 50-mL Erlenmeyer flasks containing 0.1−1.0 g of the lead mineral and the solution containing 0.5 M of EDTA (natural pH: 11.3), 0−6.5 M of CH_3COONH_4, or 0−5.0 M of NaCl acidified with 0.1 M of HCl (NaCl-HCl) (solid/liquid ratio: 0.1−1 g/10 mL). The flasks were shaken in a thermostat water bath shaker at a shaking speed of 120 rpm and amplitude of 40 mm at 25 °C. After this, the leachates were collected by filtration using 0.2 μm syringe-driven membrane filters and immediately analyzed using ICP-AES to measure the concentration of dissolved Pb. The experiments were done in triplicates to ascertain that the differences observed were statistically significant, and the extraction efficiency of lead (E_{Pb}) was calculated using the following equation.

$$E_{Pb} = \frac{[Pb]_i}{[Pb]_{tot}} \times 100 \quad (3\text{-}3)$$

where $[Pb]_{tot}$ and $[Pb]_i$ are total Pb (mM) and extracted Pb (mM), respectively.

3.2.2.2 Cementation experiments of extracted Pb^{2+}

Cementation experiments of Pb^{2+} extracted from $PbSO_4$ were conducted in 50-mL Erlenmeyer flasks. A 10 mL of the leachate obtained after extraction experiment was added to the flask, and ultrapure nitrogen gas (N_2; 99.99%) was introduced for 15 min to remove dissolved oxygen (DO) in the leachate. Then, a known amount of ZVI was added to the flask, and N_2 was further introduced for 5 min. The flask was tightly capped with a silicon rubber plug and parafilm, and shaken in a thermostat water bath shaker at a shaking speed of 120 rpm and amplitude of 40 mm at 25 °C. After this, the leachate was filtered using a 0.2 μm syringe-driven membrane filter, and the filtrate was immediately analyzed using ICP-AES to measure the concentration of dissolved Pb. Meanwhile, the residue was washed thoroughly with distilled water, dried in a vacuum drying oven at 40 °C and analyzed by a scanning electron microscopy with energy-dispersive X-ray spectroscopy (SEM-EDS, JSM-IT200TM, JEOL Co., Ltd., Japan). The experiments were done in triplicate to ascertain that the differences observed were statistically significant. The Pb recovery (R_{Pb}) was calculated using the following equation.

$$R_{Pb} = \frac{[Pb]_I - [Pb]_F}{[Pb]_I} \times 100 \quad (3\text{-}3)$$

where $[Pb]_I$ and $[Pb]_F$ are the initial and final concentrations of Pb (mM) in the leachate, respectively.

3.2.2.3 Coupled extraction-cementation experiments

Coupled extraction-cementation (CEC, described in section 3.3) experiments were conducted in 50-mL Erlenmeyer flasks. A 10 mL of NaCl-HCl was added to the flask, and N_2 was introduced for 15 min to remove DO. Then, 0.5 g of $PbSO_4$ and 0.5 g of ZVI was added to the flask, and N_2 was further introduced for 5 min. The flask was tightly capped with a silicon rubber plug and parafilm, and shaken in a thermostat water bath shaker at a shaking speed of 120 rpm and amplitude of 40 mm at 25 °C. After this, magnetic Pb-loaded ZVI was recovered from the pulp using a handheld 0.6 T magnet. The magnetic fractions were then thoroughly washed with distilled water and dried in a vacuum drying oven at 40 ºC for 24 h. After drying, the magnetic fractions were digested using aqua regia in a microwave-assisted acid digester (Ethos Advanced Microwave Lab station, Milestone Inc., USA) and the leachates were analyzed for Pb by ICP-AES. Meanwhile, the leachate was filtered using a 0.2 μm syringe-driven membrane filter, and the filtrate was immediately analyzed using ICP-AES to measure the concentration of dissolved Pb.

Distribution of Pb to magnetic fraction (R_{mag}), solution (R_{sol}), and residue (R_{res}) after treatment was calculated according to Eqs. (3-4) to (3-6).

$$R_{mag} = \frac{M_{mag} \times W_{mag}}{M_{total}} \times 100 \quad (3\text{-}4)$$

$$R_{sol} = \frac{C_{sol} \times V_{sol}}{M_{total}} \times 100 \quad (3\text{-}5)$$

$$R_{res} = 100 - R_{mag} - R_{sol} \quad (3\text{-}6)$$

where M_{total} is the mass of total Pb (g), M_{mag} is the mass of magnetic fraction (g) and W_{mag} is the ratio of Pb in magnetic fraction, C_{sol} is the Pb concentration in solution (g/L) and V_{sol} is the volume of the solution (L).

3.2.2.4 Flotation experiments

The flotation experiments were carried out using an agitator-type flotation machine (ASH-F30H, Kankyo-kanri Engineering, Akita, Japan) equipped with a 400 mL flotation cell under the following conditions: pH, 6.5; temperature, 25 °C; pulp density, 5%; impeller speed, 1000 rpm; air flow rate, 1 L/min. In a 500 mL beaker, a model sample containing 15 g of ZnS and 5 g of $PbSO_4$ was suspended in 300 mL of distilled water, and the supernatant was decanted to remove fine particles (<38 μm).

After desliming, a model sample was repulped to 400 mL with distilled water in the flotation cell and conditioned for 3 min after adding the following reagents in sequence: ~5 kg/t of $ZnSO_4$ (100 ppm Zn^{2+}), 1 kg/t of Na_2SO_3, 20 g/t of KAX, and 20 μL/L of MIBC. Afterwards, air was introduced at a flowrate of 1 L/min, and froth was recovered for 3 min. The recovered froth/tailing products were dried at 105 °C for 24 h and analyzed by XRF to determine the recovery of Zn. The experiments were performed in duplicate to ascertain that the differences observed were statistically significant. An aliquot of the pulp of about 5 mL was collected 3 min after adding the depressant, filtered through a 0.2 μm syringe-driven membrane filter, and immediately analyzed using ICP-AES to check the extent of lead activation of ZnS.

In addition, flotation experiments of ZnS/$PbSO_4$ mixture after pretreatment were conducted to check how effective the removal of $PbSO_4$ was on the depression of ZnS floatability. A mixture of 15 g ZnS and 5 g $PbSO_4$ was mixed with 100 mL of a solution containing CH_3COONH_4 3.5 M (i.e., solid/liquid ratio: 20 g/100 mL) and shaken in a thermostat water bath shaker at a shaking speed of 120 rpm and an amplitude of 40 mm at 25 °C for 30 min. After this, the leachate was filtered using a 0.2 μm syringe-driven membrane filter, and the filtrate was immediately analyzed using ICP-AES to measure the concentration of Pb^{2+}. When NaCl 5.0 M acidified with HCl 0.1 M was used, the solution was added to the flask, and N_2 was introduced for 15 min to remove DO. Then, A mixture of 15 g ZnS and 5 g $PbSO_4$ was added to the flask, and N_2 was further introduced for 5 min. The flask was tightly capped with a silicon rubber plug and parafilm and shaken in a thermostat water bath shaker at a shaking speed of 120 rpm and an amplitude of 40 mm at 25 °C. After this, magnetic Pb-loaded ZVI was recovered from the pulp using a handheld 0.6 T magnet. The magnetic fractions were then thoroughly washed with distilled water and dried in a vacuum drying oven at 40 ºC for 24 h. After drying, the magnetic fractions were digested using aqua regia in a microwave-assisted acid digester and the leachates were analyzed for Pb by ICP-AES. Meanwhile, the leachate was filtered using a 0.2 μm syringe-driven membrane filter, and the filtrate was immediately analyzed using ICP-AES to measure the concentration of Pb^{2+} to calculate lead recovery efficiency from ZnS/$PbSO_4$ mixture after treatment was calculated according to Equation 3-4. The residue obtained after pretreatment washed thoroughly with distilled water and deslimed to remove fine particles. After desliming, the residue was repulped to 400 mL with distilled water, and then flotation was conducted under the same conditions mentioned above. An aliquot of the pulp of about 5 mL was also collected 3 min after adding the depressants and filtered through a 0.2 μm syringe-driven membrane filter, and the filtrate was analyzed by ICP-AES.

3.3 Results and discussion

3.3.1 Extraction of $PbSO_4$ using EDTA, CH_3COONH_4, or NaCl-HCl

The extraction experiments of $PbSO_4$ using EDTA, CH_3COONH_4, or NaCl-HCl were conducted at solid-liquid (S/L) ratio of 0.1−1.0 g/10 mL (Figure 3-1). Almost all $PbSO_4$ was extracted by EDTA irrespective to S/L ratio. While the extraction efficiency of $PbSO_4$ using CH_3COONH_4 was 75.1% at S/L ratio of 1.0 g/10 mL, almost all $PbSO_4$ was extracted by CH_3COONH_4 at S/L ratio of 0.1−0.5 g/10 mL. The results of surface analysis using SEM-EDS indicates that the residue after extraction using CH_3COONH_4 at S/L ratio of 1.0 g/10 mL is most likely $PbSO_4$ (Figure 3-1). Extraction of $PbSO_4$ with CH_3COONH_4 would occur illustrated in Equation 3-7.

$$PbSO_4 + 2CH_3COO^- = Pb(CH_3COO)_2(aq) + SO_4^{2-} \quad (3\text{-}7)$$

NaCl-HCl extracted almost all $PbSO_4$ only at the S/L ratio = 0.1 g/10 mL, and Pb extraction was low at the S/L ratio = 0.5−1.0 g/10 mL. Extraction of $PbSO_4$ with Cl^- would occur illustrated in Equation 3-8 to 3-11 (Farahmand et al., 2009; Zhang et al., 2019).

$$PbSO_4 + Cl^- = PbCl^+ + SO_4^{2-} \quad (3\text{-}8)$$

$$PbCl^+ + Cl^- = PbCl_2 \downarrow \quad (3\text{-}9)$$

$$PbCl_2 + Cl^- = PbCl_3^- \quad (3\text{-}10)$$

$$PbCl_3^- + Cl^- = PbCl_4^{2-} \quad (3\text{-}11)$$

Figure 3-2 shows the extraction efficiency of Pb^{2+} and SO_4^{2-} after 24 h with NaCl 5 M acidified with HCl 0.1 M at various S/L ratios. As can be seen, almost all SO_4^{2-} was released from $PbSO_4$ regardless of S/L ratios, but Pb^{2+} extraction decreased at > 0.5 g/10 mL. This indicates that although almost all $PbSO_4$ dissolved, some portion of dissolved Pb was precipitated at higher S/L ratios. The results of surface analysis of the residue after extraction for 24 h with NaCl 5 M acidified with HCl 0.1 M. at S/L ratio = 1.0 g/10 mL using SEM-EDS (Figure 3-3) suggests that the residue would be $PbCl_2$. This deduction was supported by thermodynamic considerations at a $[Cl^-] = 10^{0.51}$ calculated from the initial concentration of Cl^- (Figure 3-4). To improve Pb extraction, the coupled extraction-cementation (CEC) method was applied in Section 3.3.

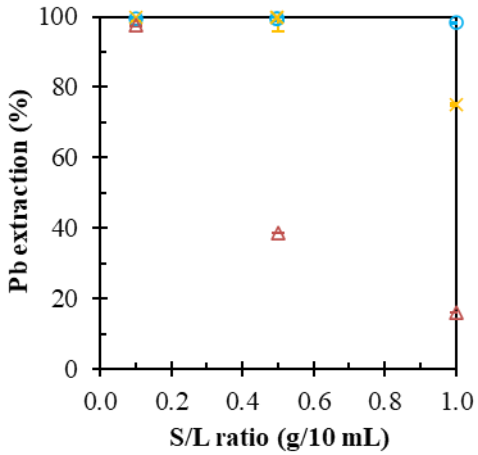

Figure 3-1. The extraction efficiency of Pb after 24 h with EDTA 0.5 M (circle), CH_3COONH_4 6.5 M (cross), and NaCl 5.0 M acidified with HCl 0.1 M (triangle).

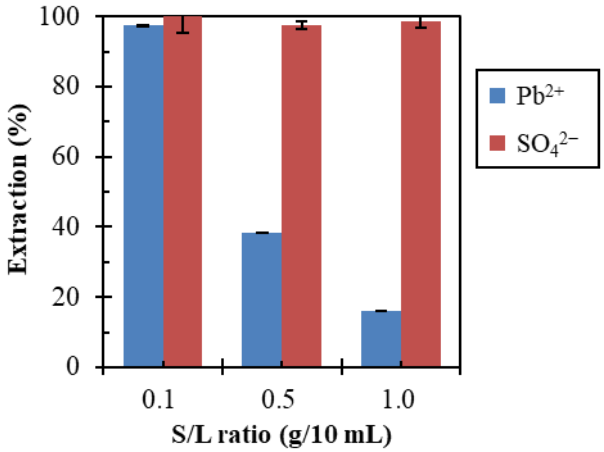

Figure 3-2. The extraction efficiency of Pb^{2+} and SO_4^{2-} after 24 h with NaCl 5.0 M acidified with HCl 0.1 M.

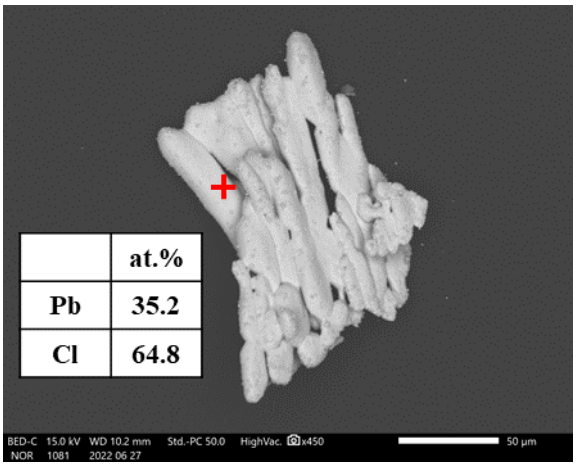

Figure 3-3. SEM photomicrograph of the residue after extraction with NaCl 5 M acidified with HCl 0.1 M 24 h at S/L ratio = 1.0 g/10 mL

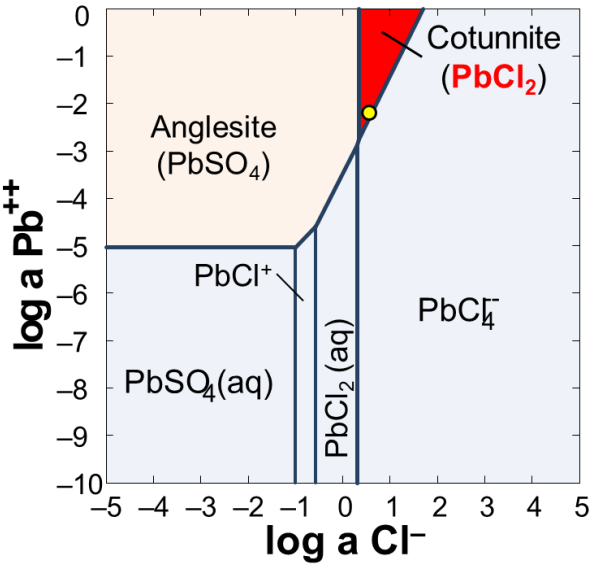

Figure 3-4. A diagram of log $a_{Pb^{2+}}$ vs log a_{Cl^-} at pH 0.64 and 25℃ created using the Geochemist's Workbench® with the MINTEQ database (Gustaffson, 2013).

3.3.2 Extraction of $PbSO_4$ using CH_3COONH_4 and recovery of extracted Pb^{2+} as zero-valent Pb by cementation using zero-valent Fe

Figure 3-5 shows the extraction efficiency of $PbSO_4$ after 24 h with different concentrations of CH_3COONH_4 (0−6.5 M). When the concentration is higher than 3.5 M, almost all $PbSO_4$ was extracted within 30 min.

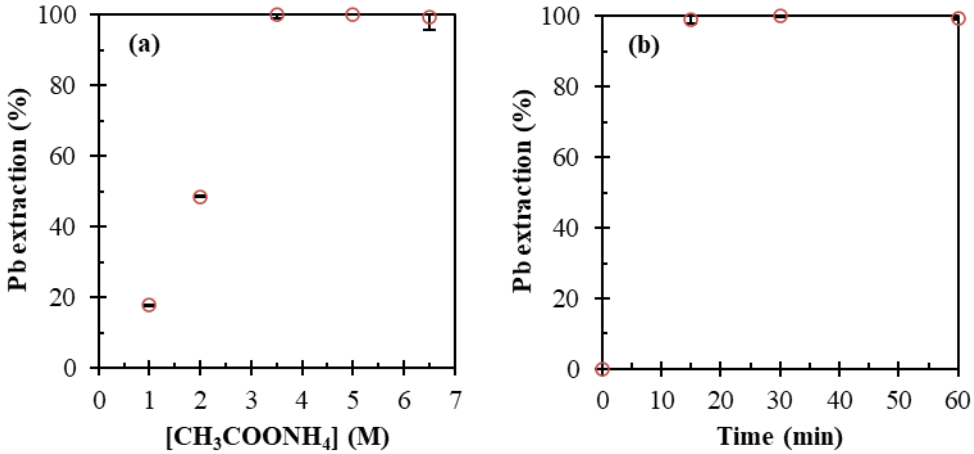

Figure 3-5. The extraction efficiency of Pb (a) after 24 h with different concentrations of CH_3COONH_4 (0−6.5 M), (b) after .0−60 min with CH_3COONH_4 3.5 M.

Cementation experiments were carried out using ZVI powder as a reductant to recover extracted Pb^{2+} as zero-valent Pb. Figure 3-6 shows the effects of the ZVI addition and cementation time on recovery of extracted Pb^{2+} in the leachate after $PbSO_4$ extraction using CH_3COONH_4 3.5 M for 30 min. Almost all extracted Pb^{2+} was recovered with more than 0.1 g of ZVI for 24 h, and with ZVI 0.5 g within 1 h. To confirm the recovery of Pb^{2+} on ZVI, the residue obtained from the cementation experiment using 1 g/10 mL of ZVI for 24 h was analyzed using SEM-EDS (Figure 3-7), suggesting that the extracted Pb^{2+} was reductively deposited on ZVI via the cementation reaction:

$$Pb(CH_3COO)_2(aq) + Fe^0 = Pb^0 + 2CH_3COO^- + Fe^{2+} \quad (3\text{-}12)$$

The elemental mapping of O suggests that the presence of O was due most likely to the oxidation of Pb^0 and ZVI surface during drying and storing of the sample (Silwamba et al., 2020a; Taylor and Perry, 1998; Xi et al., 2010).

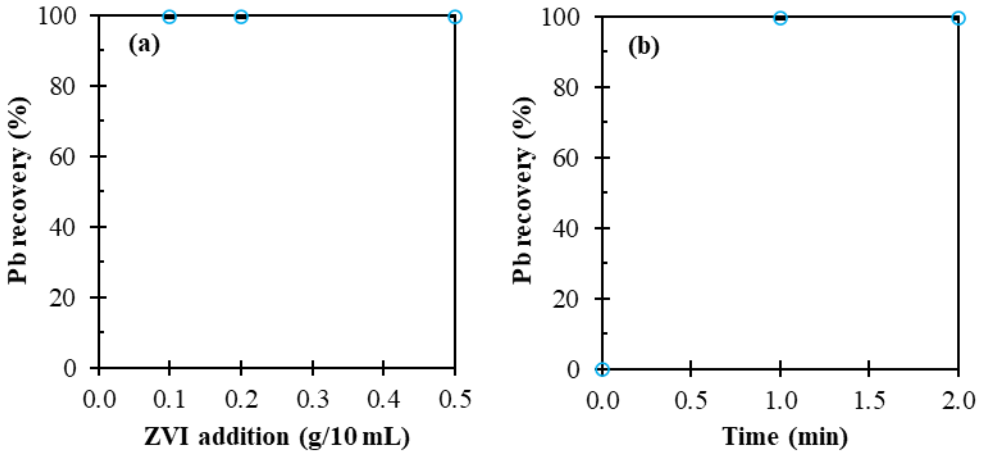

Figure 3-6. The Pb recovery in the leachate after $PbSO_4$ extraction using CH_3COONH_4 3.5 M for 30 min (a) after 24 h with different amount of ZVI (0.1−0.5 g/10 mL), (b) after 0−2 h with ZVI 0.5 g/10 mL.

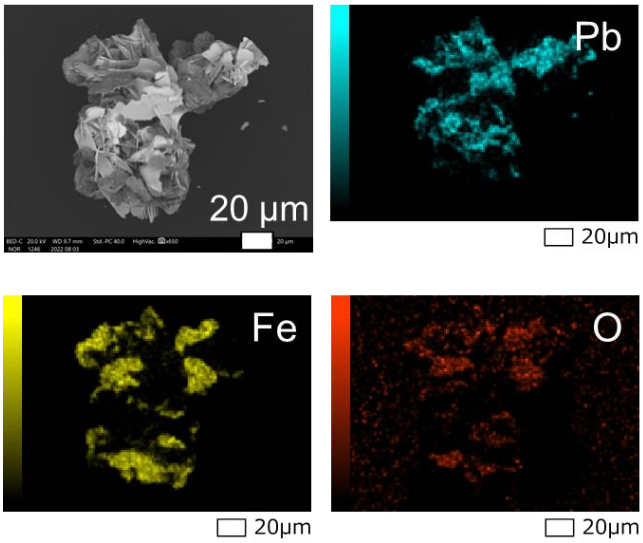

Figure 3-7. SEM photomicrograph of the residue of the cementation experiment using 0.5 g/10 mL of ZVI for 24 h with the corresponding elemental maps of Fe, Pb, and O.

3.3.4 Coupled Extraction-Cementation of $PbSO_4$ using NaCl-HCl and zero-valent Fe

As discussed in section 3.1, when $PbSO_4$ is extracted with NaCl-HCl, it was suggested that almost all $PbSO_4$ is dissolved but some portion of dissolved Pb precipitates as $PbCl_2$. Based on the thermodynamics calculation (Figure 3-4), increasing the activity of Cl^- and/or decreasing the activity of Pb^{2+} are necessary to prevent the precipitate of $PbCl_2$ and completely extract Pb species as $PbCl_4^{2-}$. To address these problems, the coupled extraction-cementation (CEC) method using ZVI as a reductant was applied for extraction of $PbSO_4$ using NaCl-HCl. The CEC is a technique that

combines two processes: extraction by NaCl-HCl and recovery of extracted metals on ZVI (Silwamba et al., 2020). Once metals are extracted by NaCl-HCl, the extracted metals are soon reductively deposited on ZVI by cementation. Therefore, this process could keep the concentration of Pb^{2+} lower than its saturation concentration in the chloride system.

Figure 3-8 shows effects of NaCl concentration and time on distribution of Pb in ZVI, residues, and solution after the CEC experiments. Almost all Pb was recovered on ZVI after CEC experiments for 24 h irrespective of NaCl concentration (0.5−5.0 M) (Figure 3-8a). As can be seen in Figure 3-8b, while almost all Pb was recovered on ZVI for 1 h, ~20 % of extracted Pb^{2+} remained in solution for 0.5 h. To confirm the recovery of extracted Pb^{2+} on ZVI, the magnetic fraction obtained from the CEC experiment using NaCl 5.0 M for 24 h was analyzed using SEM-EDS. As shown in Figure 3-9, the deposition of Pb compounds on ZVI was observed, suggesting that the extracted Pb^{2+} was reductively deposited on ZVI via the cementation reaction:

$$PbCl_4^{2-} + Fe^0 = Pb^0 + 4Cl^- + Fe^{2+} \quad (3\text{-}13)$$

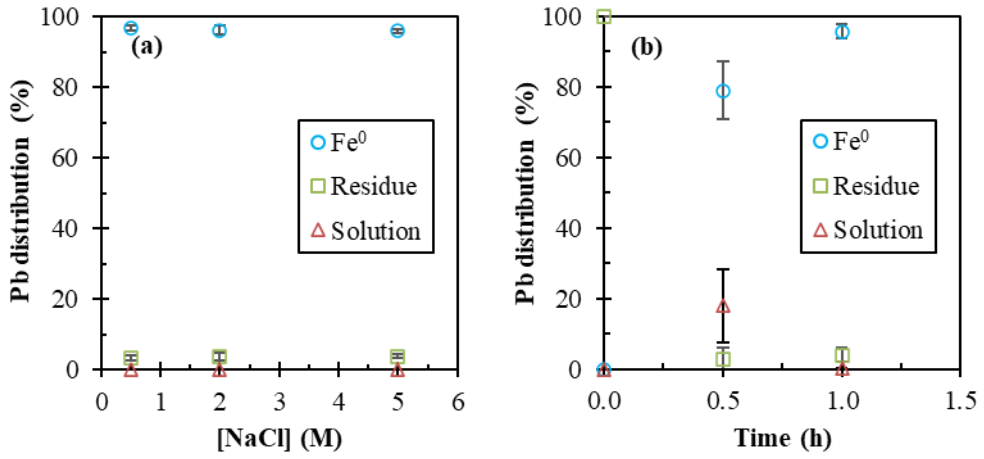

Figure 3-8. Effects of NaCl concentration and time on distribution of Pb in ZVI, residues, and solution: (a) NaCl 0.5−5.0 M for 24 h and (b) NaCl 5.0 M for 0−1 h.

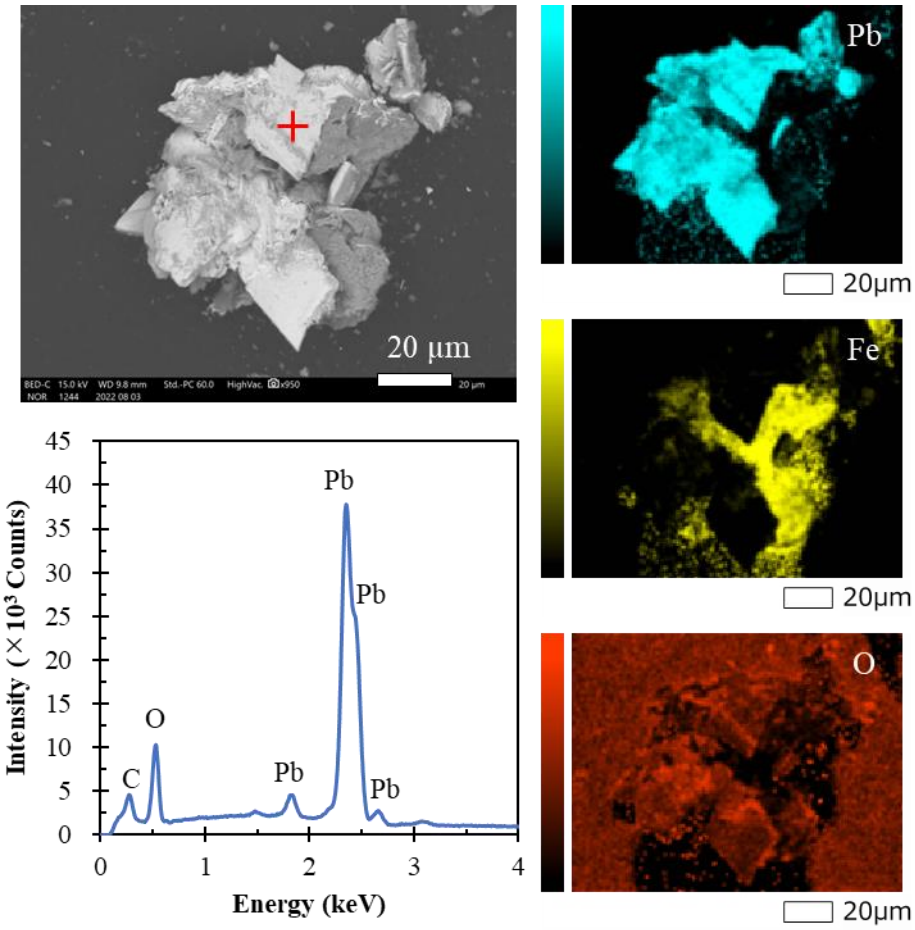

Figure 3-9. SEM photomicrograph and EDS spectrum of the residue of the CEC experiment using NaCl 5.0 M for 24 h with the corresponding elemental maps of Fe, Pb, and O.

3.3.4 Effects of pretreatments on ZnS depression in flotation

As described in Section 3.3.2 and 3.3.3, almost all $PbSO_4$ was extracted with CH_3COONH_4, and almost all $PbSO_4$ was extracted and recovered on ZVI using NaCl-HCl. Therefore, the effects of the pretreatments on ZnS depression in flotation were investigated. Flotation experiments using model samples (ZnS/$PbSO_4$ mixture) with and without the pretreatments were conducted. Prior to the flotation experiments, the mixture of 15 g ZnS and 5 g $PbSO_4$ was treated with 3.5 M of CH_3COONH_4 for 30 min or 5 M of NaCl acidified with 0.1 M of HCl and 0.5 g of ZVI for 1 h, and then flotation experiments were conducted with ~5 kg/t $ZnSO_4$ (100 ppm Zn^{2+}) and 1 kg/t Na_2SO_3 as depressants. The flotation results shows that the floatability of ZnS was clearly depressed from ~82% to ~6.7% and 1.8% with pretreatments using CH_3COONH_4 or NaCl-HCl, respectively (Figure 3-10).

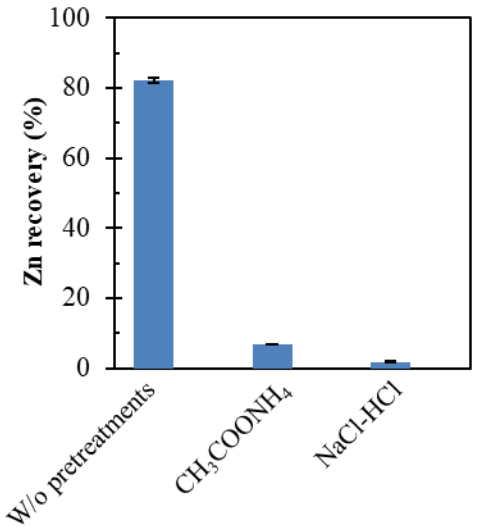

Figure 3-10. Effects of pretreatments using CH_3COONH_4 or NaCl on the floatability of ZnS in the presence of $PbSO_4$: (a) W/o pretreatments, (b) w/ a pretreatment using CH_3COONH_4, and (c) w/ a pretreatment using NaCl-HCl.

To confirm the depression of ZnS floatability with the pretreatments, pretreated samples reacted with $ZnSO_4$ for 3min and Na_2SO_3 for 3 min, a ~5 mL aliquot of the flotation pulp were collected , and the filtrate was analyzed by ICP-AES. The concentration of Pb^{2+} in the filtrate without the pretreatment was 3.3 ppm which decreased to 0.09 ppm and 0.20 ppm with pretreatments using CH3COONH4 or NaCl-HCl, respectively. On the other hand, the concentrations of Zn^{2+} in the filtrates without the pretreatment and with pretreatments using CH3COONH4 or NaCl-HCl showed 96.5, 95.4, and 95.2 ppm, respectively. Based on thermodynamics calculation using Equation(3-14), the possibility of lead activation of ZnS (Equation (3-1)) could be evaluated using the measured values of Pb^{2+} and Zn^{2+} (Aikawa et al., 2021; Basilio et al., 1996; El-Shall et al., 2000). The changes in free energy were calculated using measured values of Pb^{2+} and Zn^{2+} concentrations.

Table **3-1** showed that the calculated results of the changes in free energy based on the equilibrium constants of lead activation of ZnS (Equation (3-1)). The change in free energy without the pretreatment was negative while those with pretreatments using CH_3COONH_4 or NaCl-HCl were positive. When the change in free energy is positive, the reverse reaction of lead activation (Equation (3-1)) would occur spontaneously, indicating that lead activation would be limited by the pretreatment. These results support the flotation results that the depression of ZnS floatability was achieved by the pretreatments which decreases Pb^{2+} concentration during flotation by extracting $PbSO_4$ in advance.

$$\Delta G = -RT \ln K + \ln(Zn^{2+}/Pb^{2+}) \quad (3\text{-}14)$$

$$K = \frac{K_{sp}^{ZnS}}{K_{sp}^{PbS}} \quad (3\text{-}15)$$

Table 3-1. Calculation results of the change in free energy without pretreatments or with CH_3COONH_4 or NaCl-HCl pretreatment.

K	ΔG (kJ/mol) Without pretreatments	ΔG (kJ/mol) With CH_3COONH_4 pretreatment	ΔG (kJ/mol) With NaCl-HCl pretreatment
1000[a]	–5.9	3.1	1.2
704[b]	–5.1	4.0	2.1
1059[c]	–6.1	2.9	1.0
1127[d]	–6.2	2.8	0.9

[a] The equilibrium constant was referred from the previous study (El-Shall et al., 2000).

[b, c, d] The equilibrium constants were calculated using Equation (3-15) by the reported K_{sp} values of ZnS and PbS, respectively (Helgeson, 1969; Latimer, 1952; Leckie and James, 1974).

3.3.5 Implication of this study

In this study, alternative extractants of anglesite to EDTA using ammonium acetate and sodium chloride-hydrochloric acid for a sustainable process combined with Extraction, Flotation, and Cementation for complex sulfide ores containing anglesite were investigated. When CH_3COONH_4 is used instead of EDTA, the pretreatment can be applied to grinding systems (e.g., ball milling). The crushed samples obtained after CH_3COONH_4 pretreatment is fed to a flotation stage where ZnS floatability is effectively depressed by the conventional depressant for ZnS due to the decrease in the ratio of Pb^{2+}/Zn^{2+} of the flotation pulp.

When NaCl-HCl is used instead of EDTA, the crushed samples are treated with NaCl-HCl and ZVI followed by magnetic separation to recover Pb-loaded ZVI. The non-magnetic slurry is fed to a flotation stage where ZnS floatability is effectively depressed by the conventional depressant for ZnS due to the decrease in the ratio of Pb^{2+}/Zn^{2+} of the flotation pulp. Figure 3-1 shows that $PbSO_4$ was extracted and recovered on ZVI for 24 h using 0.5 M of NaCl acidified with 0.1 M of HCl, indicating that sea water having ~0.5 M of Cl can be used as an extractant of $PbSO_4$.

3.4 Conclusions

In this chapter, pretreatments of flotation using CH_3COONH_4 or NaCl-HCl to extract $PbSO_4$ for prevention of lead pollution the surrounding environment of tailings dam and depression of ZnS

floatability combined with recovery of extracted Pb^{2+} by cementation or CEC was investigated, and the findings of this study are summarized as follows:

1. Almost all $PbSO_4$ (> 99%) was extracted using CH_3COONH_4, and >99% of extracted Pb^{2+} could be recovered as Pb^0 by cementation using ZVI.

2. Almost all $PbSO_4$ (> 97%) was extracted and recovered on ZVI as Pb^0 by the coupled extraction-cementation method using NaCl-HCl as an extractant of $PbSO_4$ and ZVI as a reductant.

3. Pretreatments of flotation extracting $PbSO_4$ using CH_3COONH_4 or NaCl-HCl was effective in depressing ZnS floatability, indicating that CH_3COONH_4 and NaCl-HCl can be used instead of EDTA for the extraction of $PbSO_4$ to depress the floatability of ZnS.

References

Aikawa, K., Ito, M., Kusano, A., Jeon, S., Park, I., Hiroyoshi, N., 2022. Development of a Sustainable Process for Complex Sulfide Ores Containing Anglesite: Effect of Anglesite on Sphalerite Floatability, Enhanced Depression of Sphalerite by Extracting Anglesite, and Recovery of Extracted Pb2+ as Zero-Valent Pb by Cementation Using Zero-Valent Fe. Minerals 12, 723. https://doi.org/10.3390/min12060723

Aikawa, K., Ito, M., Kusano, A., Park, I., Oki, T., Takahashi, T., Furuya, H., Hiroyoshi, N., 2021. Flotation of Seafloor Massive Sulfide Ores: Combination of Surface Cleaning and Deactivation of Lead-Activated Sphalerite to Improve the Separation Efficiency of Chalcopyrite and Sphalerite. Metals (Basel) 11, 253. https://doi.org/10.3390/met11020253

Aikawa, K., Ito, M., Segawa, T., Jeon, S., Park, I., Tabelin, C.B., Hiroyoshi, N., 2020. Depression of lead-activated sphalerite by pyrite via galvanic interactions: Implications to the selective flotation of complex sulfide ores. Miner Eng 152, 106367. https://doi.org/10.1016/j.mineng.2020.106367

Ball, J.W., Nordstrom, D.K., 1991. User's manual for WATEQ4F, with revised thermodynamic data base and text cases for calculating speciation of major, trace, and redox elements in natural waters, U.S. Geological Survey Water-Resources Investigations Report. Reston, VA, USA. https://doi.org/10.3133/ofr91183

Basilio, C.I., Kartio, I.J., Yoon, R.-H., 1996. Lead activation of sphalerite during galena flotation. Miner Eng 9, 869–879. https://doi.org/10.1016/0892-6875(96)00078-7

Bilal, M., Ito, M., Akishino, R., Bu, X., Ul Hassan, F., Park, I., Jeon, S., Aikawa, K., Hiroyoshi, N., 2022. Heterogenous carrier flotation technique for recovering finely ground chalcopyrite

particles using coarse pyrite particles as a carrier. Miner Eng 180, 107518. https://doi.org/10.1016/j.mineng.2022.107518

Bilal, M., Ito, M., Koike, K., Hornn, V., Ul Hassan, F., Jeon, S., Park, I., Hiroyoshi, N., 2021. Effects of coarse chalcopyrite on flotation behavior of fine chalcopyrite. Miner Eng 163, 106776. https://doi.org/10.1016/J.MINENG.2021.106776

El-Shall, H.E., Elgillani, D.A., Abdel-Khalek, N.A., 2000. Role of zinc sulfate in depression of lead-activated sphalerite. Int J Miner Process 58, 67–75. https://doi.org/10.1016/S0301-7516(99)00055-1

Farahmand, F., Moradkhani, D., Safarzadeh, M.S., Rashchi, F., 2009. Brine leaching of lead-bearing zinc plant residues: Process optimization using orthogonal array design methodology. Hydrometallurgy 95, 316–324. https://doi.org/10.1016/J.HYDROMET.2008.07.012

Fuerstenau, M.C., Olivas, S.A., Herrera-Urbina, R., Han, K.N., 1987. The surface characteristics and flotation behavior of anglesite and cerussite. Int J Miner Process 20, 73–85. https://doi.org/10.1016/0301-7516(87)90018-4

Goal 13 | Department of Economic and Social Affairs [WWW Document], n.d. URL https://sdgs.un.org/goals/goal13 (accessed 4.26.22).

Gustaffson, J.P., 2013. Visual MINTEQ – a free equilibrium speciation model [WWW Document]. Visual MINTEQ. URL https://vminteq.lwr.kth.se/ (accessed 1.7.21).

Hák, T., Janoušková, S., Moldan, B., 2016. Sustainable Development Goals: A need for relevant indicators. Ecol Indic 60, 565–573. https://doi.org/10.1016/j.ecolind.2015.08.003

Helgeson, H.C., 1969. Thermodynamics of hydrothermal systems at elevated temperatures and pressures. Am J Sci 267, 729–804. https://doi.org/10.2475/ajs.267.7.729

Hernan, L., Morales, J., Sanchez, L., Tirado, J.L., Espinos, J.P., Gonzalez Elipe, A.R., 1995. Diffraction and XPS Studies of Misfit Layer Chalcogenides Intercalated with Cobaltocene. Chem. Mater 7, 1576–1582.

Hornn, V., Ito, M., Shimada, H., Tabelin, C.B., Jeon, S., Park, I., Hiroyoshi, N., 2020a. Agglomeration-Flotation of Finely Ground Chalcopyrite and Quartz: Effects of Agitation Strength during Agglomeration Using Emulsified Oil on Chalcopyrite. Minerals 10, 380. https://doi.org/10.3390/min10040380

Hornn, V., Ito, M., Shimada, H., Tabelin, C.B., Jeon, S., Park, I., Hiroyoshi, N., 2020b. Agglomeration–Flotation of Finely Ground Chalcopyrite Using Emulsified Oil Stabilized by Emulsifiers: Implications for Porphyry Copper Ore Flotation. Metals 2020, Vol. 10, Page 912 10, 912. https://doi.org/10.3390/MET10070912

Hornn, V., Ito, M., Yamazawa, R., Shimada, H., Tabelin, C.B., Jeon, S., Park, I., Hiroyoshi, N., 2020c. Kinetic Analysis for Agglomeration-Flotation of Finely Ground Chalcopyrite:

Comparison of First Order Kinetic Model and Experimental Results. Mater Trans 61, 1940–1948. https://doi.org/10.2320/MATERTRANS.M-M2020843

Hornn, V., Park, I., Ito, M., Shimada, H., Suto, T., Tabelin, C.B., Jeon, S., Hiroyoshi, N., 2021. Agglomeration-flotation of finely ground chalcopyrite using surfactant-stabilized oil emulsions: Effects of co-existing minerals and ions. Miner Eng 171, 107076. https://doi.org/10.1016/J.MINENG.2021.107076

Houot, R., Raveneau, P., 1992. Activation of sphalerite flotation in the presence of lead ions. Int J Miner Process 35, 253–271. https://doi.org/10.1016/0301-7516(92)90037-W

Laskowski, J.S., Liu, Q., Zhan, Y., 1997. Sphalerite activation: Flotation and electrokinetic studies. Miner Eng 10, 787–802. https://doi.org/10.1016/S0892-6875(97)00057-5

Latimer, W.M., 1952. The oxidation states of the elements and their potentials in aqueous solutions, 2nd ed.

Leckie, J.O., James, R.O., 1974. Aqueous Environmental Chemistry of Metals. Ann Arbor Science Publishers.

Liu, J., Ejtemaei, M., Nguyen, A. v., Wen, S., Zeng, Y., 2020. Surface chemistry of Pb-activated sphalerite. Miner Eng 145, 106058. https://doi.org/10.1016/J.MINENG.2019.106058

Ministry of Economic, T. and I. (METI), Japan Oil, G. and M.N.C. (JOGMEC), 2018. Summary report on comprehensive evaluations of development plan of seafloor massive sulfide deposits [WWW Document]. URL http://www.jogmec.go.jp/content/300359550.pdf (accessed 2.26.21).

Nansai, K., Nakajima, K., Kagawa, S., Kondo, Y., Suh, S., Shigetomi, Y., Oshita, Y., 2014. Global Flows of Critical Metals Necessary for Low-Carbon Technologies: The Case of Neodymium, Cobalt, and Platinum. Environ Sci Technol 48, 1391–1400. https://doi.org/10.1021/es4033452

Park, I., Hong, S., Jeon, S., Ito, M., Hiroyoshi, N., 2021a. Flotation Separation of Chalcopyrite and Molybdenite Assisted by Microencapsulation Using Ferrous and Phosphate Ions: Part II. Flotation. Metals 2021, Vol. 11, Page 439 11, 439. https://doi.org/10.3390/MET11030439

Park, I., Hong, S., Jeon, S., Ito, M., Hiroyoshi, N., 2020a. Flotation Separation of Chalcopyrite and Molybdenite Assisted by Microencapsulation Using Ferrous and Phosphate Ions: Part I. Selective Coating Formation. Metals (Basel) 10, 1667. https://doi.org/10.3390/met10121667

Park, I., Hong, S., Jeon, S., Ito, M., Hiroyoshi, N., 2020b. A Review of Recent Advances in Depression Techniques for Flotation Separation of Cu–Mo Sulfides in Porphyry Copper Deposits. Metals (Basel) 10, 1269. https://doi.org/10.3390/met10091269

Park, I., Kanazawa, Y., Sato, N., Galtchandmani, P., Jha, M.K., Tabelin, C.B., Jeon, S., Ito, M., Hiroyoshi, N., 2021b. Beneficiation of Low-Grade Rare Earth Ore from Khalzan Buregtei Deposit (Mongolia) by Magnetic Separation. Minerals 11, 1432. https://doi.org/10.3390/min11121432

Rashchi, F., Dashti, A., Arabpour-Yazdi, M., Abdizadeh, H., 2005. Anglesite flotation: a study for lead recovery from zinc leach residue. Miner Eng 18, 205–212. https://doi.org/10.1016/J.MINENG.2004.10.014

Rashchi, F., Sui, C., Finch, J.A., 2002. Sphalerite activation and surface Pb ion concentration. Int J Miner Process 67, 43–58. https://doi.org/10.1016/S0301-7516(02)00005-4

Schindler, M., Santosh, M., Dotto, G., Silva, L.F.O., Hochella, M.F., 2021. A review on Pb-bearing nanoparticles, particulate matter and colloids released from mining and smelting activities. Gondwana Research. https://doi.org/10.1016/j.gr.2021.07.011

Seng, S., Tabelin, C.B., Makino, Y., Chea, M., Phengsaart, T., Park, I., Hiroyoshi, N., Ito, M., 2019. Improvement of flotation and suppression of pyrite oxidation using phosphate-enhanced galvanic microencapsulation (GME) in a ball mill with steel ball media. Miner Eng 143, 105931. https://doi.org/10.1016/j.mineng.2019.105931

Silwamba, M., Ito, M., Hiroyoshi, N., Tabelin, C.B., Fukushima, T., Park, I., Jeon, S., Igarashi, T., Sato, T., Nyambe, I., Chirwa, M., Banda, K., Nakata, H., Nakayama, S., Ishizuka, M., 2020. Detoxification of lead-bearing zinc plant leach residues from Kabwe, Zambia by coupled extraction-cementation method. J Environ Chem Eng 8, 104197. https://doi.org/10.1016/J.JECE.2020.104197

Silwamba, M., Ito, M., Hiroyoshi, N., Tabelin, C.B., Hashizume, R., Fukushima, T., Park, I., Jeon, S., Igarashi, T., Sato, T., Nyambe, I., Nakata, H., Nakayama, S., Ishizuka, M., 2022. Alkaline Leaching and Concurrent Cementation of Dissolved Pb and Zn from Zinc Plant Leach Residues. Minerals 2022, Vol. 12, Page 393 12, 393. https://doi.org/10.3390/MIN12040393

Tabelin, C.B., Park, I., Phengsaart, T., Jeon, S., Villacorte-Tabelin, M., Alonzo, D., Yoo, K., Ito, M., Hiroyoshi, N., 2021. Copper and critical metals production from porphyry ores and E-wastes: A review of resource availability, processing/recycling challenges, socio-environmental aspects, and sustainability issues. Resour Conserv Recycl 170, 105610. https://doi.org/10.1016/J.RESCONREC.2021.105610

Taylor, J.A., Perry, D.L., 1998. An x-ray photoelectron and electron energy loss study of the oxidation of lead. Journal of Vacuum Science & Technology A: Vacuum, Surfaces, and Films 2, 771. https://doi.org/10.1116/1.572569

Trahar, W.J., Senior, G.D., Heyes, G.W., Creed, M.D., 1997. The activation of sphalerite by lead — a flotation perspective. Int J Miner Process 49, 121–148. https://doi.org/10.1016/S0301-7516(96)00041-5

WBG, 2020. Minerals for Climate Action: The Mineral Intensity of the Clean Energy Transition [WWW Document]. URL https://pubdocs.worldbank.org/en/961711588875536384/Minerals-for-Climate-Action-The-Mineral-Intensity-of-the-Clean-Energy-Transition.pdf (accessed 4.25.22).

Wills, B.A., Finch, J.A., 2016. Mineral processing technology: an introduction to the practical aspects of ore treatment and mineral recovery, 8th ed.

Woodcock, J.T., Sparrow, G.J., Bruckard, W.J., Johnson, N.W., Dunne, R., 2007. Plant Practice: Sulfide Minerals and Precious Metals, in: Froth Flotation A Century of Innovation. pp. 781–844.

Xi, Y., Mallavarapu, M., Naidu, R., 2010. Reduction and adsorption of Pb2+ in aqueous solution by nano-zero-valent iron—A SEM, TEM and XPS study. Mater Res Bull 45, 1361–1367. https://doi.org/10.1016/J.MATERRESBULL.2010.06.046

Zeng, Z., Chen, Z., Qi, H., 2021. Two Processes of Anglesite Formation and a Model of Secondary Supergene Enrichment of Bi and Ag in Seafloor Hydrothermal Sulfide Deposits. J Mar Sci Eng 10, 35. https://doi.org/10.3390/jmse10010035

Zhang, Y., Jin, B., Song, Q., Chen, B., Wang, C., 2019. Leaching Behavior of Lead and Silver from Lead Sulfate Hazardous Residues in NaCl-CaCl2-NaClO3 Media. JOM 71, 2388–2395. https://doi.org/10.1007/S11837-019-03472-1/FIGURES/8

CHAPTER 4 – EFFECTS OF PYRITE ON Cu/Zn SEPARATION AND AN EFFICIENT METHOD TO ENHANCE SPHALERITE DEPRESSION

4.1 Introduction

Copper (Cu) has excellent electrical and thermal conductivities, high corrosion resistance, and outstanding malleability and ductility, which make it an essential component in various applications (e.g., building and construction, electrical and electronic products, industrial machinery and equipment, transportation, etc.) (Bilal et al., 2022b; Spatari et al., 2005). Moreover, copper is one of 17 critical metals used across a variety of clean energy generation and storage technologies, so its demand is projected to increase continuously to achieve a low-carbon future (Park et al., 2021b; WBG, 2020). Porphyry copper deposits (PCDs) are the most important sources of copper worldwide, accounting for more than 60% of the annual production of copper and they constitute about 65% of known copper ore resources(Park et al., 2020a). Ores excavated from these deposits are typically processed by flotation—a separation technique based on the difference in surface wettabilities of minerals—to recover copper sulfides (mostly chalcopyrite ($CuFeS_2$)) while removing associated gangue minerals such as pyrite (FeS_2) and quartz (SiO_2) (Bilal et al., 2022a; Hornn et al., 2020a). After a multi-stage flotation of copper ores, the produced copper concentrates are processed via pyrometallurgical routes to produce copper metal (Park et al., 2020b).

To meet the high forecasted demand for copper, mining industries are finding it necessary to mine ores at increasingly deeper positions since copper reserves are finite and easy-to-mine ore deposits are dwindling (Hornn et al., 2021; Park, 2022; Tabelin et al., 2021). In the case of PCDs, as mining areas become deeper laterally, it could be extended to the peripheral zone, where the amount of sphalerite (ZnS) increases compared to the ore zone (John et al., 2010). When processing copper ores containing sphalerite via flotation, the depression of sphalerite floatability is an important issue for producing saleable copper concentrates because the impurities in copper concentrates have a negative impact on copper smelting and penalties are imposed for their treatment in the smelting process (Haga et al., 2012, 2018; Tongamp et al., 2009). In general, Cu-Zn sulfide ores consisting of a Cu/Zn ratio of 0.4–1:1 (*w*/*w*) (Bıçak et al., 2012; Kant et al., 1994; Natarajan et al., 1997; Sinche-Gonzalez and Fornasiero, 2021; Soltani et al., 2014) are processed by a two-step flotation: (i) the selective flotation of Cu minerals while depressing sphalerite using zinc sulfate ($ZnSO_4$)—a sphalerite depressant—and other gangue minerals such as pyrite (FeS_2) and silicate minerals under alkaline conditions, and (ii) the recovery of sphalerite after its activation using copper sulfate ($CuSO_4$) (Aikawa et al., 2022; Woodcock et al., 2007). However, it is unclear whether the conventional approach for Cu-Zn and Cu-Zn-Pb ores (i.e., depression of sphalerite using zinc sulfate) is effective in Cu/Zn separation in the processing of the copper ores excavated from PCDs with a

much lower level of Zn (e.g., a Cu/Zn ratio of 7:1 (*w*/*w*)) compared to Cu-Zn or Cu-Zn-Pb sulfide ores (Ito et al., 2020). Thus, this chapter investigated the flotation behaviors of chalcopyrite and sphalerite in ores with high Cu/Zn ratios such as PCDs. Specifically, flotation tests of a single mineral (chalcopyrite or sphalerite) and mixed minerals (chalcopyrite and sphalerite with and without pyrite—a major impurity of PCDs) were conducted. Finally, a method to enhance sphalerite depression in the flotation of the chalcopyrite–sphalerite–pyrite mixture was proposed.

4.2 Materials and methods

4.2.1 Materials

Four types of minerals were used in this chapter: chalcopyrite ($CuFeS_2$, Copper Queen Mine, Cochise County, AZ, USA), sphalerite (ZnS, Kamioka Mine, Hida, Japan), pyrite (FeS_2, Huanzala Mine, Huanuco, Peru), and quartz (SiO_2, 99% purity, FUJIFILM Wako Pure Chemical Corporation, Osaka, Japan). They were characterized by X-ray fluorescence spectroscopy (XRF, EDXL300, Rigaku Corporation, Tokyo, Japan) and X-ray powder diffraction (XRD, MultiFlex, Rigaku Corporation, Tokyo, Japan). The chemical and mineralogical compositions of these samples are summarized in Table 4-1 and shown in Figure 4-1, respectively. The XRD pattern of chalcopyrite (Figure 4-1a) showed that it contains impurities such as ferro-actinolite ($Ca_2(Fe^{2+}, Mg)_5Si_8O_{22}(OH)_2$), sphalerite, and quartz, whereas those of sphalerite and pyrite (Figure 4-1b,c) showed that these samples are highly pure as indicated by the absence of peaks from common minerals such as quartz. The samples were ground using a vibratory disc mill (RS 200, Retsch Inc., Haan, Germany) and screened to obtain a size fraction of –75 + 38 μm.

For the flotation experiments, potassium isopropyl xanthate (PIPX, Tokyo Chemical Industry Co., Ltd., Tokyo, Japan) as a collector, methyl isobutyl carbinol (MIBC, Tokyo Chemical Industry Co., Ltd., Tokyo, Japan) as a frother, and zinc sulfate ($ZnSO_4$, FUJIFILM Wako Pure Chemical Corporation, Osaka, Japan) as a depressant for sphalerite were used. Sodium hydroxide (NaOH, FUJIFILM Wako Pure Chemical Corporation, Osaka, Japan) and sulfuric acid (H_2SO_4, FUJIFILM Wako Pure Chemical Corporation, Osaka, Japan) were used as pH adjusters.

Table 4-1. The chemical composition of mineral samples based on XRF.

Mineral specimens	**Mass fraction (%)**					
	Cu	**Zn**	**Fe**	**S**	**Si**	**Ca**
Chalcopyrite	28.3	0.5	32.8	17.7	11.0	8.4
Sphalerite	–	54.0	6.4	32.3	3.3	1.9
Pyrite	–	–	42.3	52.5	1.0	–

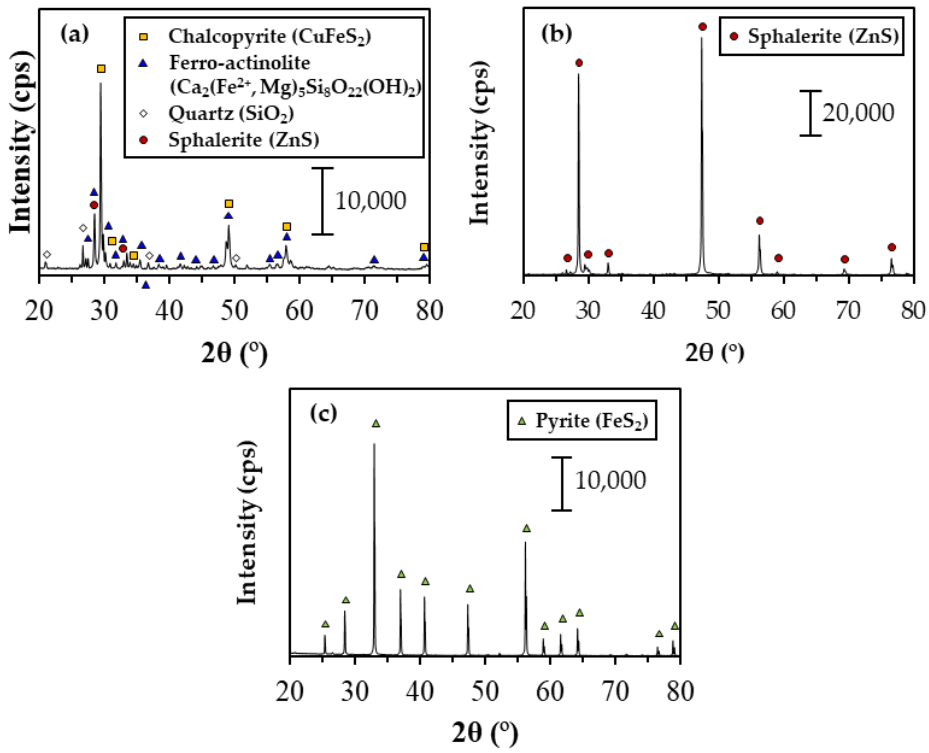

Figure 4-1. XRD patterns of mineral samples: (a) chalcopyrite ($CuFeS_2$), (b) sphalerite (ZnS), and (c) pyrite (FeS_2). Note differences in the scales of the y-axes.

4.2.2 Experimental methods

4.2.2.1 Flotation

Flotation experiments were carried out using an agitator-type flotation machine (ASH-F30H, Kankyo-kanri Engineering, Akita, Japan) equipped with a 400 mL flotation cell under the following conditions: pH, 9; temperature, 25 °C; impeller speed, 1000 rpm; air flow rate, 1 L/min. The mixtures of ground sphalerite, chalcopyrite, pyrite, and quartz (–75 + 38 µm) were used as model samples. Three types of model samples were prepared: (i) 18 g of chalcopyrite or sphalerite and 2 g of quartz, (ii) 13 g of chalcopyrite, 1 g of sphalerite, and 6 g of quartz, (iii) 13 g of chalcopyrite, 1 g of sphalerite, 4 g of pyrite, and 2 g of quartz. The ratios of Cu and Zn in model samples (ii) and (iii) were based on the Cu ore sample obtained from South America. Meanwhile, quartz was added to not only adjust the amount of the model samples to 20 g but also to check the entrainment of minerals into the froth products.

Prior to the flotation experiments, each mineral sample was deslimed with 300 mL of distilled water, respectively (Aikawa et al., 2021). After desliming, each mineral sample was mixed and

repulped to 400 mL with distilled water containing various concentrations of zinc sulfate (0, 1, or 10 kg/t) in the flotation cell and conditioned with MIBC for 3 min, and then the flotation experiments were carried out based on the flowchart consisting of conditioning with PIPX for 3 min, followed by froth recovery for 3 min, which was repeated until the cumulative PIPX dosage reached 500 g/t (Figure 4-2). After flotation, froth and tailings were dried at 105 °C for 24 h and analyzed by XRF to determine the recovery of Cu, Zn, Fe, and Si. Some experiments were carried out in duplicate to ascertain that the differences observed were statistically significant.

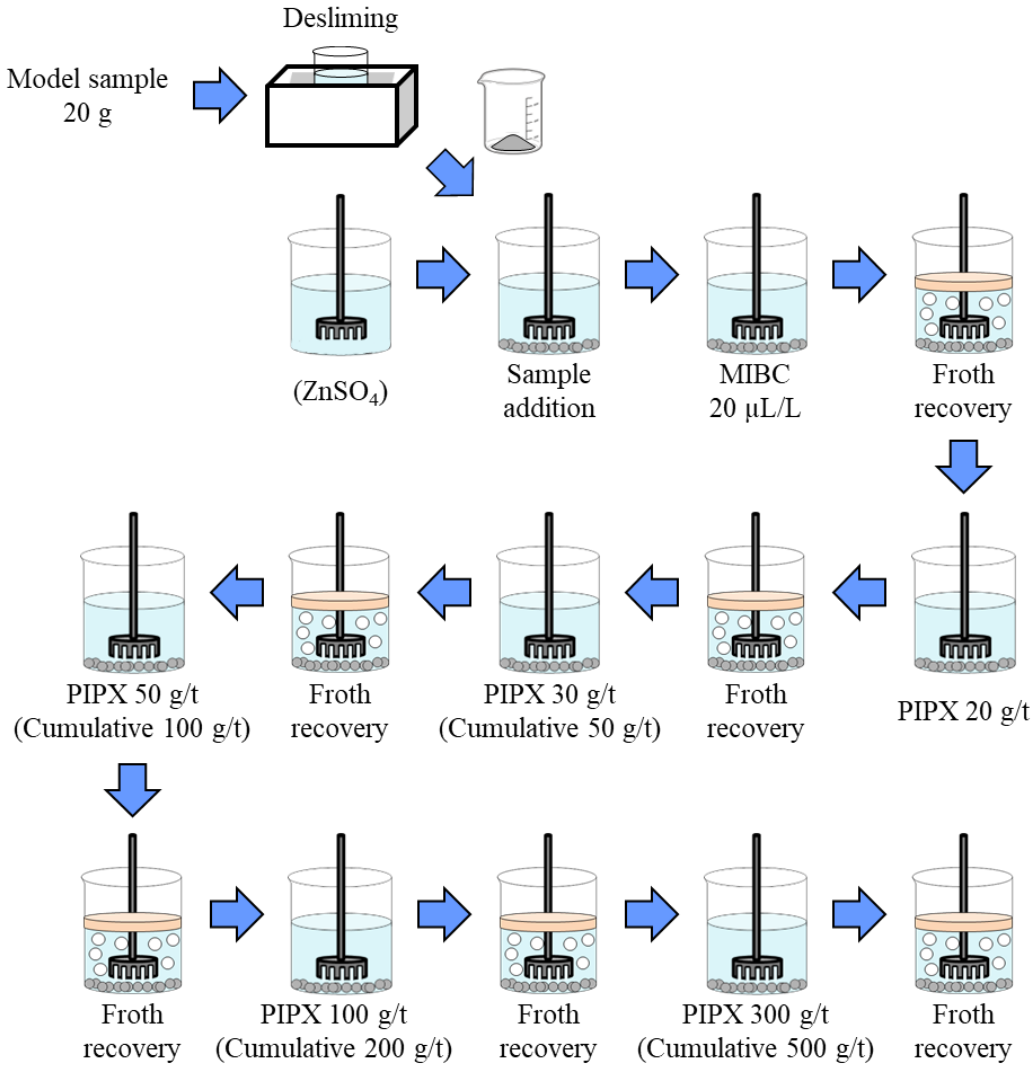

Figure 4-2. Flotation procedure with sequential addition of the collector (PIPX).

4.2.2.2 Contact Angle Measurements

Contact angle measurements were carried out in a solution containing 50 ppm zinc sulfate, 5 ppm PIPX, and 20 µL/L MIBC at pH 9 and 25 °C. A small cuboid crystal of sphalerite and pyrite (~10

mm (w) × 10 mm (d) × 10 mm (h)) was obtained by cutting the sphalerite and pyrite mineral specimens using a diamond cutter and fixed inside a plastic holder using Technovit® non-conductive resin (Kulzer GmbH, Wehrheim, Germany). The mineral surface was polished with a polishing machine (SAPHIR 250 M1, ATM GmbH, Mammelzen, Germany) against silicon carbide papers of increasing grit numbers (P180 → P320 → P600 → P1200), followed by polishing with diamond suspensions (3 and 1 μm). After this, the polished mineral sample was cleaned using an ultrasonicator (W-113 MK-II, Honda Electronics Co., Ltd., Toyohashi, Japan) for 5 min to remove any residually attached diamond particles, washed thoroughly with distilled water, and then immediately used for the experiments. The sphalerite and pyrite surfaces were reacted with a solution containing 50 ppm zinc sulfate in the flotation cell and conditioned for 3 min after adding the following reagents in sequence: 5 ppm PIPX and 20 μL/L MIBC. The concentrations of zinc sulfate, PIPX, and MIBC were the same as that used in the flotation experiments: 1 kg/t zinc sulfate, 100 g/t PIPX, and 20 μL/L MIBC, respectively. Bubble contact angles on the surfaces of sphalerite and pyrite were measured using the captive bubble method. A high-magnification digital microscope (VHX-1000, Keyence Corporation, Japan) and AutoCAD 2023 (Autodesk, Inc., San Rafael, CA, USA) were used to measure the bubble contact angles. The experiments were conducted in triplicates at various spots on the mineral surface to ascertain that the differences observed were statistically significant.

4.3 Results and discussion

4.3.1 Single Mineral Flotation of Chalcopyrite or Sphalerite

To investigate the floatabilities of chalcopyrite and sphalerite, single mineral flotation experiments of chalcopyrite or sphalerite were carried out without Zn depressants. The Cu recovery in the absence of PIPX was 58% but significantly increased to 86% by adding 20 g/t PIPX because chalcopyrite has a high affinity with xanthate (Bilal et al., 2021; Hornn et al., 2020b, 2020c; Park et al., 2021a). As the PIPX dosage increased from 20 to 200 g/t, the Cu recovery was mildly increased to 95% and remained constant after 200 g/t PIPX (Figure 4-3a). On the other hand, the Zn recovery was lower than 30% even at 500 g/t PIPX (Figure 4-3b) because sphalerite has a low affinity with xanthate, thus adding PIPX cannot improve the floatability of sphalerite (Wills and Finch, 2016).

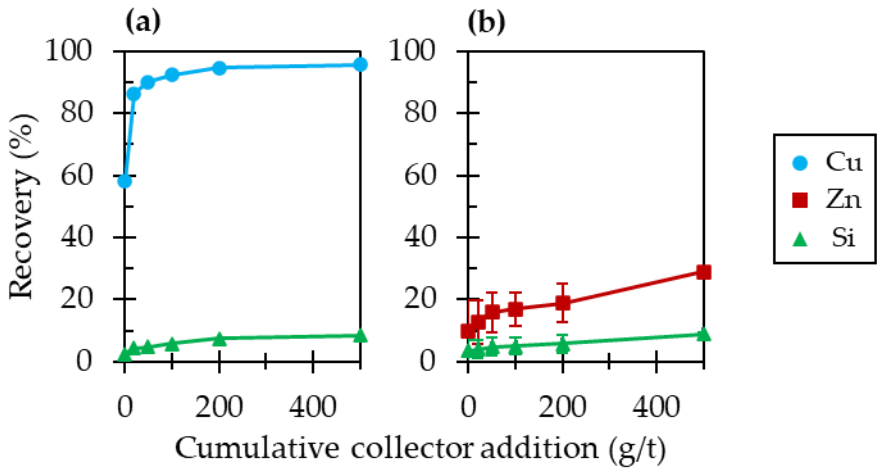

Figure 4-3. Results of single mineral flotation of (a) chalcopyrite or (b) sphalerite.

4.3.2 Effects of Chalcopyrite on the Floatability of Sphalerite

To investigate how the flotation behaviors of chalcopyrite and sphalerite are affected when they coexist in the absence of Zn depressants, flotation tests of mixed minerals (chalcopyrite and sphalerite) were conducted with various PIPX dosages. Compared to the results of the single mineral flotation of sphalerite (Figure 4-4a), the mixed mineral flotation results show that sphalerite floated together with chalcopyrite, indicating that the coexistence of chalcopyrite improved the floatability of sphalerite (Figure 4-4b). To elucidate why the floatability of sphalerite increased in the presence of chalcopyrite, the mixture of sphalerite and chalcopyrite was conditioned in the flotation cell following the flotation procedure, and the surface of sphalerite was analyzed by a scanning electron microscopy with energy-dispersive X-ray spectroscopy (SEM-EDS, JSM-IT200TM, JEOL Co., Ltd., Tokyo, Japan). Figure 4-5 shows the SEM photomicrograph of sphalerite after conditioning with chalcopyrite and the corresponding elemental maps of Zn, S, Cu, Fe, and O. The elemental mapping results showed that Cu was detected on the surface of sphalerite after conditioning with chalcopyrite and associated with the maps of S and O, whereas that of Cu did not correspond to that of Fe. These indicate that sphalerite was activated by Cu^{2+} dissolved from chalcopyrite, that is, a CuS-like and/or $Cu(OH)_2$-like layer was formed on the surface of sphalerite as described in Equation (4-1) (Chandra and Gerson, 2009).

$$ZnS_{(s)} + Cu^{2+} = CuS_{(s)} + Zn^{2+} \quad (4\text{-}1)$$

Cu^{2+} was dissolved from copper oxides formed on the surface of chalcopyrite and caused unwanted activation of sphalerite (Lascelles and Finch, 2002; Wei et al., 2021). The copper activation of sphalerite caused an increase in the floatability of sphalerite because xanthate was readily adsorbed on the Cu-compounds present on the sphalerite surface as illustrated in Figure 4-6.

These results indicate that the increase in the floatability of sphalerite in the presence of chalcopyrite made the separation of sphalerite from chalcopyrite difficult without the aid of Zn depressants.

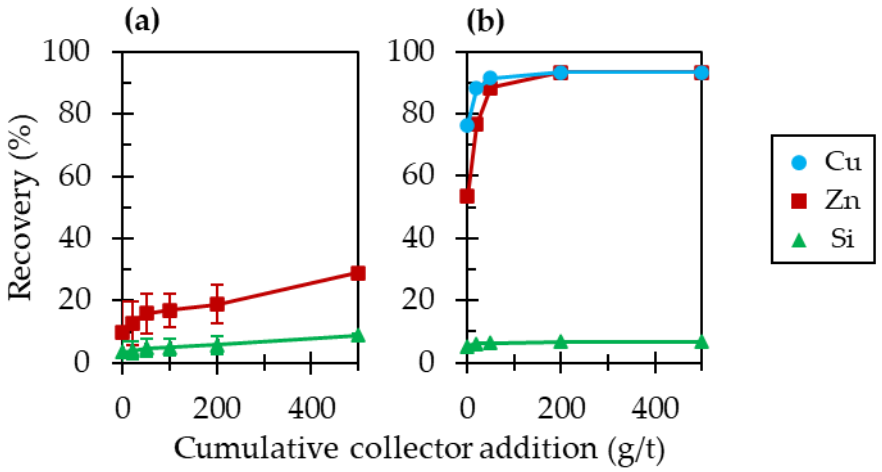

Figure 4-4. Flotation results of sphalerite in the absence of Zn depressants (a) without chalcopyrite and (b) with chalcopyrite. Note that the data at 100 g/t of collector in Figure 4-4b were absent due to the lack of froth amounts for the XRF.

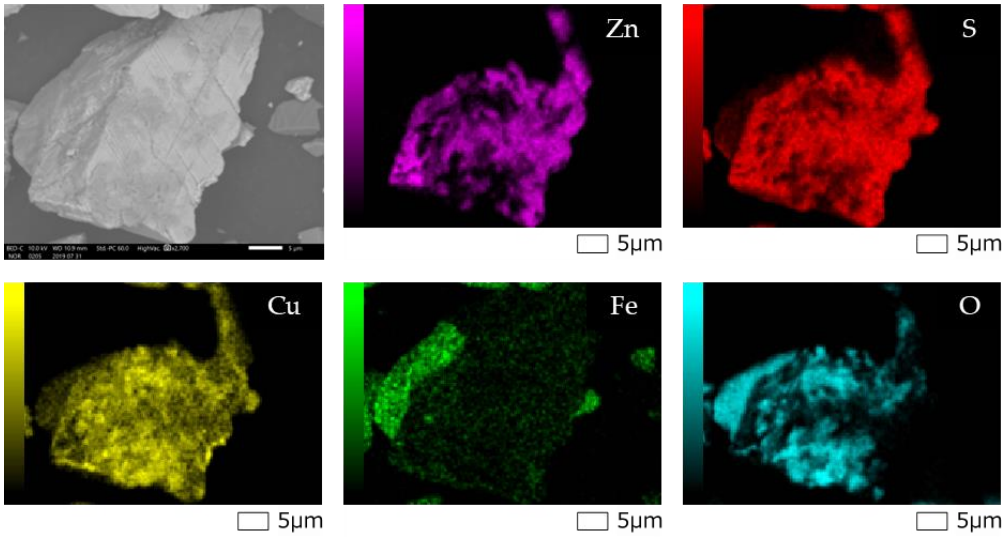

Figure 4-5. SEM photomicrograph of sphalerite after conditioning with chalcopyrite in the flotation cell with the corresponding elemental maps of Zn, S, Cu, Fe, and O.

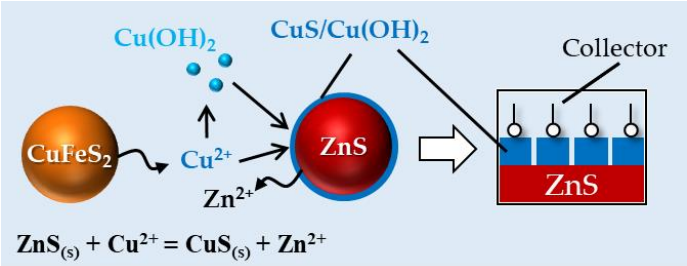

Figure 4-6. A schematic diagram of copper activation of sphalerite in the presence of chalcopyrite.

To depress the floatability of sphalerite in the presence of chalcopyrite, the effect of zinc sulfate, a conventional depressant, on sphalerite floatability was investigated. Figure 4-7 shows the flotation results of chalcopyrite and sphalerite with and without 1 kg/t zinc sulfate. As illustrated in Figure 4-7a, sphalerite was recovered as froth together with chalcopyrite in the absence of zinc sulfate; however, when zinc sulfate was added as a depressant for sphalerite, the Zn recovery was dramatically decreased to ~12% even at 500 g/t PIPX (Figure 4-7b). Meanwhile, the floatability of chalcopyrite was not affected by zinc sulfate; >90% of Cu recovery was achieved irrespective of the presence of zinc sulfate at >50 g/t PIPX (Figure 4-7). These results indicate that zinc sulfate is effective in depressing the floatability of sphalerite even in the presence of chalcopyrite. The possible mechanisms of how zinc sulfate could depress the floatability of sphalerite in the presence of chalcopyrite are as follows: (i) adsorption of zinc precipitates such as $Zn(OH)_2$ on the surface of sphalerite, rendering the surface of sphalerite hydrophilic where the adsorption of the collector is limited, (ii) inhibition of Cu activation by zinc precipitates, and/or (iii) deactivation of Cu-activated sphalerite via reverse reaction of Equation (4-1) (Cao and Liu, 2006; Wills and Finch, 2016).

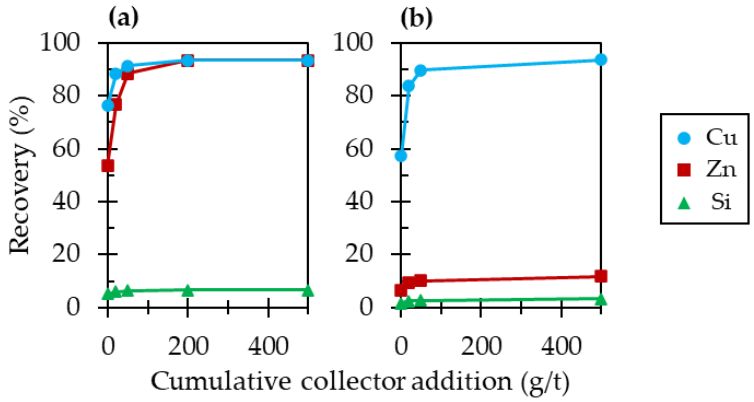

Figure 4-7. Flotation results of sphalerite and chalcopyrite with zinc sulfate (a) 0 kg/t and (b) 1 kg/t. Note that the data at 100 g/t of collector in Figure 4-7a and those at 100 and 200 g/t of collector in Figure 4-7b were absent due to the lack of froth amounts for the XRF.

4.3.3 Effects of Pyrite on Sphalerite Floatability in the Presence of Chalcopyrite

Copper ores contain not only valuable minerals such as chalcopyrite and sphalerite but also gangue minerals such as pyrite—a major gangue mineral of sulfide ores. The presence of pyrite has been reported to have a significant impact on the flotation behavior of minerals (Aikawa et al., 2020; Barker et al., 2014; Pecina-Treviño et al., 2003; Wenqing Qin et al., 2015; Wen-qing Qin et al., 2015; Wang et al., 2020). Although the addition of zinc sulfate improved the flotation separation of chalcopyrite from the chalcopyrite–sphalerite binary mixed minerals system, it is necessary to further investigate whether zinc sulfate would also be effective in the presence of pyrite. To clarify this, flotation tests of mixed minerals consisting of chalcopyrite, sphalerite, and pyrite were conducted with zinc sulfate (Figure 4-8). When pyrite coexisted with sphalerite and chalcopyrite, the recovery of Zn was dramatically increased (Figure 4-8b) compared to that in the absence of pyrite (Figure 4-8a). Though the amount of zinc sulfate increased from 1 to 10 kg/t, the floatability of sphalerite was high (>80%) (Figure 4-8c). These results indicate that pyrite inhibits the depressive effect of zinc sulfate toward sphalerite in the presence of chalcopyrite, which could be attributed to two possible mechanisms: (i) the reduced amount of zinc precipitates adsorbed onto the surface of sphalerite due to the presence of pyrite whose surface also attracts zinc precipitates, and (ii) the galvanic interaction between chalcopyrite and pyrite that promotes the anodic half-cell reaction of chalcopyrite, releasing more Cu^{2+} into the aqueous solution (Figure 4-9). These two possible mechanisms will be explored in more detail in the next sub-section.

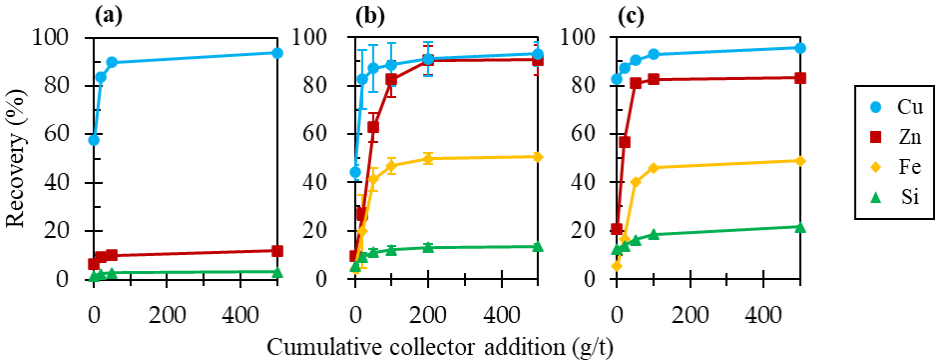

Figure 4-8. Flotation results of sphalerite and chalcopyrite (a) in the absence of pyrite and with zinc sulfate 1 kg/t, (b) in the presence of pyrite and zinc sulfate 1kg/t, and (c) in the presence of pyrite and zinc sulfate 10 kg/t. Note that the data at 100 and 200 g/t of collector in Figure 4-8a and those at 200 g/t of collector in Figure 4-8c were absent due to the lack of froth amounts for the XRF.

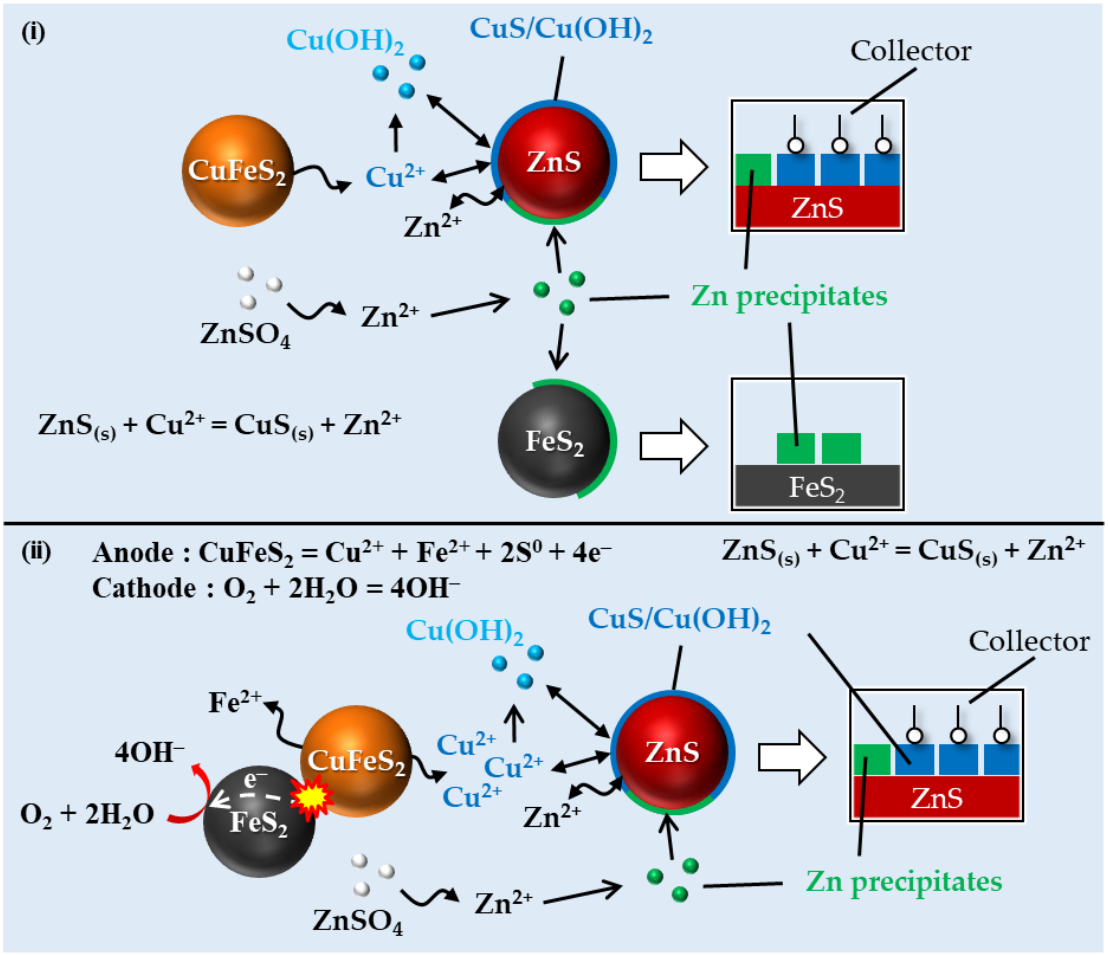

Figure 4-9. A schematic diagram of two possible mechanisms for why pyrite inhibits the depression of sphalerite with zinc sulfate in the presence of chalcopyrite: (i) the reduced amount of zinc precipitates adsorbed onto the surface of sphalerite due to the presence of pyrite whose surface also attracts zinc precipitates, (ii) galvanic interaction between chalcopyrite and pyrite that promotes the anodic half-cell reaction of chalcopyrite, releasing more Cu^{2+} into the aqueous solution.

4.3.4. Mechanisms of Losing the Depressive Effect of Zinc Sulfate Toward Sphalerite in the Presence of Both Pyrite and Chalcopyrite

4.3.4.1 Effects of Pyrite on the Hydrophilicity of Sphalerite

One of the considerable mechanisms of depressing sphalerite floatability with zinc sulfate may be due to the adsorption of zinc precipitates such as $Zn(OH)_2$ on the surface sphalerite, rendering its surface hydrophilic, thus limiting the adsorption of a collector (Cao and Liu, 2006; Wills and Finch, 2016). If Zn precipitates are adsorbed onto the surface of not only sphalerite but also pyrite, it would result in reducing the amount of Zn precipitates adsorbed onto the surface of sphalerite, and thus the depression of sphalerite floatability by zinc sulfate may not be achieved. To investigate whether

pyrite affects the adsorption of Zn precipitates on sphalerite, the contact angles of sphalerite in the absence and presence of pyrite were measured using a small cuboid crystal of sphalerite and pyrite under the same conditions as the flotation experiments; 50 ppm zinc sulfate, 5 ppm PIPX, and 20 μL/L MIBC at pH 9 and 25 °C. As shown in Figure 4-10, the difference in the contact angles between the sphalerite and air bubble in the absence and presence of pyrite was almost negligible, indicating that the reduced amount of Zn precipitates adsorbed onto the sphalerite surface by pyrite is not the reason for losing the depressive effect of zinc sulfate toward sphalerite.

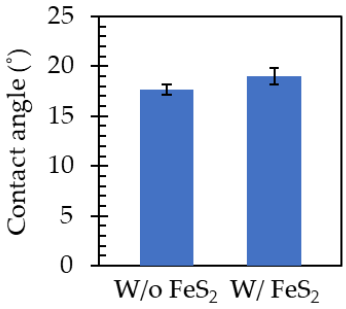

Figure 4-10. The contact angle of sphalerite in the absence and presence of pyrite.

4.3.4.2 Effects of the Galvanic Interaction between Chalcopyrite and Pyrite on the Floatability of Sphalerite

Pyrite is known to strongly affect the floatability of target minerals due to their electrochemical interactions with each other (Mu et al., 2018; Owusu et al., 2014). When pyrite and chalcopyrite are in contact, they form a galvanic cell where the former (i.e., pyrite) acts as a cathode due to a higher rest potential, whereas the latter (i.e., chalcopyrite) having a lower rest potential behaves as an anode (Nazari et al., 2011). The formation of a galvanic cell is well-known to enhance the dissolution of minerals or metals that act as anodes while it protects the cathode from corrosion (Jeon et al., 2022a, 2022b; Park et al., 2019; Seng et al., 2019a, 2019b; Tabelin et al., 2018). That is, the dissolution of chalcopyrite as an anodic reaction (Equation (4-2)) is accelerated via the galvanic interaction, whereas on the surface of pyrite, the reduction reaction of dissolved oxygen (DO) as a cathodic reaction (Equation (4-3)) occurs (Ekmekçi and Demirel, 1997)

$$CuFeS_2 = Cu^{2+} + Fe^{2+} + 2S^0 + 4e^- \quad (4\text{-}2)$$

$$O_2 + 2H_2O + 4e^- = 4OH^- \quad (4\text{-}3)$$

This indicates that the amount of dissolved Cu^{2+} in the flotation pulp would increase due to the galvanic interaction between chalcopyrite and pyrite, and the degree of sphalerite activation by Cu^{2+} would also be enhanced, resulting in the difficulty in depressing sphalerite floatability by zinc sulfate. Therefore, the enhanced dissolution of chalcopyrite due to the galvanic interaction with pyrite is one

of the possible mechanisms that inhibits the ability of zinc sulfate to depress sphalerite floatability in the presence of both pyrite and chalcopyrite.

To investigate the effect of the galvanic interaction between chalcopyrite and pyrite on the floatability of sphalerite, mixed minerals flotation experiments of chalcopyrite, sphalerite, and pyrite with 1 kg/t zinc sulfate were carried out, where the amount of DO in the flotation pulp was limited. DO is an essential reactant for the galvanic interaction to take place, and thus the effect of the galvanic interaction between chalcopyrite and pyrite on the floatability of sphalerite can be clarified by conducting flotation experiments in the absence and presence of oxygen in the system. For the flotation under anaerobic conditions, ultrapure nitrogen (N_2) gas (99.99%) was introduced to distilled water for 15 min before conditioning to remove DO from the flotation pulp, and froth recovery was also conducted by injecting N_2 gas instead of air to limit the appearance of oxygen in the system. As shown in Figure 4-11, the recovery of Zn was dramatically decreased under anaerobic conditions; at 100 g/t PIPX, Zn recoveries under aerobic and anaerobic conditions were ~90% and ~20%, respectively. As confirmed in Figure 4-8c, when the galvanic interaction between pyrite and chalcopyrite occurred, it was impossible to depress the floatability of sphalerite even with the addition of 10 kg/t zinc sulfate. These results indicate that the effects of the galvanic interaction between pyrite and chalcopyrite on sphalerite floatability were minimized when the amount of DO in the flotation pulp was limited by employing N_2 gas, resulting in effective depression of sphalerite floatability in the presence of both chalcopyrite and pyrite. Therefore, the galvanic interaction between pyrite and chalcopyrite would be the most likely mechanism for pyrite inhibiting the depression of sphalerite floatability with zinc sulfate in the presence of chalcopyrite.

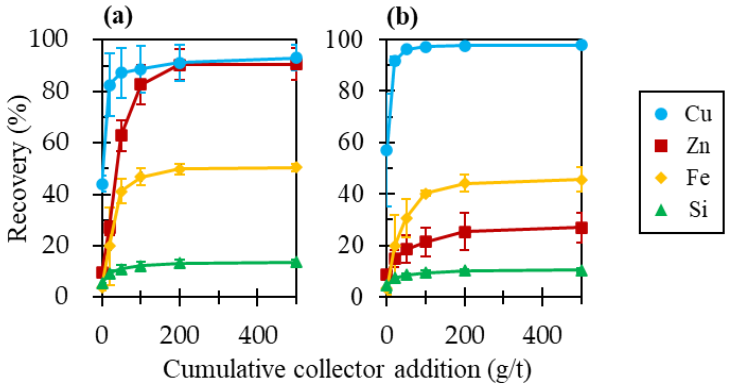

Figure 4-11. Flotation results of chalcopyrite, sphalerite, and pyrite in the presence of 1 kg/t zinc sulfate (a) with air and (b) with N_2 gas.

4.3.5 A Proposed Method to Efficiently Depress Sphalerite in Flotation of Cu Ores with a High Cu/Zn Ratio

Figure 4-12 shows the proposed method to efficiently depress sphalerite in the flotation of Cu ores with a high Cu/Zn ratio. When chalcopyrite and pyrite coexisted with sphalerite, zinc sulfate lost its ability to depress sphalerite floatability (Figure 4-8). This is most likely due to the galvanic interaction between chalcopyrite and pyrite that enhances the dissolution of chalcopyrite, and thus the amount of dissolved Cu^{2+} in the flotation pulp would be increased. As a result, Cu activation of sphalerite could be enhanced, so zinc sulfate becomes inefficient in depressing sphalerite (Figure 4-9ii). The cathodic reaction, i.e., the reduction of DO occurring on the pyrite surface (Equation (4-3)), is the first step of the galvanic interaction, so the application of N_2 gas minimizing the amount of DO in the system could limit the galvanic interaction, and as a result, zinc sulfate becomes effective in depressing sphalerite floatability. As the ratio of pyrite to chalcopyrite in copper ores increased, the galvanic interaction between them would become more intensive, which negatively would affect the floatability of chalcopyrite (Lee et al., 2022). Copper ores contain not only chalcopyrite but also other copper sulfide minerals (e.g., chalcocite and bornite), which could also form a galvanic cell with pyrite due to their lower rest potential than pyrite (Allison et al., 1972). Therefore, the application of N_2 gas to limit the galvanic interaction of copper sulfide minerals with pyrite could be a promising method to achieve Cu/Zn separation by effectively depressing sphalerite floatability in the actual processing of copper ores containing many mineralogical species such as several copper sulfide minerals and pyrite.

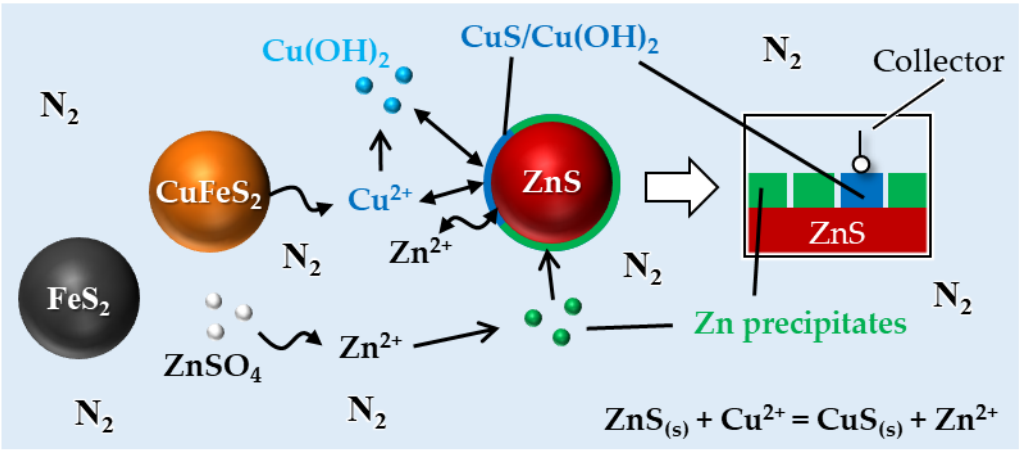

Figure 4-12. A schematic diagram of the proposed efficient method to depress sphalerite in flotation of Cu ores containing sphalerite and pyrite with zinc sulfate.

4.4 Conclusions

In this chapter, the flotation behaviors of chalcopyrite and sphalerite in model samples mimicking Cu ores with high Cu/Zn ratios were investigated.

1. The recovery of Zn was low in single mineral flotation of sphalerite, but it was dramatically increased when chalcopyrite coexisted due to the activation of sphalerite by Cu^{2+} dissolved from chalcopyrite.

2. The addition of zinc sulfate could successfully depress the sphalerite floatability; however, the presence of pyrite inhibited its ability to depress sphalerite floatability due most likely to galvanic interaction between pyrite and chalcopyrite.

3. Application of N_2 gas that limits galvanic interaction between pyrite and chalcopyrite by reducing DO concentration in the system is an effective option to depress sphalerite with zinc sulfate when the amounts of chalcopyrite and pyrite are much higher than sphalerite.

This chapter is edited from "Aikawa et al., 2022b. Flotation of copper ores with high Cu/Zn Ratio: Effects of Pyrite on Cu/Zn Separation and an Efficient Method to Enhance Sphalerite Depression. Minerals 1103, 12(9)."

References

Aikawa, K., Ito, M., Kusano, A., Jeon, S., Park, I., Hiroyoshi, N., 2022. Development of a Sustainable Process for Complex Sulfide Ores Containing Anglesite: Effect of Anglesite on Sphalerite Floatability, Enhanced Depression of Sphalerite by Extracting Anglesite, and Recovery of Extracted Pb2+ as Zero-Valent Pb by Cementation Using Zero-Valent Fe. Minerals 12, 723. https://doi.org/10.3390/min12060723

Aikawa, K., Ito, M., Kusano, A., Park, I., Oki, T., Takahashi, T., Furuya, H., Hiroyoshi, N., 2021. Flotation of Seafloor Massive Sulfide Ores: Combination of Surface Cleaning and Deactivation of Lead-Activated Sphalerite to Improve the Separation Efficiency of Chalcopyrite and Sphalerite. Metals (Basel) 11, 253. https://doi.org/10.3390/met11020253

Aikawa, K., Ito, M., Segawa, T., Jeon, S., Park, I., Tabelin, C.B., Hiroyoshi, N., 2020. Depression of lead-activated sphalerite by pyrite via galvanic interactions: Implications to the selective flotation of complex sulfide ores. Miner Eng 152, 106367. https://doi.org/10.1016/j.mineng.2020.106367

Allison, S.A., Goold, L.A., Nicol, M.J., Granville, A., 1972. A determination of the products of reaction between various sulphide minerals and aqueous xanthate. Metallurgical Transactions 3, 2613–2618. https://doi.org/10.1007/BF02644237

Barker, G.J., Gerson, A.R., Menuge, J.F., 2014. The impact of iron sulfide on lead recovery at the giant Navan Zn–Pb orebody, Ireland. Int J Miner Process 128, 16–24. https://doi.org/10.1016/j.minpro.2014.02.001

Bilal, M., Ito, M., Akishino, R., Bu, X., Ul Hassan, F., Park, I., Jeon, S., Aikawa, K., Hiroyoshi, N., 2022a. Heterogenous carrier flotation technique for recovering finely ground chalcopyrite particles using coarse pyrite particles as a carrier. Miner Eng 180, 107518. https://doi.org/10.1016/j.mineng.2022.107518

Bilal, M., Ito, M., Koike, K., Hornn, V., Ul Hassan, F., Jeon, S., Park, I., Hiroyoshi, N., 2021. Effects of coarse chalcopyrite on flotation behavior of fine chalcopyrite. Miner Eng 163, 106776. https://doi.org/10.1016/J.MINENG.2021.106776

Bilal, M., Park, I., Hornn, V., Ito, M., Hassan, F., Jeon, S., Hiroyoshi, N., 2022b. The Challenges and Prospects of Recovering Fine Copper Sulfides from Tailings Using Different Flotation Techniques: A Review. Minerals 12, 586. https://doi.org/10.3390/min12050586

Bıçak, Ö., Ekmekçi, Z., Can, M., Öztürk, Y., 2012. The effect of water chemistry on froth stability and surface chemistry of the flotation of a Cu–Zn sulfide ore. Int J Miner Process 102–103, 32–37. https://doi.org/10.1016/j.minpro.2011.09.005

Cao, M., Liu, Q., 2006. Reexamining the functions of zinc sulfate as a selective depressant in differential sulfide flotation—The role of coagulation. J Colloid Interface Sci 301, 523–531. https://doi.org/10.1016/J.JCIS.2006.05.036

Chandra, A.P., Gerson, A.R., 2009. A review of the fundamental studies of the copper activation mechanisms for selective flotation of the sulfide minerals, sphalerite and pyrite. Adv Colloid Interface Sci. https://doi.org/10.1016/j.cis.2008.09.001

Ekmekçi, Z., Demirel, H., 1997. Effects of galvanic interaction on collectorless flotation behaviour of chalcopyrite and pyrite. Int J Miner Process 52, 31–48. https://doi.org/10.1016/s0301-7516(97)00050-1

Haga, K., Altansukh, B., Shibayama, A., 2018. Volatilization of Arsenic and Antimony from Tennantite/Tetrahedrite Ore by a Roasting Process. Mater Trans 59, 1396–1403. https://doi.org/10.2320/matertrans.M2017400

Haga, K., Tongamp, W., Shibayama, A., 2012. Investigation of Flotation Parameters for Copper Recovery from Enargite and Chalcopyrite Mixed Ore. Mater Trans 53, 707–715. https://doi.org/10.2320/matertrans.M2011354

Hornn, V., Ito, M., Shimada, H., Tabelin, C.B., Jeon, S., Park, I., Hiroyoshi, N., 2020a. Agglomeration-Flotation of Finely Ground Chalcopyrite and Quartz: Effects of Agitation

Strength during Agglomeration Using Emulsified Oil on Chalcopyrite. Minerals 10, 380. https://doi.org/10.3390/min10040380

Hornn, V., Ito, M., Shimada, H., Tabelin, C.B., Jeon, S., Park, I., Hiroyoshi, N., 2020b. Agglomeration–Flotation of Finely Ground Chalcopyrite Using Emulsified Oil Stabilized by Emulsifiers: Implications for Porphyry Copper Ore Flotation. Metals 2020, Vol. 10, Page 912 10, 912. https://doi.org/10.3390/MET10070912

Hornn, V., Ito, M., Yamazawa, R., Shimada, H., Tabelin, C.B., Jeon, S., Park, I., Hiroyoshi, N., 2020c. Kinetic Analysis for Agglomeration-Flotation of Finely Ground Chalcopyrite: Comparison of First Order Kinetic Model and Experimental Results. Mater Trans 61, 1940–1948. https://doi.org/10.2320/MATERTRANS.M-M2020843

Hornn, V., Park, I., Ito, M., Shimada, H., Suto, T., Tabelin, C.B., Jeon, S., Hiroyoshi, N., 2021. Agglomeration-flotation of finely ground chalcopyrite using surfactant-stabilized oil emulsions: Effects of co-existing minerals and ions. Miner Eng 171, 107076. https://doi.org/10.1016/J.MINENG.2021.107076

Ito, M., Orii, N., Aikawa, K., Jeon, S., Park, I., Hiroyoshi, N., Magwaneng, R., Kudo, K., Sunada, K., Takahashi, T., 2020. Effects of several depressants on the floatability of sphalerite in the flotation of copper-zinc sulfides, in: The Mining and Materials Processing Institute of Japan (MMIJ) Fall Meeting 2020. The Mining and Materials Processing Institute of Japan.

Jeon, S., Bright, S., Park, I., Kuze, A., Ito, M., Hiroyoshi, N., 2022a. A Kinetic Study on Enhanced Cementation of Gold Ions by Galvanic Interactions between Aluminum (Al) as an Electron Donor and Activated Carbon (AC) as an Electron Mediator in Ammonium Thiosulfate System. Minerals 2022, Vol. 12, Page 91 12, 91. https://doi.org/10.3390/MIN12010091

Jeon, S., Bright, S., Park, I., Tabelin, C.B., Ito, M., Hiroyoshi, N., 2022b. A simple and efficient recovery technique for gold ions from ammonium thiosulfate medium by galvanic interactions of zero-valent aluminum and activated carbon: A parametric and mechanistic study of cementation. Hydrometallurgy 208, 105815. https://doi.org/10.1016/J.HYDROMET.2021.105815

John, D.A., Ayuso, R.A., Barton, M.D., Blakely, R.J., Bodnar, R.J., Dilles, J.H., Gray, F., Graybeal, F.T., Mars, J.C., McPhee, D.K., Seal, R.R., Taylor, R.D., Vikre, P.G., 2010. Porphyry Copper Deposit Model, Chapter B of Mineral Deposit Models for Resource Assessment. Menlo Park, CA, USA.

Kant, C., Rao, S.R., Finch, J.A., 1994. Distribution of surface metal ions among the products of chalcopyrite flotation. Miner Eng 7, 905–916. https://doi.org/10.1016/0892-6875(94)90132-5

Lascelles, D., Finch, J.A., 2002. Quantifying accidental activation. Part I. Cu ion production. Miner Eng 15, 567–571. https://doi.org/10.1016/S0892-6875(02)00081-X

Lee, R.L.J., Chen, X., Peng, Y., 2022. Flotation performance of chalcopyrite in the presence of an elevated pyrite proportion. Miner Eng 177, 107387. https://doi.org/10.1016/J.MINENG.2021.107387

Mu, Y., Peng, Y., Lauten, R.A., 2018. The galvanic interaction between chalcopyrite and pyrite in the presence of lignosulfonate-based biopolymers and its effects on flotation performance. Miner Eng 122, 91–98. https://doi.org/10.1016/j.mineng.2018.03.048

Natarajan, R., Nirdosh, I., Muthuswami, S. v., 1997. Flotation of a Copper-Zinc Ore Using p-Nonylcupferron as Collector. Developments in Chemical Engineering and Mineral Processing 5, 183–193. https://doi.org/10.1002/apj.5500050302

Nazari, G., Dixon, D.G., Dreisinger, D.B., 2011. Enhancing the kinetics of chalcopyrite leaching in the GalvanoxTM process. Hydrometallurgy 105, 251–258. https://doi.org/10.1016/J.HYDROMET.2010.10.013

Owusu, C., Brito e Abreu, S., Skinner, W., Addai-Mensah, J., Zanin, M., 2014. The influence of pyrite content on the flotation of chalcopyrite/pyrite mixtures. Miner Eng 55, 87–95. https://doi.org/10.1016/j.mineng.2013.09.018

Park, I., 2022. Advances in Selective Flotation and Leaching Process in Metallurgy. Metals (Basel) 12, 144. https://doi.org/10.3390/met12010144

Park, I., Hong, S., Jeon, S., Ito, M., Hiroyoshi, N., 2021a. Flotation Separation of Chalcopyrite and Molybdenite Assisted by Microencapsulation Using Ferrous and Phosphate Ions: Part II. Flotation. Metals 2021, Vol. 11, Page 439 11, 439. https://doi.org/10.3390/MET11030439

Park, I., Hong, S., Jeon, S., Ito, M., Hiroyoshi, N., 2020a. Flotation Separation of Chalcopyrite and Molybdenite Assisted by Microencapsulation Using Ferrous and Phosphate Ions: Part I. Selective Coating Formation. Metals (Basel) 10, 1667. https://doi.org/10.3390/met10121667

Park, I., Hong, S., Jeon, S., Ito, M., Hiroyoshi, N., 2020b. A Review of Recent Advances in Depression Techniques for Flotation Separation of Cu–Mo Sulfides in Porphyry Copper Deposits. Metals (Basel) 10, 1269. https://doi.org/10.3390/met10091269

Park, I., Kanazawa, Y., Sato, N., Galtchandmani, P., Jha, M.K., Tabelin, C.B., Jeon, S., Ito, M., Hiroyoshi, N., 2021b. Beneficiation of Low-Grade Rare Earth Ore from Khalzan Buregtei Deposit (Mongolia) by Magnetic Separation. Minerals 11, 1432. https://doi.org/10.3390/min11121432

Park, I., Tabelin, C.B., Jeon, S., Li, X., Seno, K., Ito, M., Hiroyoshi, N., 2019. A review of recent strategies for acid mine drainage prevention and mine tailings recycling. Chemosphere 219, 588–606. https://doi.org/10.1016/j.chemosphere.2018.11.053

Pecina-Treviño, E.T., Uribe-Salas, A., Nava-Alonso, F., 2003. Effect of dissolved oxygen and galvanic contact on the floatability of galena and pyrite with Aerophine 3418A. Miner Eng 16, 359–367. https://doi.org/10.1016/S0892-6875(03)00022-0

Qin, Wen-qing, Wang, X., Ma, L., Jiao, F., Liu, R., Gao, K., 2015. Effects of galvanic interaction between galena and pyrite on their flotation in the presence of butyl xanthate. Transactions of Nonferrous Metals Society of China 25, 3111–3118. https://doi.org/10.1016/S1003-6326(15)63940-1

Qin, Wenqing, Wang, X., Ma, L., Jiao, F., Liu, R., Yang, C., Gao, K., 2015. Electrochemical characteristics and collectorless flotation behavior of galena: With and without the presence of pyrite. Miner Eng 74, 99–104. https://doi.org/10.1016/j.mineng.2015.01.010

Seng, S., Tabelin, C.B., Kojima, M., Hiroyoshi, N., Ito, M., 2019a. Galvanic Microencapsulation (GME) Using Zero-Valent Aluminum and Zero-Valent Iron to Suppress Pyrite Oxidation. Mater Trans 60, 277–286. https://doi.org/10.2320/matertrans.M-M2018851

Seng, S., Tabelin, C.B., Makino, Y., Chea, M., Phengsaart, T., Park, I., Hiroyoshi, N., Ito, M., 2019b. Improvement of flotation and suppression of pyrite oxidation using phosphate-enhanced galvanic microencapsulation (GME) in a ball mill with steel ball media. Miner Eng 143, 105931. https://doi.org/10.1016/j.mineng.2019.105931

Sinche-Gonzalez, M., Fornasiero, D., 2021. Understanding the effect of sulphate in mining-process water on sulphide flotation. Miner Eng 165, 106865. https://doi.org/10.1016/j.mineng.2021.106865

Soltani, F., Koleini, S.M.J., Abdollahy, M., 2014. Optimization of Cu–Zn Massive Sulphide Flotation by Selective Reagents. Journal of The Institution of Engineers (India): Series D 95, 125–134. https://doi.org/10.1007/s40033-014-0043-7

Spatari, S., Bertram, M., Gordon, R.B., Henderson, K., Graedel, T.E., 2005. Twentieth century copper stocks and flows in North America: A dynamic analysis. Ecological Economics 54, 37–51. https://doi.org/10.1016/J.ECOLECON.2004.11.018

Tabelin, C.B., Igarashi, T., Villacorte-Tabelin, M., Park, I., Opiso, E.M., Ito, M., Hiroyoshi, N., 2018. Arsenic, selenium, boron, lead, cadmium, copper, and zinc in naturally contaminated rocks: A review of their sources, modes of enrichment, mechanisms of release, and mitigation strategies. Science of The Total Environment 645, 1522–1553. https://doi.org/10.1016/j.scitotenv.2018.07.103

Tabelin, C.B., Park, I., Phengsaart, T., Jeon, S., Villacorte-Tabelin, M., Alonzo, D., Yoo, K., Ito, M., Hiroyoshi, N., 2021. Copper and critical metals production from porphyry ores and E-wastes: A review of resource availability, processing/recycling challenges, socio-environmental aspects, and sustainability issues. Resour Conserv Recycl 170, 105610. https://doi.org/10.1016/J.RESCONREC.2021.105610

Tongamp, W., Takasaki, Y., Shibayama, A., 2009. Arsenic removal from copper ores and concentrates through alkaline leaching in NaHS media. Hydrometallurgy 98, 213–218. https://doi.org/10.1016/j.hydromet.2009.04.020

Wang, X., Qin, W., Jiao, F., Wu, J., 2020. The influence of galvanic interaction on the dissolution and surface composition of galena and pyrite in flotation system. Miner Eng 156, 106525. https://doi.org/10.1016/J.MINENG.2020.106525

WBG, 2020. Minerals for Climate Action: The Mineral Intensity of the Clean Energy Transition [WWW Document]. URL https://pubdocs.worldbank.org/en/961711588875536384/Minerals-for-Climate-Action-The-Mineral-Intensity-of-the-Clean-Energy-Transition.pdf (accessed 4.25.22).

Wei, Q., Jiao, F., Dong, L., Liu, X., Qin, W., 2021. Selective depression of copper-activated sphalerite by polyaspartic acid during chalcopyrite flotation. Transactions of Nonferrous Metals Society of China 31, 1784–1795. https://doi.org/10.1016/S1003-6326(21)65616-9

Wills, B.A., Finch, J.A., 2016. Mineral processing technology: an introduction to the practical aspects of ore treatment and mineral recovery, 8th ed.

Woodcock, J.T., Sparrow, G.J., Bruckard, W.J., Johnson, N.W., Dunne, R., 2007. Plant Practice: Sulfide Minerals and Precious Metals, in: Froth Flotation A Century of Innovation. pp. 781–844.

CHAPTER 5 – DEPRESSION OF LEAD-ACTVATED SPHALERITE BY PYRITE VIA GALVANIC INTERACTIONS

5.1 Introduction

The current high demand for critical metals like copper (Cu), zinc (Zn), nickel (Ni), and cobalt (Co) in electronics and computers, aviation and transportation, electric and hybrid vehicles, and clean/renewal energies, which are still projected to significantly increase in the future(Nansai et al., 2014) . One of the most widespread and promising deposits that contain many critical metals is loosely classified as 'complex sulfides' (Herzig and Hannington, 1995a; Ikumapayi and Rao, 2015; Marston et al., 1981; Martin et al., 1989). Complex sulfide ores are generally defined as mixtures of several metal-sulfide minerals associated intimately with each other (e.g., Cu-Pb-Zn-Fe sulfides and Cu-Ni-Co-Fe sulfides) that make them very difficult to process using traditional mineral processing techniques including flotation (Majima, 1969; Martin et al., 1989). Although the recovery of valuable minerals from complex sulfide ores still remains very challenging, the high demand for critical metals, the abundance of complex sulfide ores in continental and submarine deposits, and the substantial critical metal content found in complex sulfide ores have driven a renewed interests in the processing of these ores especially via selective flotation. A typical complex sulfide ore contains sphalerite (ZnS), chalcopyrite ($CuFeS_2$), galena (PbS), pyrite (FeS_2), and barite ($BaSO_4$) and its selective flotation involves the recovery of sphalerite by surface modification using an 'activator' such as copper sulfate ($CuSO_4$) to form CuS-like surface compounds as explained in Equation (5-1) (Wills and Finch, 2016). These CuS-like surface compounds have higher affinities for short-chained thiol collectors like xanthate than sphalerite, so the surface modification of sphalerite using CuSO4 enhances collector adsorption on and floatability of the mineral (Chandra and Gerson, 2009; Leppinen, 1990; Wills and Finch, 2016). The surface modifications of sulfide minerals using metal ions have been studied in great detail for many years and are typically composed of two steps (Finkelstein, 1997; Fornasiero and Ralston, 2006; Gerson et al., 1999): (1) activation to form surface compounds with strong affinities to xanthate (e.g., CuS-like compounds) (the solubility product (K_{sp}) of Cu^{2+} and Zn^{2+} are $10^{-24.2}$ and $10^{-8.2}$, respectively (Du Reitz, 1975)), and (2) xanthate adsorption on the surface of activated sphalerite.

$$ZnS(s) + Cu^{2+} = CuS(s) + Zn^{2+} \quad (5\text{-}1)$$

Some complex sulfide ores contain not only galena but also anglesite with higher solubility (Ksp of anglesite and galena are $10^{-7.79}$ and $10^{-26.77}$, respectively) (Ball and Nordstrom, 1991; Park et al., 2018; Tabelin et al., 2012; Tabelin and Igarashi, 2009), which could complicate flotation process because anglesite releases Pb^{2+} that activates unwanted minerals. For example, the flotation separation of Cu-Pb-Zn ores is generally conducted via two-step: Cu- and Pb-minerals are first recovered, followed by Zn flotation (Woodcock et al., 2007). However, if anglesite is contained in

the ores, Pb^{2+} released during Cu-Pb flotation process could activate sphalerite, so some portion of sphalerite is recovered together with Cu- and Pb-minerals. This means that another process to separate Cu-Pb concentrates and sphalerite is necessary. When anglesite dissolution releases Pb^{2+}, sphalerite is activated via the formation of PbS-like surface compounds on the mineral as explained in Eq. 2. Activation of sphalerite by Pb^{2+} has a similar effect to flotation as that of Cu^{2+}; that is, sphalerite floatability is significantly increased (Houot and Raveneau, 1992; Laskowski et al., 1997; Rashchi et al., 2002a; Trahar et al., 1997).

$$ZnS(s) + Pb^{2+} = PbS(s) + Zn^{2+} \quad (5\text{-}2)$$

In practice, chalcopyrite and galena are floated first followed by sphalerite, so activation of sphalerite by Pb^{2+} is an unwelcomed side reaction because it dramatically limits the separation of these three sulfide minerals by selective flotation. Co-existing gangue sulfide minerals like pyrite and pyrrhotite ($Fe_{1-x}S$; where x is 0.0–0.2) are also known to strongly affect the floatability of target minerals due to their electrochemical interactions with each other (Majima, 1969), a phenomenon that occurs when two conducting or semiconducting materials with different redox or rest potentials come in close contact with each other in ionic solutions (Jeon et al., 2019, 2018; Park et al., 2019; Seng et al., 2019a; Tabelin et al., 2017a). Below pH 4, for example, pyrite has a higher rest potential (0.62–0.66 V vs. SHE) than those of chalcopyrite (0.53–0.56 V vs. SHE), galena (0.23–0.4 V vs. SHE) and sphalerite (-0.2–0.46 V vs. SHE) (Allison et al., 1972; Majima, 1969), so when target minerals come in close contact with pyrite, galvanic interactions could not only enhance their oxidations but also release co-existing ions into solution (e.g., Pb^{2+}, Cu^{2+}, and Zn^{2+}) (Figure 5-1) that complicate separation via selective flotation.

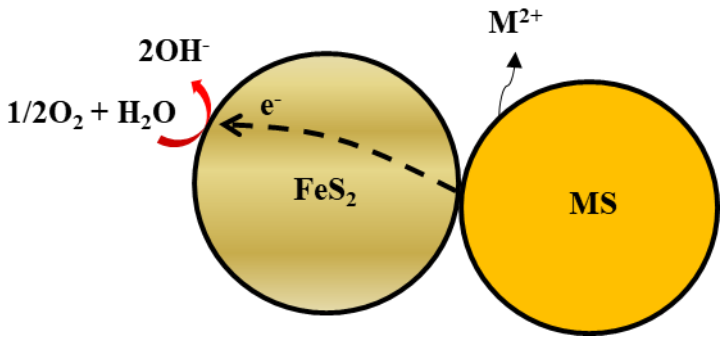

Figure 5-1. A schematic diagram of galvanic interaction between pyrite and sulfides with lower rest potentials (MS) (e.g., chalcopyrite, galena, and sphalerite).

Although many studies have been reported about the galvanic/electrochemical interactions of sulfide minerals and/or conducting materials in grinding circuits (Azizi et al., 2013; Huang and Grano, 2005; Palm et al., 2010; Rabieh et al., 2018; Seng et al., 2019b), acid mine drainage formation in sulfidic mine wastes (Chopard et al., 2017; Igarashi et al., 2020; Tabelin et al., 2018; Tatsuhara et al., 2012; Tomiyama et al., 2020, 2019), hydrometallurgical systems (Calderon et al.,

2019; Choi et al., 2020b; Jeon et al., 2020b, 2020a; Phuong Thao et al., 2020), and flotation systems (Barker et al., 2014; Ekmekçi and Demirel, 1997; Eslami Andargoli et al., 2012; Mu et al., 2018; Pecina-Treviño et al., 2003; Wenqing Qin et al., 2015; Wen-qing Qin et al., 2015; Rao and Finch, 1988; Yelloji Rao and Natarajan, 1989), very few have been conducted to explore galvanic interactions between pyrite and lead-activated sphalerite and how this phenomenon affects flotation.

In this chapter, the effects of pyrite on the floatability of lead-activated sphalerite were investigated using flotation tests and electrochemical techniques coupled with contact angle measurements. Moreover, factors important on lead-activated sphalerite floatability were elucidated in detail using dissolution experiments and X-ray photoelectron spectroscopy (XPS). Finally, a mechanism for lead-activated sphalerite depression by pyrite is proposed.

5.2 Materials and methods

5.2.1 Materials

Three types of mineral specimens were used in this chapter: sphalerite (Kamioka Mine, Japan), pyrite (Huanzala Mine, Peru), and galena (Beni Tadjit, Morocco), which were characterized by X-ray fluorescence spectroscopy (XRF, EDXL300, Rigaku Corporation, Japan) and X-ray powder diffraction (XRD, MultiFlex, Rigaku Corporation, Japan). The chemical and mineralogical compositions of these samples are summarized in Table 5-1 and shown in Figure 5-2, respectively. The XRD patterns of sphalerite, pyrite, and galena (Figure 5-2 a–c) implied that these samples are relatively pure based on the absence of peaks from common minerals like quartz. In preparation for the flotation experiments, the mineral samples were ground by a vibratory disc mill (RS 100, Retsch Inc., Germany), screened to obtain a size fraction of −75 μm and then used immediately to limit their oxidation in air.

For the flotation experiments, potassium amyl xanthate (KAX, Tokyo Chemical Industry Co., Ltd., Japan), AEROFROTH®76A (Cytec Industries Japan LLC., Japan), and sodium sulfite (Na_2SO_3, Wako Pure Chemical Industries, Ltd., Japan) were used as the collector, frother, and depressant for pyrite, respectively. Lead(II) nitrate ($Pb(NO_3)_2$, Wako Pure Chemical Industries Ltd., Japan) was used as the source of Pb^{2+} for sphalerite activation. Iron(II) sulfate heptahydrate ($FeSO_4 \cdot 7H_2O$, Wako Pure Chemical Industries Ltd., Japan) and sodium sulfate (Na_2SO_4, Wako Pure Chemical Industries, Ltd., Japan) were used to investigate the effects of Fe^{2+} and SO_4^{2-} on sphalerite floatability. Sodium hydroxide (NaOH, Wako Pure Chemical Industries Ltd., Japan) and sulfuric acid (H_2SO_4, Wako Pure Chemical Industries, Ltd., Japan) were used as pH adjusters.

Table 5-1. Chemical composition of mineral samples based on XRF.

Mineral specimens	Mass fraction (%)				
	Zn	Fe	Pb	S	Si
Sphalerite	66.5	3.5	0.1	24.8	2.7
Pyrite	–	42.3	–	52.5	1.0
Galena	–	–	84.8	8.3	1.5

Note: "–" denotes below detection limit.

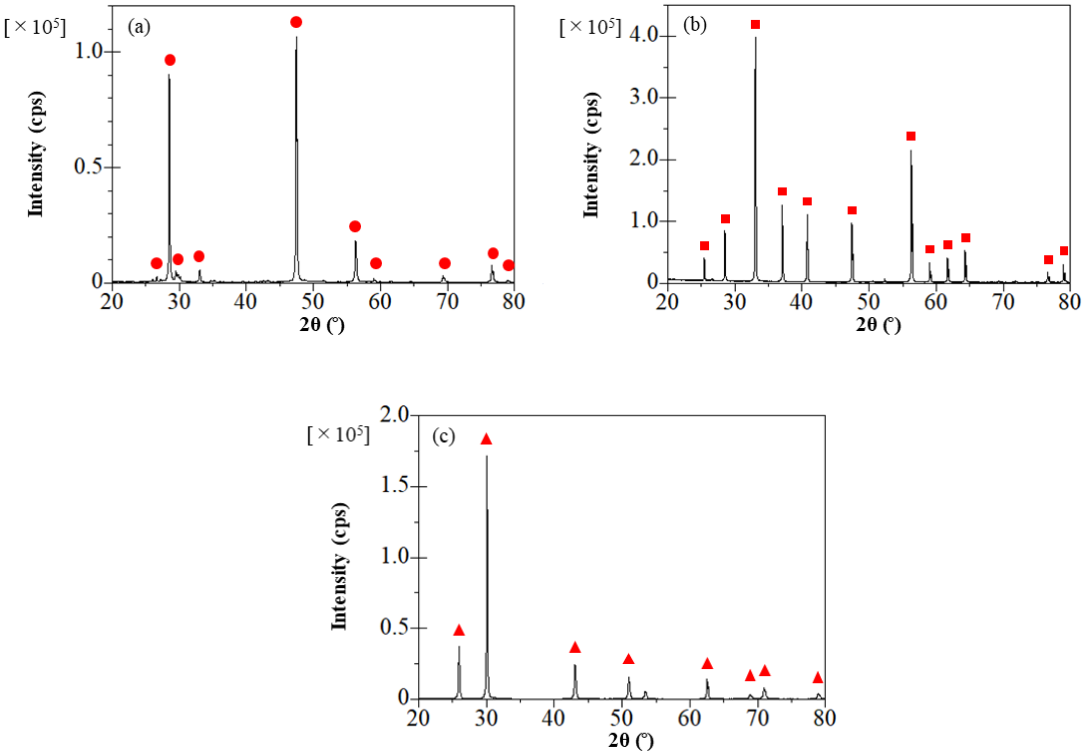

Figure 5-2. XRD patterns of mineral samples of (a) sphalerite (ZnS), (b) pyrite (FeS_2), (c) galena (PbS). Note differences in the scale of the y-axes.

5.2.2 Flotation

Flotation experiments were carried out using an agitator-type flotation machine (FT-1000, Heiko-Seisakusyo, Japan) equipped with a 400-mL flotation cell under the following conditions: 25 °C, impeller speed of 1000 rpm, and air flow rate of 1 L/min. Ground sphalerite and pyrite (−75 μm) were used as model samples. After flotation for 10 min, froth and tailings were dried at 105 °C for 24 h and analyzed by XRF to determine the recovery of Zn and Fe. All the experiments were done in duplicates to ascertain that the differences observed were statistically significant.

5.2.2.1 Single mineral flotation tests

In the flotation cell, a suspension of 10 g of sphalerite and 400 mL of distilled water was conditioned for 3 min after adding the following reagents in sequence: 1 kg/t Na_2SO_3, 0 or 5 ppm Pb^{2+}, 20 g/t KAX, and 20 μL/L AEROFROTH®76A.

5.2.2.2 Mixed sphalerite-pyrite flotation tests

In the flotation cell, 10 g of sphalerite and 10 g of pyrite were conditioned in 400 mL of distilled water for 3 min after adding the following reagents in sequence: 1 kg/t of Na_2SO_3, 5 ppm of Pb^{2+}, 20 g/t KAX, and 20 μL/L AEROFROTH®76A.

5.2.2.3 Single mineral flotation in the presence of Fe^{2+} or SO_4^{2-}

In the flotation cell, a suspension of 10 g of sphalerite and 400 mL of distilled water was conditioned for 3 min after adding the following reagents sequentially: pre-determined concentrations of Fe^{2+} (0 or 1 mM) or SO_4^{2-} (0 or 2 mM), 1 kg/t of Na_2SO_3, 5 ppm of Pb^{2+}, 20 g/t KAX, and 20 μL/L AEROFROTH®76A.

5.2.3 Contact angle measurements

Contact angle measurements were carried out using galena and pyrite electrodes in a solution containing 0.1 M of Na_2SO_4 and 10 μL/L of AEROFROTH®76A at pH 7 and 25 °C. The mineral electrodes were prepared following the procedure described by the authors (Li et al., 2019; Park et al., 2020c; Tabelin et al., 2017b), which involves cutting the galena and pyrite specimens using a diamond cutter to obtain a small cuboid crystal, connecting the crystal to copper wires with silver conducting paste (DOTITE, Fujikura Kasei Co. Ltd., Japan), and fixing them inside a plastic holder using Technovit® non-conductive resin (Heraeus Kulzer GmbH, Germany). The mineral surface was exposed by polishing the 'working' side of the electrode against silicon carbide papers of increasing grit numbers (#200 → #600 → #1200 → #1500) followed by polishing with alumina (Al_2O_3) pastes (5 and 1 μm) on a smooth glass plate. After this, the polished electrode was cleaned using an ultrasonicator (W-113, Honda Electronics Co., Ltd., Japan) for 5 min to remove any residually attached Al_2O_3 particles, washed thoroughly with distilled water and then immediately used for the experiments. The galena electrode was pre-treated for 5 min in a solution containing 5 ppm of KAX. Bubble contact angles on the surface of galena were measured using the captive bubble method as illustrated in Figure 5-3. A high-magnification digital microscope (VHX-1000, Keyence Corporation,

Japan) with built-in image analysis capability was used to measure the bubble contact angles with and without electrical connection between galena and pyrite electrodes.

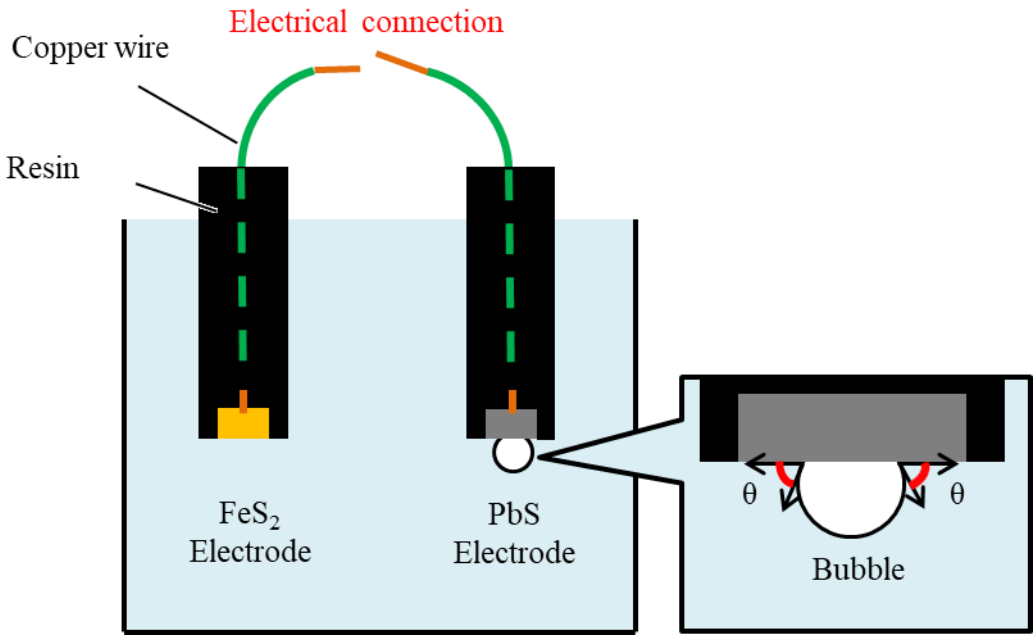

Figure 5-3. A schematic diagram of the contact angle measurements with and without electrical connection.

5.2.4 Dissolution tests of galena

The model sample (2.5 g of galena mixed with 0.0, 2.5, or 5.0 g of pyrite) and 100 mL of distilled water were put in a 100 mL beaker, and the pH of suspension was adjusted to 7 using dilute NaOH and H_2SO_4 solutions. The suspension was then magnetically stirred at 500 rpm for 30 min. After this, the leachates were collected by filtration using 0.2 μm syringe-driven membrane filters and immediately analyzed using an inductively coupled plasma atomic emission spectrometer (ICP-AES, ICPE 9820, Shimadzu Corporation, Japan) (margin of error = ± 2%) to measure the concentration of Pb^{2+} released from galena. Meanwhile, the residues were collected, thoroughly washed with distilled water, dried in a vacuum oven at 40 °C for 24 h and analyzed by X-ray photoelectron spectroscopy (XPS, JPS-9200, JEOL Ltd., Japan) to characterize the surface of galena after the leaching experiments with and without pyrite.

The XPS analysis was conducted using an Al Kα X-ray source (1486.7 eV) operated at 100 W (voltage = 10 kV; current = 10 mA) under ultrahigh vacuum conditions (~6.7×10^{-7} Pa). The binding energies of photoelectrons were calibrated using C 1s (285 eV) for charge correction. The XPS data were analyzed by XPSPEAK version 4.1 and deconvolutions of the spectra were done

using an 80% Gaussian–20% Lorentzian peak model and a true Shirley background (Nesbitt and Muir, 1994; Park et al., 2020c; Shirley, 1972; Tabelin et al., 2019; Zoleta et al., 2020b).

5.3 Results and discussion

5.3.1 Flotation experiments

5.3.1.1 Effects of pyrite on the floatability of lead-activated sphalerite

Figure 5-4 shows the results of single mineral flotation of sphalerite with and without 5 ppm of Pb^{2+}. Only ~15% of Zn was recovered as froth products without Pb^{2+}, but in the presence of Pb^{2+}, recovery of Zn dramatically increased to ~80%. This could be attributed to lead activation of sphalerite consistent with Equation (5-2) and the reports of other authors.

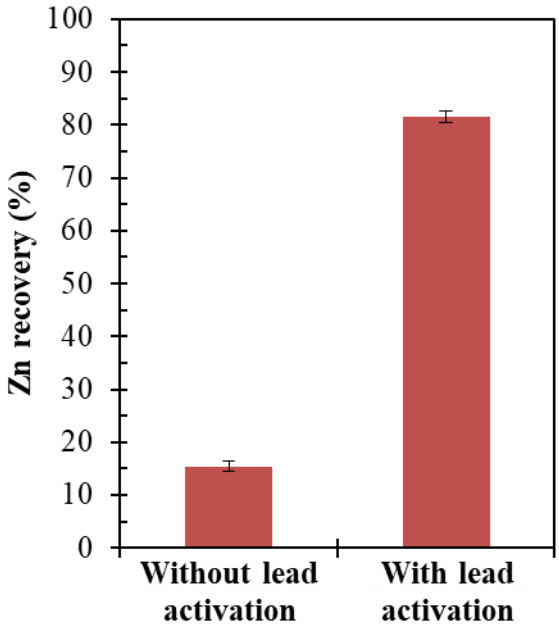

Figure 5-4. Zn recovery in single mineral flotation of sphalerite with and without lead activation.

Mixed sphalerite-pyrite flotation was carried out to evaluate the effects of pyrite on Zn recovery. Prior to the flotation experiments with KAX, two types of samples (sphalerite only and sphalerite with pyrite) were treated with 5 ppm Pb^{2+}. As shown in Figure 5-5, the floatability of lead-activated sphalerite was dramatically depressed by pyrite, which could be attributed to three possible mechanisms as illustrated in Figure 5-6: (1) effects of dissolved Fe and S released from pyrite oxidation, (2) inhibition of sphalerite activation with Pb^{2+} by pyrite, and (3) suppression of xanthate

adsorption on lead-activated sphalerite by pyrite. These three possible mechanisms are explored in more detail in the next sub-sections.

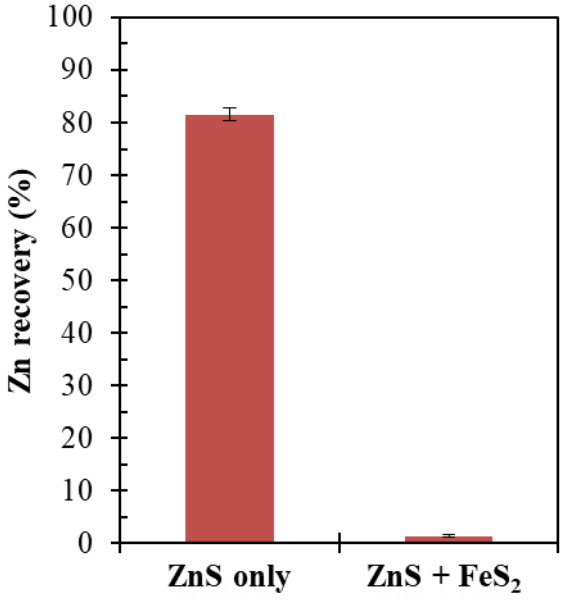

Figure 5-5. Zn recovery in mixed sphalerite-pyrite flotation.

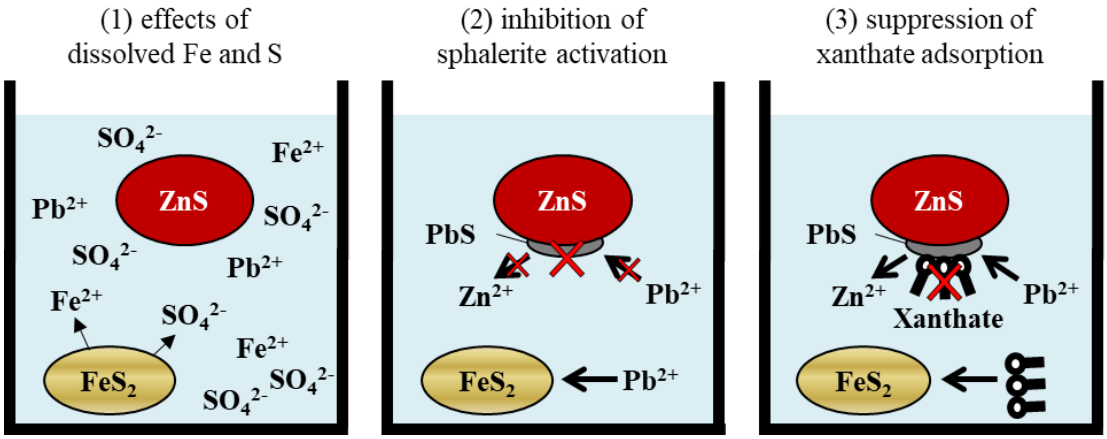

Figure 5-6. Schematic diagrams of three possible mechanisms for the depression of lead-activated sphalerite floatability by pyrite.

5.3.1.2 Lead-activated sphalerite flotation with dissolved Fe and S

To elucidate how pyrite depressed the floatability of lead-activated sphalerite, the effects of dissolved Fe and S, both known oxidation products of pyrite (Equation (5-3)), were first investigated (Figure 5-6 (1)). This was done by adding either 1 mM Fe^{2+} or 2 mM SO_4^{2-} during the flotation

experiments of lead-activated sphalerite. The concentration of Fe^{2+} or SO_4^{2-} in these experiments was based on the previous study of the authors on pyrite oxidation (Park et al., 2018).

$$FeS_{2(s)} + 7/2O_{2(aq)} + H_2O = Fe^{2+} + 2SO_4^{2-} + 2H^+ \quad (5\text{-}3)$$

As shown in Figure 5-7, dissolved Fe and S had negligible effects on the floatability of lead-activated sphalerite, indicating that the mechanism of lead-activated sphalerite depression by pyrite was not entirely due to the effects of co-existing ions released during pyrite oxidation.

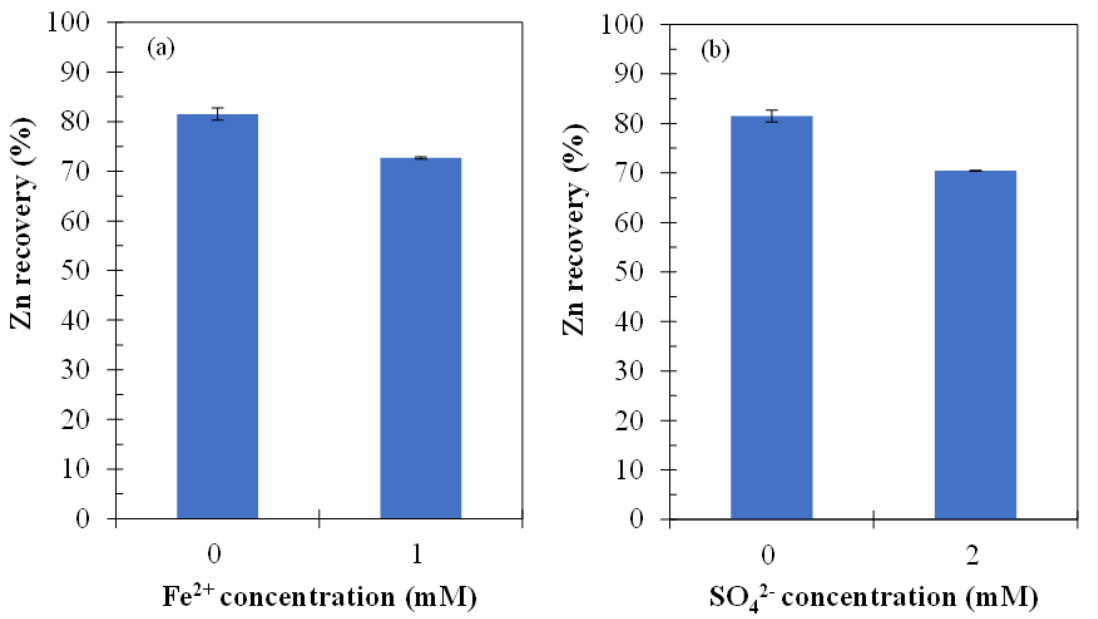

Figure 5-7. Zn recovery in single lead-activated sphalerite flotation in the absence and presence of (a) Fe^{2+} and (b) SO_4^{2-}.

5.3.1.3 Lead-activated sphalerite flotation with pyrite

To investigate the remaining two mechanisms of lead-activated sphalerite floatability depression by pyrite shown in Figure 5-6, flotation experiments were carried out by changing when pyrite was added. In case A, pyrite was added before lead activation of sphalerite and KAX addition (Figure 5-8A) while in case B, pyrite was added after lead activation of sphalerite (Figure 5-8B). For the third case (case C), pyrite was added after lead activation and KAX addition (Figure 5-8C). Case A was conducted to investigate the effects of co-existing FeS_2 before lead activation of sphalerite while case B and case C were done to elucidate the effects of pyrite on lead-activated sphalerite (i.e., PbS–ZnS) and xanthate adsorption on lead-activated sphalerite (i.e., X—PbS–ZnS; where X denotes xanthate), respectively. As shown in Figure 5-9 (case A), the floatability of sphalerite was less than 4%, indicating that pyrite inhibited (1) sphalerite activation by Pb^{2+}, and (2) consumption of xanthate ions by pyrite. To elucidate the effects of pyrite on xanthate adsorption to lead-activated sphalerite, case B was conducted (Figure 5-8B) where sphalerite is activated by Pb^{2+} (i.e., PbS–ZnS) first prior

to pyrite addition. The results showed very low recovery of Zn in case B (Figure 5-9), indicating that depression of sphalerite floatability by pyrite could be related to its consumption of xanthate ions or interference during xanthate ion adsorption to sphalerite/lead-activated sphalerite. To clarify the effects of pyrite on adsorbed xanthate on lead-activated sphalerite, case C (Figure 5-8C) where sphalerite is treated with Pb^{2+} followed by KAX addition (i.e., X—PbS–ZnS) before pyrite is added was carried out. As shown in Figure 5-9 (case C), the floatability of sphalerite treated with Pb^{2+} and KAX was also very low in the presence of pyrite. This means that another possible depression mechanism of lead-activated sphalerite floatability by pyrite was the removal of 'activated' surface layers (i.e., PbS-like compounds) on sphalerite with adsorbed xanthate. From the results of case B and case C, the dissolution of PbS layer was considered to be the most possible scenario that depresses the floatability of lead-activated sphalerite, so it will be examined in more detail in the next sub-section.

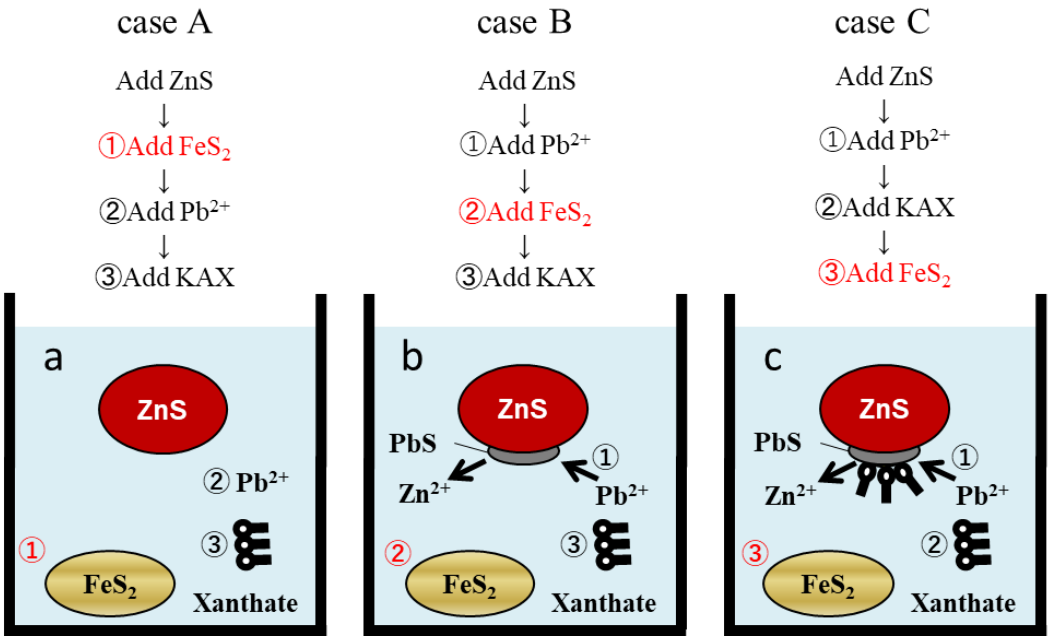

Figure 5-8. Conditioning methods of sphalerite flotation with various orders of pyrite addition.

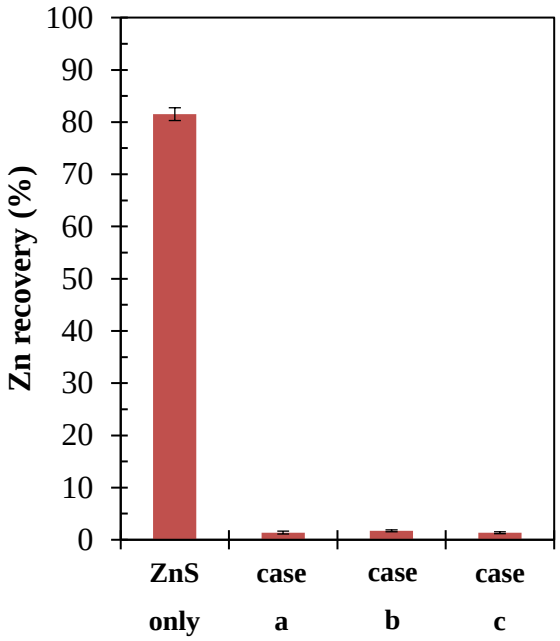

Figure 5-9. Zn recovery in mixed sphalerite-pyrite flotation by changing when pyrite was added. Note that the cases A–C are denoted as follows: A) pyrite was added before lead activation of sphalerite and KAX addition, B) pyrite was added after lead activation of sphalerite, and C) pyrite was added after lead activation and KAX addition.

5.3.2 Effects of pyrite on the dissolution of PbS formed on sphalerite

When pyrite and lead-activated sphalerite are stirred in the flotation cell, PbS-like compounds formed on sphalerite could be dissolved electrochemically due to galvanic interactions and/or peeled off by attrition. It follows that after the dissolution and/or exfoliation of PbS-like compounds formed on sphalerite, xanthate adsorbed on these compounds will also be desorbed, resulting in the lower floatability of lead-activated sphalerite in the presence of pyrite. To evaluate this mechanism in more detail, the changes in contact angle of galena treated in a KAX solution with and without electrical connection to pyrite as well as the extent of galena dissolution with varying amounts of pyrite were investigated.

5.3.2.1 Contact angle measurements of xanthate-treated galena with and without electrical connection with pyrite

The changes in contact angle of xanthate-treated galena with and without electrical connection to pyrite (Figure 5-3) were measured to evaluate the effects of galvanic interactions on xanthate-treated PbS hydrophobicity. Changes in bubble contact angle would be more accurately measured when the distribution of adsorbed xanthate on PbS is homogenous and uniform, so instead of lead-activated sphalerite, which will typically have uneven distribution of PbS-like compounds, galena was used. For the measurements, the xanthate-treated galena electrode was immersed into an electrolyte solution either with or without electrical connection to the pyrite electrode (Figure 5-3). As shown in Figure 5-10, the contact angle of galena decreased faster with time when the mineral was electrically connected to pyrite. The rest potentials of galena and pyrite are 0.06 and 0.22 V (vs. SCE) (Allison et al., 1972), respectively, indicating that galena is preferentially dissolved due to its galvanic interactions with pyrite. The enhanced dissolution of minerals or metals that act as anodes in galvanic systems is a well-known phenomenon. It has also been reported that when minerals having different rest potentials are in contact, the one with a lower rest potential acts as an anode and is preferentially dissolved (Rao, 2004). For example, it was reported that in their leaching and ball mill experiments, galvanic interactions between pyrite as cathode and steel ball media or zero-valent iron as anode were observed and anode materials were preferentially dissolved (Seng et al., 2019a, 2019b). This means the preferential dissolution of galena via galvanic interactions would occur as an anodic reaction (Eq. (4)) while on pyrite, reduction of dissolved oxygen (DO) occurs as the cathodic reaction (Eq. (5)).

$$PbS = Pb^{2+} + S^0 + 2e^- \quad (5\text{-}4)$$

$$1/2O_{2(aq)} + H_2O + 2e^- = 2OH^- \quad (5\text{-}5)$$

This enhanced dissolution of galena due to galvanic interactions could cause xanthate desorption and the release of Pb^{2+}, which could precipitate as lead hydroxide on galena and make it

less hydrophobic (i.e., lower contact angle). To confirm these deductions, dissolution tests of galena were carried out with and without pyrite and the results are discussed in the next sub-section.

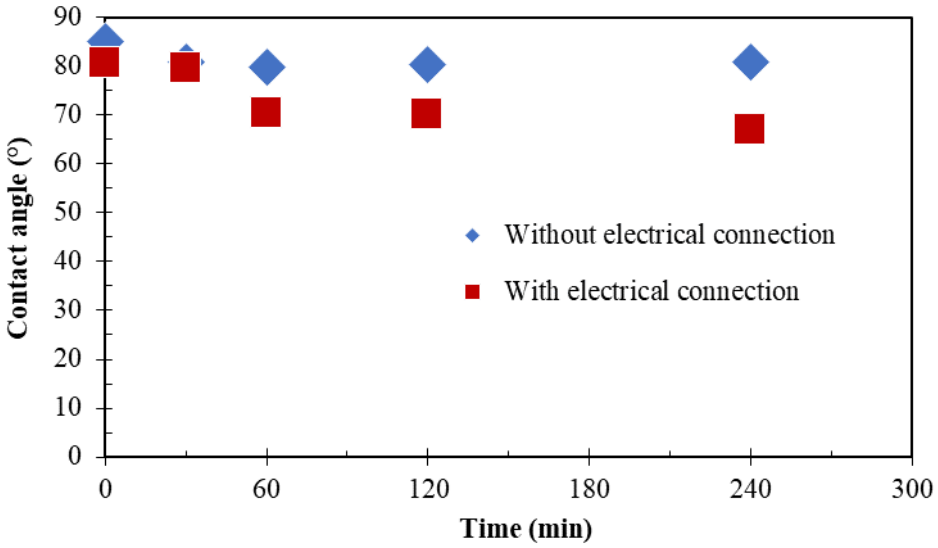

Figure 5-10 Change of contact angle with and without electrical connection as a function of time.

5.3.3 Dissolution tests of galena with and without pyrite

Dissolution tests of galena (2.5 g) with varying amounts of pyrite (0.0, 2.5, and 5.0 g) were conducted to confirm whether the presence of pyrite enhances the dissolution of galena due to their galvanic interaction or not. In this experiment, galena was used instead of lead-activated sphalerite because the estimated concentration of Pb^{2+} released from lead-activated sphalerite would be below the detection limit of ICP-AES. As shown in Figure 5-11, dissolved Pb concentration was around 1.2 ppm in the absence of pyrite, but with pyrite, the dissolution of galena was more extensive (i.e., about 2.5 ppm at the ratio of 2 (FeS_2/PbS, w/w), which indicates that galvanic interaction occurred, and this phenomenon enhanced the dissolution of galena. To characterize the surface of galena after the dissolution tests with and without pyrite, XPS analysis of dissolution test residues was conducted. The XPS spectra (Pb $4f_{(7/2)}$) of the residues are shown in Figure 5-12 and the corresponding curve fitting parameters are summarized in Table 5-2. As illustrated in Figure 5-12a, the deconvoluted XPS spectrum of galena treated without pyrite showed two types of Pb species on the surface of galena: (1) Pb2+—S of galena (142.1 and 137.2 eV), and (2) Pb2+—OH of Pb(OH)2 and/or Pb2+—SO4 of PbSO4 (143.4 and 138.4 eV) (Chernyshova and Andreev, 1997; Fornasiero et al., 1994; Mikhlin et al., 2004). The XPS spectrum of galena with pyrite also had two types of Pb species (Figure 5-12b), but the relative abundance of Pb^{2+}—OH and/or Pb^{2+}—SO_4 was substantially higher; that is, oxidized products (e.g., $Pb(OH)_2$/$PbSO_4$) increased from 9.2 to 59.2% in the presence of pyrite (Table 5-2). It is important to note that the peak positions of Pb species for $Pb(OH)_2$ and $PbSO_4$ are located closed

to each other and distinguishing between the two is difficult. Based on thermodynamic considerations, however, the formation of $Pb(OH)_2$ is more favorable than $PbSO_4$ in our experiments because the activity of SO_4^{2-} calculated by GWB was around −3.11 (Figure 5-11 and Figure 5-13). This means that Pb^{2+} released from galena via its galvanic interactions with pyrite is most likely precipitated as $Pb(OH)_2$. In other words, pyrite enhanced the dissolution of galena due to galvanic interactions (Figure 5-11) and Pb^{2+} was precipitated as $Pb(OH)_2$ on the surface of galena (Eq. (6)).

$$Pb^{2+} + 2H_2O = Pb(OH)_2 + 2H^+ \quad (5\text{-}6)$$

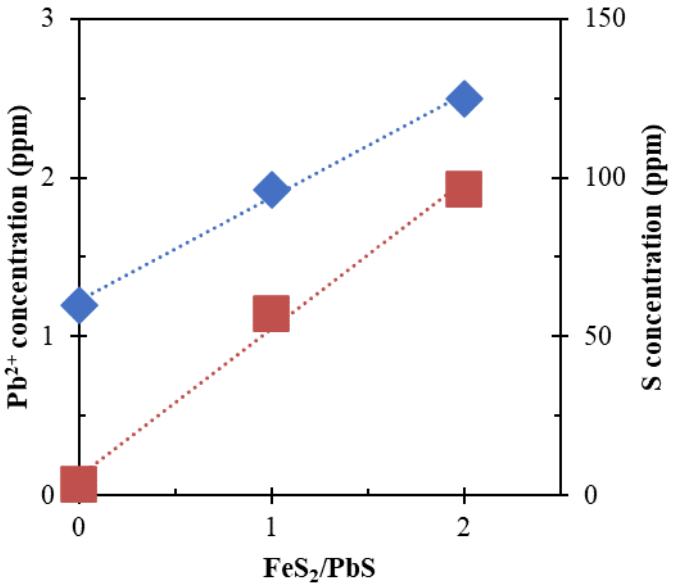

Figure 5-11. Dissolved Pb (blue) and S (red) concentration after the dissolution tests of galena with and without pyrite.

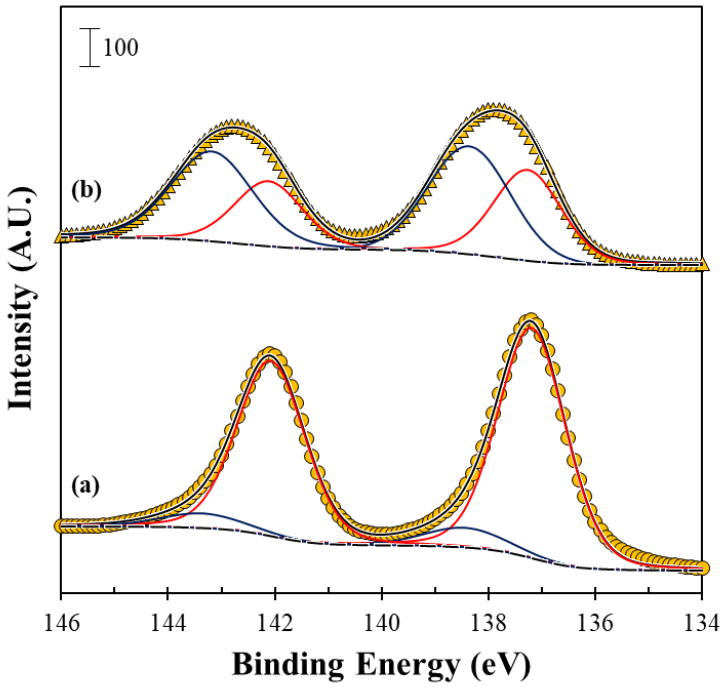

Figure 5-12. XPS spectra of Pb $4f_{(7/2)}$ of residues after dissolution tests: (a) galena only, and (b) galena with pyrite.

Table 5-2. XPS peak parameters for Pb $4f_{(7/2)}$ spectra and the relative abundances of Pb species.

Binding energy (eV)	**FWHM**	**Assignments**	**Contents (at.%)**	
			Galena only	**Galena + Pyrite**
137.2 ± 0.05 142.1 ± 0.05	1.5	PbS	90.8	40.8
138.4 ± 0.05 143.3 ± 0.05	1.8	$Pb(OH)_2$, $PbSO_4$	9.2	59.2

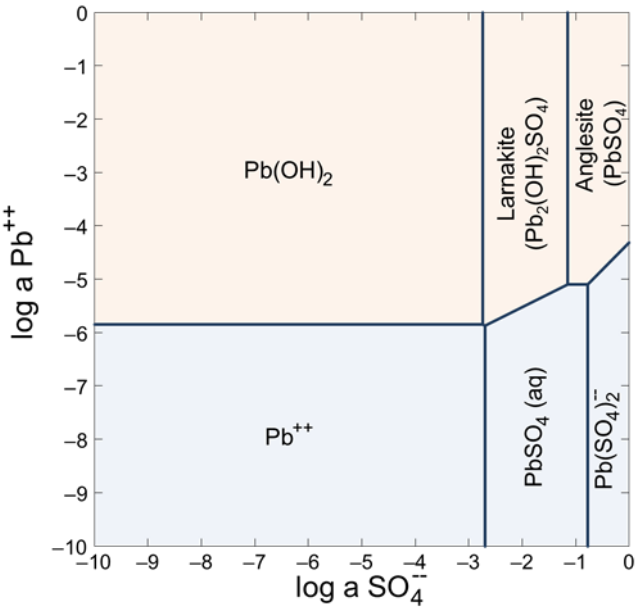

Figure 5-13. A diagram of log $\boldsymbol{a}_{\mathbf{Pb^{2+}}}$ vs log $\boldsymbol{a}_{\mathbf{SO_4^{2-}}}$ at pH 7 and 25℃ created using the Geochemist's Workbench® with the MINTEQ database (Gustaffson, 2013).

5.3.4 Proposed mechanism of depression of lead-activated sphalerite floatability by pyrite

Figure 5-14 illustrates the proposed mechanism of how pyrite depressed the floatability of lead-activated sphalerite. Pyrite significantly depressed the floatability of sphalerite even in the presence of activator (Pb^{2+}) and collector (KAX) (Figure 5-5 and Figure 5-9) because of its galvanic interactions with the PbS-like compounds on the surface of lead-activated sphalerite. This depression mechanism occurred directly via the enhanced dissolution of PbS-like compounds on sphalerite with adsorbed xanthate, and indirectly due to the precipitation of $Pb(OH)_2$, a well-known hydrophilic phase, on sphalerite.

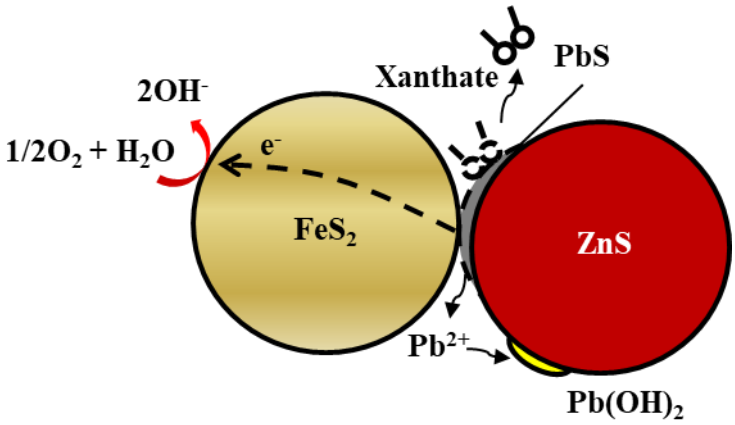

Figure 5-14. A schematic diagram of the proposed depression mechanism of lead-activated sphalerite floatability by pyrite.

5.4 Conclusions

In this chapter, the effects of pyrite on the floatability of lead-activated sphalerite were investigated and the findings of this chapter are summarized as follows:

1. Lead activation improved sphalerite floatability but pyrite significantly depressed lead-activated sphalerite flotation.

2. Dissolved Fe and S released from pyrite had negligible effects on the floatability of lead-activated sphalerite.

3. Contact angle on xanthate-treated galena with electrical connection to pyrite was lower than that without electrical connection, which indicates the desorption of xanthate and/or the formation of $Pb(OH)_2$ from Pb^{2+} generated via PbS dissolution.

4. Pyrite enhanced the dissolution of galena due to galvanic interactions and made the surface of galena less hydrophobic due to the formation of surface $Pb(OH)_2$ phases.

5. The floatability of lead-activated sphalerite was suppressed directly via galvanic interaction that dissolved PbS-like phases with adsorbed xanthate and indirectly due to the formation of hydrophilic $Pb(OH)_2$ on sphalerite.

This chapter is edited from “Aikawa et al., 2020. Depression of lead-activated sphalerite by pyrite via galvanic interactions: Implications to the selective flotation of complex sulfide ores. Miner. Eng. 152, 106367.”

References

Allison, S.A., Goold, L.A., Nicol, M.J., Granville, A., 1972. A determination of the products of reaction between various sulphide minerals and aqueous xanthate. Metallurgical Transactions 3, 2613–2618. https://doi.org/10.1007/BF02644237

Azizi, A., Shafaei, S.Z., Noaparast, M., Karamoozian, M., 2013. Galvanic interaction between chalcopyrite and pyrite with low alloy and high carbon chromium steel ball. J Chem 2013. https://doi.org/10.1155/2013/817218

Ball, J.W., Nordstrom, D.K., 1991. User's manual for WATEQ4F, with revised thermodynamic data base and text cases for calculating speciation of major, trace, and redox elements in natural waters, U.S. Geological Survey Water-Resources Investigations Report. Reston, VA, USA. https://doi.org/10.3133/ofr91183

Barker, G.J., Gerson, A.R., Menuge, J.F., 2014. The impact of iron sulfide on lead recovery at the giant Navan Zn–Pb orebody, Ireland. Int J Miner Process 128, 16–24. https://doi.org/10.1016/j.minpro.2014.02.001

Calderon, A.R.M., Alorro, R.D., Tadesse, B., Yoo, K., Tabelin, C.B., 2019. Evaluation of Maghemite-Rich Iron Oxide Composite Prepared from Magnetite as Adsorbent for Gold from Chloride Solution. JOM 71, 4639–4646. https://doi.org/10.1007/s11837-019-03514-8

Chandra, A.P., Gerson, A.R., 2009. A review of the fundamental studies of the copper activation mechanisms for selective flotation of the sulfide minerals, sphalerite and pyrite. Adv Colloid Interface Sci. https://doi.org/10.1016/j.cis.2008.09.001

Chernyshova, I. V., Andreev, S.I., 1997. Spectroscopic study of galena surface oxidation in aqueous solutions: I. Identification of surface species by XPS and ATR/FTIR spectroscopy. Appl Surf Sci 108, 225–236. https://doi.org/10.1016/S0169-4332(96)00579-X

Choi, S., Yoo, K., Alorro, R.D., Tabelin, C.B., 2020. Cementation of Co ion in leach solution using Zn powder followed by magnetic separation of cementation-precipitate for recovery of unreacted Zn powder. Miner Eng 145, 106061. https://doi.org/10.1016/j.mineng.2019.106061

Chopard, A., Plante, B., Benzaazoua, M., Bouzahzah, H., Marion, P., 2017. Geochemical investigation of the galvanic effects during oxidation of pyrite and base-metals sulfides. Chemosphere 166, 281–291. https://doi.org/10.1016/j.chemosphere.2016.09.129

Ekmekçi, Z., Demirel, H., 1997. Effects of galvanic interaction on collectorless flotation behaviour of chalcopyrite and pyrite. Int J Miner Process 52, 31–48. https://doi.org/10.1016/s0301-7516(97)00050-1

Eslami Andargoli, M.B., Jannesar Malakooti, S., Doulati Ardejani, F., Abdollahi, H., 2012. Effect of galvanic contact on the flotability of galena in the presence and absence of a collector. Int J Min Sci Technol 22, 629–632. https://doi.org/10.1016/j.ijmst.2012.08.006

Finkelstein, N.P., 1997. The activation of sulphide minerals for flotation: a review. Int J Miner Process 52, 81–120. https://doi.org/10.1016/S0301-7516(97)00067-7

Fornasiero, D., Li, F., Ralston, J., Smart, R.S.C., 1994. Oxidation of galena surfaces I. x-ray photoelectron spectroscopic and dissolution kinetics studies. J Colloid Interface Sci 164, 333–344. https://doi.org/10.1006/jcis.1994.1175

Fornasiero, D., Ralston, J., 2006. Effect of surface oxide/hydroxide products on the collectorless flotation of copper-activated sphalerite. Int J Miner Process 78, 231–237. https://doi.org/10.1016/j.minpro.2005.10.006

Gerson, A.R., Lange, A.G., Prince, K.E., Smart, R.St.C., 1999. The mechanism of copper activation of sphalerite. Appl Surf Sci 137, 207–223. https://doi.org/10.1016/S0169-4332(98)00499-1

Gustaffson, J.P., 2013. Visual MINTEQ – a free equilibrium speciation model [WWW Document]. Visual MINTEQ. URL https://vminteq.lwr.kth.se/ (accessed 1.7.21).

Herzig, P.M., Hannington, M.D., 1995. Polymetallic massive sulfides at the modern seafloor a review. Ore Geol Rev 10, 95–115. https://doi.org/10.1016/0169-1368(95)00009-7

Houot, R., Raveneau, P., 1992. Activation of sphalerite flotation in the presence of lead ions. Int J Miner Process 35, 253–271. https://doi.org/10.1016/0301-7516(92)90037-W

Huang, G., Grano, S., 2005. Galvanic interaction of grinding media with pyrite and its effect on floatation. Miner Eng 18, 1152–1163. https://doi.org/10.1016/j.mineng.2005.06.005

Igarashi, T., Herrera, P.S., Uchiyama, H., Miyamae, H., Iyatomi, N., Hashimoto, K., Tabelin, C.B., 2020. The two-step neutralization ferrite-formation process for sustainable acid mine drainage treatment: Removal of copper, zinc and arsenic, and the influence of coexisting ions on ferritization. Science of The Total Environment 715, 136877. https://doi.org/10.1016/j.scitotenv.2020.136877

Ikumapayi, F., Rao, K.H., 2015. Recycling process water in complex sulfide ore flotation: Effect of calcium and sulfate on sulfide minerals recovery. Mineral Processing and Extractive Metallurgy Review 36, 45–64. https://doi.org/10.1080/08827508.2013.868346

Jeon, S., Ito, M., Tabelin, C.B., Pongsumrankul, R., Tanaka, S., Kitajima, N., Saito, A., Park, I., Hiroyoshi, N., 2019. A physical separation scheme to improve ammonium thiosulfate leaching of gold by separation of base metals in crushed mobile phones. Miner Eng 138, 168–177. https://doi.org/10.1016/j.mineng.2019.04.025

Jeon, S., Tabelin, C.B., Park, I., Nagata, Y., Ito, M., Hiroyoshi, N., 2020a. Ammonium thiosulfate extraction of gold from printed circuit boards (PCBs) of end-of-life mobile phones and its recovery from pregnant leach solution by cementation. Hydrometallurgy 191, 105214. https://doi.org/10.1016/j.hydromet.2019.105214

Jeon, S., Tabelin, C.B., Takahashi, H., Park, I., Ito, M., Hiroyoshi, N., 2020b. Enhanced cementation of gold via galvanic interactions using activated carbon and zero-valent aluminum: A novel

approach to recover gold ions from ammonium thiosulfate medium. Hydrometallurgy 191, 105165. https://doi.org/10.1016/j.hydromet.2019.105165

Jeon, S., Tabelin, C.B., Takahashi, H., Park, I., Ito, M., Hiroyoshi, N., 2018. Interference of coexisting copper and aluminum on the ammonium thiosulfate leaching of gold from printed circuit boards of waste mobile phones. Waste Management 81, 148–156. https://doi.org/10.1016/j.wasman.2018.09.041

Laskowski, J.S., Liu, Q., Zhan, Y., 1997. Sphalerite activation: Flotation and electrokinetic studies. Miner Eng 10, 787–802. https://doi.org/10.1016/S0892-6875(97)00057-5

Leppinen, J.O., 1990. FTIR and flotation investigation of the adsorption of ethyl xanthate on activated and non-activated sulfide minerals. Int J Miner Process 30, 245–263. https://doi.org/10.1016/0301-7516(90)90018-T

Li, X., Gao, M., Hiroyoshi, N., Tabelin, C.B., Taketsugu, T., Ito, M., 2019. Suppression of pyrite oxidation by ferric-catecholate complexes: An electrochemical study. Miner Eng 138, 226–237. https://doi.org/10.1016/j.mineng.2019.05.005

Majima, H., 1969. How oxidation affects selective flotation of complex sulphide ores. Canadian Metallurgical Quarterly 8, 269–273. https://doi.org/10.1179/cmq.1969.8.3.269

Marston, R.J., Groves, D.I., Hudson, D.R., Ross, J.R., 1981. Nickel sulfide deposits in Western Australia: a review. Economic Geology 76, 1330–1363. https://doi.org/10.2113/gsecongeo.76.6.1330

Martin, C.J., Rao, S.R., Finch, J.A., Leroux, M., 1989. Complex sulphide ore processing with pyrite flotation by nitrogen. Int J Miner Process 26, 95–110. https://doi.org/10.1016/0301-7516(89)90045-8

Mikhlin, Y., Kuklinskiy, A., Mikhlina, E., Kargin, V., Asanov, I., 2004. Electrochemical behaviour of galena (PbS) in aqueous nitric acid and perchloric acid solutions. J Appl Electrochem 34, 37–46. https://doi.org/10.1023/B:JACH.0000005566.28289.c0

Mu, Y., Peng, Y., Lauten, R.A., 2018. The galvanic interaction between chalcopyrite and pyrite in the presence of lignosulfonate-based biopolymers and its effects on flotation performance. Miner Eng 122, 91–98. https://doi.org/10.1016/j.mineng.2018.03.048

Nansai, K., Nakajima, K., Kagawa, S., Kondo, Y., Suh, S., Shigetomi, Y., Oshita, Y., 2014. Global Flows of Critical Metals Necessary for Low-Carbon Technologies: The Case of Neodymium, Cobalt, and Platinum. Environ Sci Technol 48, 1391–1400. https://doi.org/10.1021/es4033452

Nesbitt, H.W., Muir, I.J., 1994. X-ray photoelectron spectroscopic study of a pristine pyrite surface reacted with water vapour and air. Geochim Cosmochim Acta 58, 4667–4679. https://doi.org/10.1016/0016-7037(94)90199-6

Palm, N.A., Shackleton, N.J., Malysiak, V., O'Connor, C.T., 2010. The effect of using different comminution procedures on the flotation of sphalerite. Miner Eng 23, 1053–1057. https://doi.org/10.1016/j.mineng.2010.08.001

Park, I., Tabelin, C.B., Jeon, S., Li, X., Seno, K., Ito, M., Hiroyoshi, N., 2019. A review of recent strategies for acid mine drainage prevention and mine tailings recycling. Chemosphere 219, 588–606. https://doi.org/10.1016/j.chemosphere.2018.11.053

Park, I., Tabelin, C.B., Seno, K., Jeon, S., Inano, H., Ito, M., Hiroyoshi, N., 2020. Carrier-microencapsulation of arsenopyrite using Al-catecholate complex: nature of oxidation products, effects on anodic and cathodic reactions, and coating stability under simulated weathering conditions. Heliyon 6, e03189. https://doi.org/10.1016/j.heliyon.2020.e03189

Park, I., Tabelin, C.B., Seno, K., Jeon, S., Ito, M., Hiroyoshi, N., 2018. Simultaneous suppression of acid mine drainage formation and arsenic release by Carrier-microencapsulation using aluminum-catecholate complexes. Chemosphere 205, 414–425. https://doi.org/10.1016/j.chemosphere.2018.04.088

Pecina-Treviño, E.T., Uribe-Salas, A., Nava-Alonso, F., 2003. Effect of dissolved oxygen and galvanic contact on the floatability of galena and pyrite with Aerophine 3418A. Miner Eng 16, 359–367. https://doi.org/10.1016/S0892-6875(03)00022-0

Phuong Thao, N.T., Tsuji, S., Jeon, S., Park, I., Tabelin, C.B., Ito, M., Hiroyoshi, N., 2020. Redox potential-dependent chalcopyrite leaching in acidic ferric chloride solutions: Leaching experiments. Hydrometallurgy 194, 105299. https://doi.org/10.1016/j.hydromet.2020.105299

Qin, Wen-qing, Wang, X., Ma, L., Jiao, F., Liu, R., Gao, K., 2015. Effects of galvanic interaction between galena and pyrite on their flotation in the presence of butyl xanthate. Transactions of Nonferrous Metals Society of China 25, 3111–3118. https://doi.org/10.1016/S1003-6326(15)63940-1

Qin, Wenqing, Wang, X., Ma, L., Jiao, F., Liu, R., Yang, C., Gao, K., 2015. Electrochemical characteristics and collectorless flotation behavior of galena: With and without the presence of pyrite. Miner Eng 74, 99–104. https://doi.org/10.1016/j.mineng.2015.01.010

Rabieh, A., Eksteen, J.J., Albijanic, B., 2018. Galvanic interaction of grinding media with arsenopyrite and pyrite and its effect on gold cyanide leaching. Miner Eng 116, 46–55. https://doi.org/10.1016/j.mineng.2017.10.018

Rao, S.R., 2004. Surface Chemistry of Froth Flotation, Surface Chemistry of Froth Flotation. Springer US, Boston, MA. https://doi.org/10.1007/978-1-4757-4302-9

Rao, S.R., Finch, J.A., 1988. Galvanic Interaction Studies on Sulphide Minerals. Canadian Metallurgical Quarterly 27, 253–259. https://doi.org/10.1179/cmq.1988.27.4.253

Rashchi, F., Sui, C., Finch, J.A., 2002. Sphalerite activation and surface Pb ion concentration. Int J Miner Process 67, 43–58. https://doi.org/10.1016/S0301-7516(02)00005-4

Seng, S., Tabelin, C.B., Kojima, M., Hiroyoshi, N., Ito, M., 2019a. Galvanic Microencapsulation (GME) Using Zero-Valent Aluminum and Zero-Valent Iron to Suppress Pyrite Oxidation. Mater Trans 60, 277–286. https://doi.org/10.2320/matertrans.M-M2018851

Seng, S., Tabelin, C.B., Makino, Y., Chea, M., Phengsaart, T., Park, I., Hiroyoshi, N., Ito, M., 2019b. Improvement of flotation and suppression of pyrite oxidation using phosphate-enhanced galvanic microencapsulation (GME) in a ball mill with steel ball media. Miner Eng 143, 105931. https://doi.org/10.1016/j.mineng.2019.105931

Shirley, D.A., 1972. High-Resolution X-Ray Photoemission Spectrum of the Valence Bands of Gold. Phys Rev B 5, 4709–4714. https://doi.org/10.1103/PhysRevB.5.4709

Tabelin, C.B., Corpuz, R.D., Igarashi, T., Villacorte-Tabelin, M., Ito, M., Hiroyoshi, N., 2019. Hematite-catalysed scorodite formation as a novel arsenic immobilization strategy under ambient conditions. Chemosphere 233, 946–953. https://doi.org/10.1016/j.chemosphere.2019.06.020

Tabelin, C.B., Igarashi, T., 2009. Mechanisms of arsenic and lead release from hydrothermally altered rock. J Hazard Mater 169, 980–990. https://doi.org/10.1016/j.jhazmat.2009.04.049

Tabelin, C.B., Igarashi, T., Tamoto, S., Takahashi, R., 2012. The roles of pyrite and calcite in the mobilization of arsenic and lead from hydrothermally altered rocks excavated in Hokkaido, Japan. J Geochem Explor 119–120, 17–31. https://doi.org/10.1016/j.gexplo.2012.06.003

Tabelin, C.B., Igarashi, T., Villacorte-Tabelin, M., Park, I., Opiso, E.M., Ito, M., Hiroyoshi, N., 2018. Arsenic, selenium, boron, lead, cadmium, copper, and zinc in naturally contaminated rocks: A review of their sources, modes of enrichment, mechanisms of release, and mitigation strategies. Science of The Total Environment 645, 1522–1553. https://doi.org/10.1016/j.scitotenv.2018.07.103

Tabelin, C.B., Veerawattananun, S., Ito, M., Hiroyoshi, N., Igarashi, T., 2017a. Pyrite oxidation in the presence of hematite and alumina: I. Batch leaching experiments and kinetic modeling calculations. Science of The Total Environment 580, 687–698. https://doi.org/10.1016/j.scitotenv.2016.12.015

Tabelin, C.B., Veerawattananun, S., Ito, M., Hiroyoshi, N., Igarashi, T., 2017b. Pyrite oxidation in the presence of hematite and alumina: I. Batch leaching experiments and kinetic modeling calculations. Science of The Total Environment 580, 687–698. https://doi.org/10.1016/j.scitotenv.2016.12.015

Tatsuhara, T., Arima, T., Igarashi, T., Tabelin, C.B., 2012. Combined neutralization-adsorption system for the disposal of hydrothermally altered excavated rock producing acidic leachate with hazardous elements. Eng Geol 139–140, 76–84. https://doi.org/10.1016/j.enggeo.2012.04.006

Tomiyama, S., Igarashi, T., Tabelin, C.B., Tangviroon, P., Ii, H., 2020. Modeling of the groundwater flow system in excavated areas of an abandoned mine. J Contam Hydrol 230, 103617. https://doi.org/10.1016/j.jconhyd.2020.103617

Tomiyama, S., Igarashi, T., Tabelin, C.B., Tangviroon, P., Ii, H., 2019. Acid mine drainage sources and hydrogeochemistry at the Yatani mine, Yamagata, Japan: A geochemical and isotopic study. J Contam Hydrol 225, 103502. https://doi.org/10.1016/j.jconhyd.2019.103502

Trahar, W.J., Senior, G.D., Heyes, G.W., Creed, M.D., 1997. The activation of sphalerite by lead — a flotation perspective. Int J Miner Process 49, 121–148. https://doi.org/10.1016/S0301-7516(96)00041-5

Wills, B.A., Finch, J.A., 2016. Mineral processing technology: an introduction to the practical aspects of ore treatment and mineral recovery, 8th ed.

Woodcock, J.T., Sparrow, G.J., Bruckard, W.J., Johnson, N.W., Dunne, R., 2007. Plant Practice: Sulfide Minerals and Precious Metals, in: Froth Flotation A Century of Innovation. Pp. 781–844.

Yelloji Rao, M.K., Natarajan, K.A., 1989. Electrochemical effects of mineral-mineral interactions on the flotation of chalcopyrite and sphalerite. Int J Miner Process 27, 279–293. https://doi.org/10.1016/0301-7516(89)90069-0

Zoleta, J.B., Itao, G.B., Resabal, V.J.T., Lubguban, A.A., Corpuz, R.D., Ito, M., Hiroyoshi, N., Tabelin, C.B., 2020. Improved pyrolysis behavior of ammonium polyphosphate-melamine-expandable (APP-MEL-EG) intumescent fire retardant coating system using ceria and dolomite as additives for I-beam steel application. Heliyon 6, e03119. https://doi.org/10.1016/j.heliyon.2019.e03119

CHAPTER 6 – GENERAL CONCLUSION

This dissertation is comprised of six chapters which detail the different methodologies used in the experiments and their outcomes.

Chapter 1 describes the statement of the problem and objectives of this study, and a literature review on depression of sphalerite floatability in flotation of complex sulfide ores. Complex sulfide ores, some of the most important sources of critical metals, are typically composed of several metal sulfide minerals like chalcopyrite, galena and sphalerite. Complex sulfides consisting of copper (Cu), lead (Pb), and zinc (Zn)-sulfide minerals are typically processed via flotation—a separation technique based on the differences in wettability of minerals—to produce concentrates of each mineral. Some complex sulfides (e.g., seafloor massive sulfides obtained from around Japan, one of the promising sources of critical metals in the future) contain not only galena but also anglesite, which is not typically contained in the conventional ores. The presence of anglesite is problematic for the separation of Cu, Pb and Zn-sulfide minerals by flotation due to the unwanted activation of sphalerite by lead ions released from anglesite. In addition, anglesite rejected to tailings dam contaminates its surrounding environment. To address these problems, a sufficient method for depressing sphalerite floatability to separate it from Cu and Pb-minerals and preventing lead pollution around the surrounding environment of tailings dam are necessary. In this study, a promising process of mineral processing for complex sulfide ores combined with extraction, flotation, and cementation for sustainable development of complex sulfide deposits in harmony with environment. In addition, effects of unwanted activation of sphalerite by Cu^{2+} and Pb^{2+} on Cu/Zn flotation and Pb/Zn flotation were investigated.

In Chapter 2, a process of mineral processing for complex sulfide ores combined with extraction, flotation, and cementation using ethylene diamine tetra acetic acid (EDTA) was investigated. The results of sphalerite flotation in the presence and absence of anglesite showed that sphalerite floatability increased in the presence of anglesite. The conventional depressants for sphalerite, zinc sulfate and sodium sulfite, were not effective in depressing the floatability of sphalerite when anglesite was present. The results of extraction experiments of anglesite using EDTA and cementation experiments using zero-valent iron (ZVI) showed that almost all anglesite (>97%) was extracted using EDTA, and >97% of the extracted Pb^{2+} could be recovered as Pb^{0} by cementation using ZVI. When a pretreatment of flotation extracting anglesite using EDTA was applied, sphalerite floatability was effectively depressed. The proposed method for complex sulfide ores containing anglesite, a combination of extraction of anglesite using EDTA and recovery of

extracted Pb^{2+} as zero-valent Pb by cementation using ZVI, could achieve enhanced selective flotation of complex sulfide ores (depression of sphalerite floatability) while preventing lead pollution to the surrounding environment of tailings dams (removal of toxic anglesite before flotation) and maximizing the recovery of critical elements by cementation (recovery of Pb^0 using ZVI).

In Chapter 3, alternative extractants of anglesite to EDTA were investigated using ammonium acetate and sodium chloride-hydrochloric acid. The results of extraction experiments of anglesite using ammonium acetate and cementation experiments using ZVI showed that Almost all anglesite (> 99%) was extracted using ammonium acetate, and >99% of extracted Pb^{2+} could be recovered as Pb^0 by cementation using ZVI. The results of CEC experiments using sodium chloride-hydrochloric acid and ZVI showed that almost all anglesite (> 97%) was extracted and recovered on ZVI as Pb^0 by the coupled extraction-cementation method using sodium chloride-hydrochloric acid as an extractant of anglesite and ZVI as a reductant. Based on these results Pretreatments of flotation extracting anglesite using ammonium acetate or sodium chloride-hydrochloric acid was effective in depressing sphalerite floatability, indicating that ammonium acetate and sodium chloride-hydrochloric acid can be used instead of EDTA for the extraction of anglesite to depress the floatability of sphalerite.

In Chapter 4, effects of pyrite on the separation of chalcopyrite and sphalerite were investigated to further depress the floatability of sphalerite in the cleaner stage of Cu flotation. The results of single mineral flotation of sphalerite showed that Zn recovery was low, but it was dramatically increased when chalcopyrite coexisted due to the activation of sphalerite by Cu^{2+} dissolved from chalcopyrite. When zinc sulfate was used as a depressant, sphalerite floatability was successfully depressed; however, the presence of pyrite inhibited its ability to depress sphalerite floatability due most likely to galvanic interaction between pyrite and chalcopyrite. When nitrogen gas was applied to flotation experiments to limit galvanic interaction between pyrite and chalcopyrite by reducing dissolved oxygen concentration in the system, sphalerite was effectively depressed with zinc sulfate even in the presence of much higher amounts of chalcopyrite and pyrite.

In Chapter 5, effects of pyrite on the floatability of lead-activated sphalerite were investigated to clarify whether the addition of activators such as copper sulfate is necessary to separate lead-activated sphalerite from pyrite in Zn flotation. The results of sphalerite flotation in the presence and absence of pyrite showed that pyrite significantly depressed the floatability of lead-activated sphalerite. Dissolved Fe and S released from pyrite had negligible effects on the floatability of lead-activated sphalerite. Contact angle on xanthate-treated galena with electrical connection to pyrite was lower than that without electrical connection, indicating that the desorption of xanthate and/or the formation of $Pb(OH)_2$ from Pb^{2+} generated via PbS dissolution. The results of dissolution tests of

PbS with and without pyrite, combined with the surface analysis of the residues after dissolution tests using XPS indicated that Pyrite enhanced the dissolution of galena due to galvanic interactions and made the surface of galena less hydrophobic due to the formation of surface $Pb(OH)_2$ phases, resulting in the depression of lead-activated sphalerite directly via galvanic interaction that dissolved PbS-like phases with adsorbed xanthate and indirectly due to the formation of hydrophilic $Pb(OH)_2$ on sphalerite.

Taking all of these results into consideration, a more sustainable process was proposed as illustrated in Figure 6-1 and the details of pretreatments are illustrated in Figure 6-2. The processing flowcharts are decided based on the presence of soluble minerals in complex sulfide ores; (i) no soluble minerals, (ii) only soluble Pb minerals, (iii) soluble minerals releasing not only Pb^{2+} but also other ions such Cu^{2+}, Zn^{2+}, $Fe^{2+/3+}$. (i) The ores without soluble minerals are directly subjected to the conventional flotation process after comminution without pretreatments. (ii) The ores containing soluble Pb minerals such as anglesite are pretreated with ammonium acetate or sodium chloride-hydrochloric acid to extract/remove anglesite from the ores. The ammonium acetate pretreatment is applied to wet-grinding systems (e.g., ball mill, SAG mill, etc.), and then the residue and the filtrate are fed to Cu-Pb/Zn flotation and cementation after S/L separation, respectively. Cementation to recover extracted Pb^{2+} by ammonium acetate as Pb^0 is conducted using ZVI as a reductant. After S/L separation, the filtrate containing ammonium acetate is reused as an extractant of soluble Pb minerals. The sodium chloride-hydrochloric acid pretreatment based on the coupled extraction-cementation (CEC) method is applied after dry grinding system (e.g., high pressure grinding rolls (HPGR)) to avoid Pb activation of sphalerite during wet grinding. Dry-ground ores are treated in sodium chloride-hydrochloric acid solution with ZVI to extract and recover anglesite as Pb^0. After Pb^0-loaded ZVI is separated using magnets, S/L separation of non-magnetic fraction is conducted, and then the residue is fed to Cu-Pb/Zn flotation and the filtrate containing sodium chloride-hydrochloric acid is reused as an extractant of soluble Pb minerals. Pb^0-loaded ZVI (the residue) from the ammonium acetate/sodium chloride-hydrochloric acid pretreatment is further treated to separate Pb^0 from ZVI or directly fed to Pb smelting. After pretreatments of the ores to extract soluble minerals, Cu-Pb/Zn flotation is conducted to recover chalcopyrite and galena as froth and depress the floatability of sphalerite. The concentrate of Cu-Pb/Zn flotation is further treated in Cu/Pb flotation and chalcopyrite is separated from galena. Cu/Pb flotation should be conducted under anoxic conditions to depress the floatability of sphalerite if the Zn grade in Cu-Pb/Zn flotation is high to prevent activation of sphalerite by Cu^{2+} and Pb^{2+} released from chalcopyrite/galena due to galvanic interactions with pyrite. In Zn flotation to separate sphalerite from gangue minerals, copper sulfate is used as an activator for sphalerite to improve the Zn recovery.

The results of this study have significant implications for future-oriented mineral processing, considering the upcoming situations to process ores from small-scale, complex, and heterogeneous deposits. Terrestrial deposits being developed are large-scale, and their mineralogical compositions are typically uniform. Because of this, concentrates that meet the requirements of smelters can be produced stably, so the modification of the operating conditions is not often required once optimized. Meanwhile, large-scale deposits are getting depleted, and the remaining deposits are small-scale, complex, and heterogeneous, which make the conventional mineral processing inapplicable. Therefore, the development of future-oriented mineral processing is necessary; in particular, (i) Monitoring (Ore characteristics are variable), (ii) simulation/optimization (Optimization of flotation process/conditions based on ore characteristics), and (iii) automatic control (Optimized flotation process). Outcomes of this dissertation could attribute to (ii) simulation/optimization. To develop (ii) simulation/optimization, it is necessary to clarify (a) physical properties (e.g., mineral composition, degree of liberation, etc.) and (b) estimation of chemical reaction (interaction between mineral surface and dissolved ions/mineral surface).

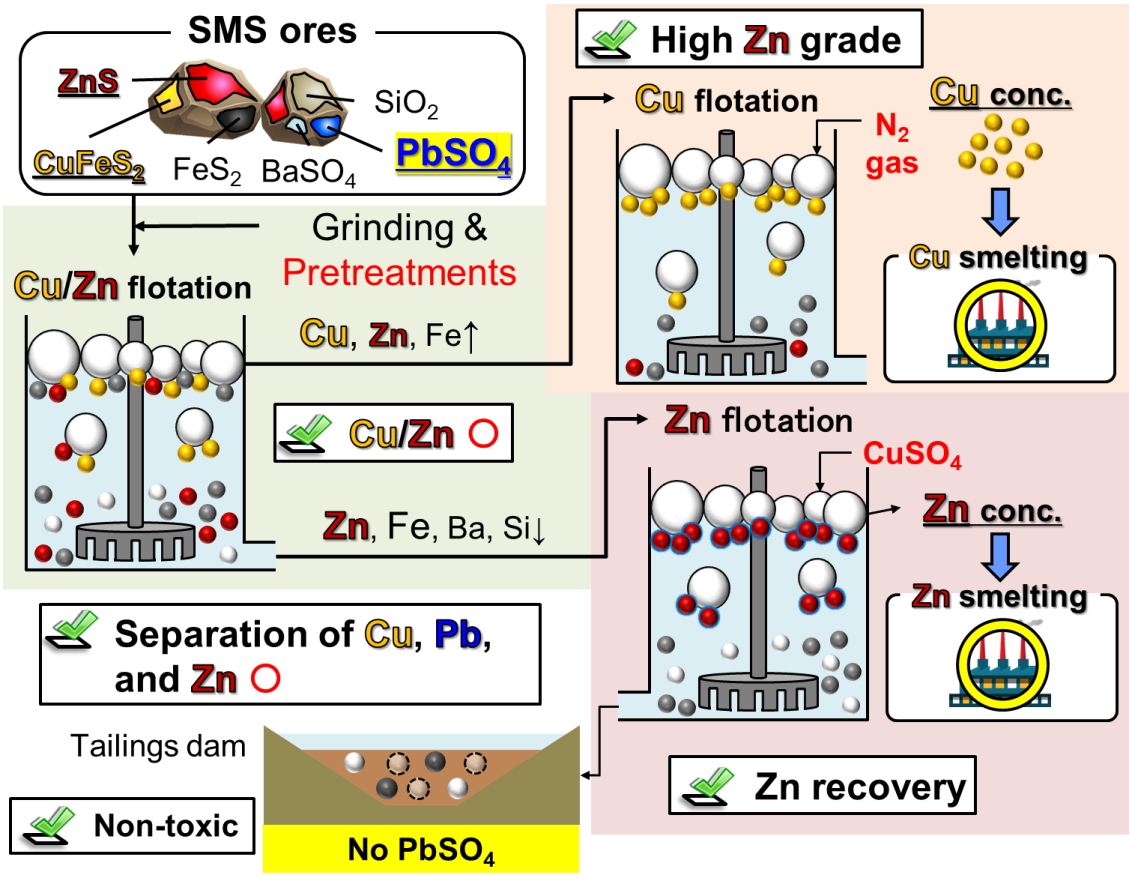

Figure 6-1. The proposed flowsheet of selective flotation of complex sulfide ores based on pretreatments to extract soluble minerals in complex sulfide ores.

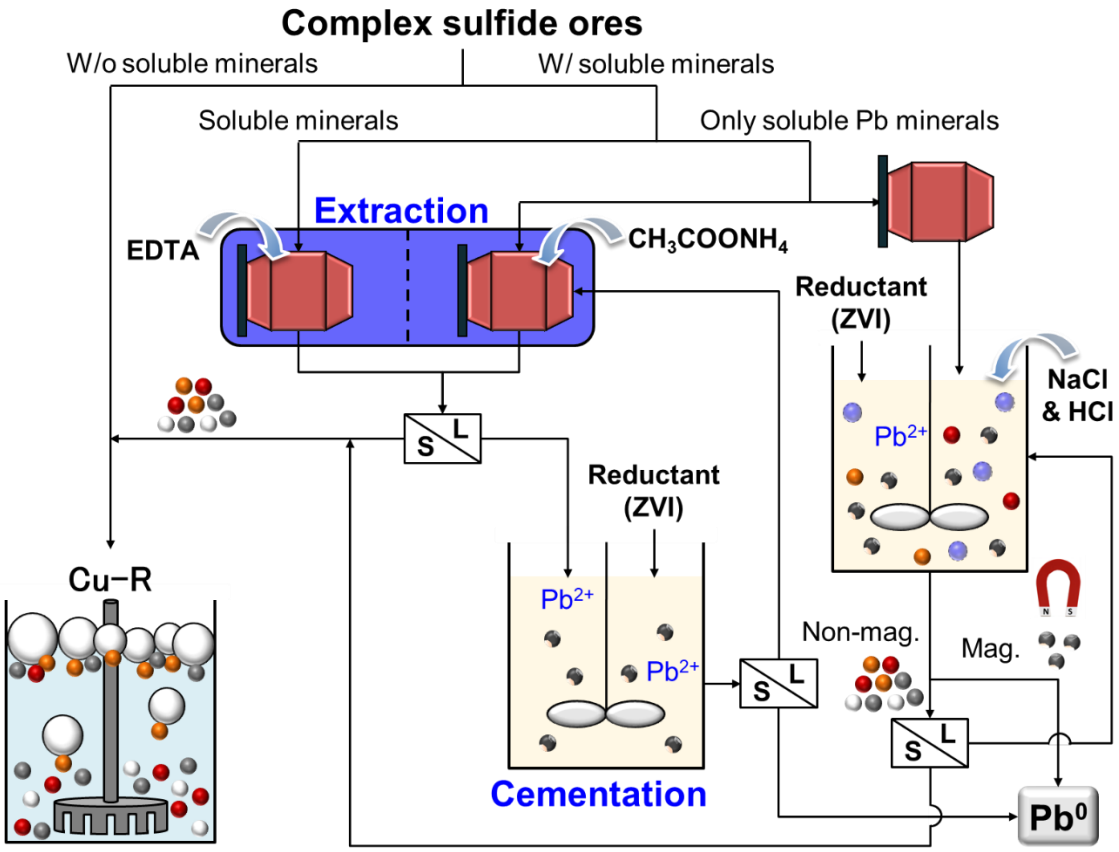

Figure 6-2. The detailed flowsheet of pretreatments to extract anglesite using EDTA and ammonium acetate combined with cementation using ZVI, and to extract and recover soluble Pb minerals using a CEC method using sodium chloride-hydrochloric acid and ZVI.

ACKNOLEDGEMENT

This dissertation could be successfully completed thanks to many people, so I wish to express my sincere appreciation to each of them.

I would like to acknowledge to my supervisor, Professor Mayumi Ito, who gave me a lot of constructive advice to succeed in my research. She also guided me to walk through the path of a researcher. I will never forget your enthusiasm to do your best to inspire not only me but also all the students.

I am very grateful to Professor Naoki Hiroyoshi, who encouraged me in the completion of this dissertation. His valuable advice and critical comments for the improvements of my research are gratefully appreciated.

My sincere thanks are extended to my co-supervisor, Assistant Professor Ilhwan Park. He always strived to inspire me when I was in trouble with research works, rather than giving me a direct answer. His continual encouragement made my dissertation successful.

Special appreciation goes to Professor Tsubasa Otake (Division of Sustainable Resources Engineering, Faculty of Engineering, Hokkaido University) and Associate Professor Masatoshi Sakairi (Division of Materials Science and Engineering, Faculty of Hokkaido University), who served as co-examiners of my dissertation. Thanks to their efforts and advice, this dissertation could have been improved considerably.

To my colleagues from the Laboratory of Mineral Processing and Resources Recycling, thank you very much for being warm during my Ph.D. course. Thanks to your kind support and companionship, I think I was able to complete a 2-year journey. Special thanks are extended to my junior students, Atsuhiro Kusano, Nodoka Orii, and Shunki Tanaka. I would like to say thank you for putting your trust in me and for always helping me in academic and university matters.

Finally, I would like to thank heartily my family for their continual support and encouragement.